Fundamentals and Applications of Spatial Dissipative Solitons in Photonic Devices

T. Ackemann, W. J. Firth, G.-L. Oppo

SUPA and Department of Physics, University of Strathclyde, Glasgow G4 ONG, Scotland, UK

Abstract

We review the properties of optical spatial dissipative solitons (SDS). These are stable, self-localized optical excitations sitting on a uniform, or quasi-uniform, background in a dissipative environment like a nonlinear optical cavity. Indeed in optics they are often termed 'cavity solitons'. We discuss their dynamics and interactions in both ideal and imperfect systems, making comparison with experiments. SDS in lasers offer important advantages for applications. We review candidate schemes and the tremendous recent progress in semiconductor-based cavity soliton lasers. We examine SDS in periodic structures, and we show how SDS can be quantitatively related to the locking of fronts. We conclude with an assessment of potential applications of SDS in photonics, arguing that best use of their particular features is made by exploiting their mobility, e.g. in all-optical delay lines.

Key words: dissipative spatial solitons, cavity solitons, nonlinear photonics, optical pattern formation, homoclinic snaking, cavity soliton lasers, spatial effects in optical bistability, VCSEL, all-optical delay lines

1 Introduction

1.1 Basic definitions and scope

Spontaneous pattern formation is a widespread consequence of nonlinearity in spatially-extended systems driven out of equilibrium (Cross and Hohenberg, 1993), and has been predicted and/or observed in a wide variety of systems, including fluid dynamics (Manneville, 1990), chemistry (Ross et al., 1988), biology (Murray, 2003), ferro-fluids (Richter and Barashenkov, 2005), gas discharges (Müller et al., 1999), granular media (Umbanhowar et al., 1996) and optics (McLaughlin et al. (1983); Lugiato and Lefever (1987); Abraham and

Firth (1990); Lugiato et al. (1994); Neubecker (1996); Rosanov (1996); Lugiato et al. (1999); Arecchi et al. (1999); Ackemann and Lange (2001); Firth and Weiss (2002); Rosanov (2002); Oppo (2009)).

Possibly even more fascinating is *self-localization*, i.e. the formation of nonlinearity-sustained localized objects, which is again a quite universal feature in nonlinear science, e.g. (Umbanhowar et al. (1996); Müller et al. (1999); Riecke (1999); Coullet (2002); Richter and Barashenkov (2005); Akhmediev and Ankiewicz (2005a, 2008)). Although dissipation plays a major role in most natural systems, much of early research into self-localization concentrated on the conservative limit, and in particular on *solitons*, i.e. exact solutions to integrable, conservative, nonlinear wave equations, see, e.g., (Remoissenet, 1994).

In optics, *spatial optical solitons* are beams of light in which nonlinearity counter-balances diffraction, leading to a robust structure which propagates without change of form (see Fig. 1a) (Stegeman and Segev (1999); Segev (2002)). In the conservative case, the range of materials is rather limited – they need to be self-focusing – and in many cases the existence of stable spatial solitons is also limited to one-dimensional systems. Such is the case for the simplest soliton medium, one with a Kerr nonlinearity, i.e. a refractive index which changes in proportion to the intensity of the light. However, as many researchers demonstrated over the last years and as we are trying to review and elucidate here, more general schemes can support stable soliton-like solutions with lots of intriguing and new properties, if dissipation and driving and/or feedback are explicitly introduced. Among these, localized bright spots (see Fig. 2) in driven optical cavities (Fig. 1b, c) have received a great deal of attention because of their experimental realizability in semiconductor microresonators and potential applications in information processing. These are usually referred to as *cavity solitons* (CS) (Firth and Harkness (1998); Firth and Weiss (2002); Barland et al. (2002)). Actually, a "half-cavity" turns out to be enough, i.e. very similar objects are found in arrangements in which feedback is provided by a single-mirror only (Fig. 1d, "single-mirror feedback scheme" (Firth (1990); D'Alessandro and Firth (1991); Ackemann and Lange (2001)), see Figs. 3, 4). They can be named *feedback solitons* (FS). In the nonlinear science literature self-localized dissipative structures are variously referred to as "localized states" (Burke and Knobloch, 2006), "localized structures" (LS) (Coullet et al. (2000); Coullet (2002)), "localized patterns" (Coullet (2002); Dawes (2008)) or *spatial dissipative solitons* (SDS) (Akhmediev and Ankiewicz (2005a, 2008)). Perhaps the earliest term of all is "autosoliton", still much used in the Russian literature (Rosanov and Khodova (1988); Kerner and Osipov (1989); Rosanov and Khodova (1990)). Here we adopt SDS because, in our opinion, it nicely stresses similarities and differences between these structures and "solitons".

The history of cavity solitons probably began with the seminal theoretical

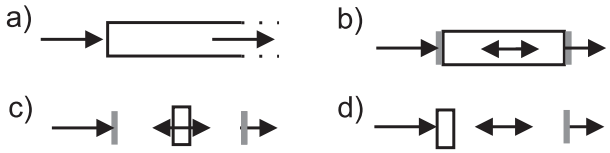

Fig. 1. Nonlinear optical systems supporting pattern formation and solitons (plane mirrors are drawn in gray): a) nonlinear beam propagation, b) cavity filled with nonlinear medium, c) cavity with a short medium, d) single-mirror feedback arrangement.

papers of Moloney and co-workers (McLaughlin et al., 1983) and Rosanov and coworkers (Rosanov and Semenov (1980); Rosanov and Khodova (1988, 1990); Fedorov et al. (1991)) stemming from interest in spatial aspects of optical bistability (Gibbs (1985); Lugiato (1984)). Early experiments followed soon afterwards (Kreuzer et al. (1991); Neubecker and Tschudi (1994); Bazhenov et al. (1991)). Overviews and reviews of the early stage of the field can be found in Abraham and Firth (1990); Lugiato et al. (1994); Rosanov (1996); Neubecker et al. (1999); Lugiato et al. (1999); Arecchi et al. (1999); Weiss et al. (1999); Trillo and Torruellas (2001); Ackemann and Lange (2001); Firth (2001); Firth and Weiss (2002); Rosanov (2002); Lugiato (2003).

In this contribution we want to review more recent developments, prompted by the fact that SDS have been realized in photonic devices like semiconductor microcavities, which belong to mainstream research in applied optoelectronics (Barland et al., 2002). SDS in these robust, compact and comparatively fast systems appeal not only to those interested in the fundamentals of self-organization but also offer a new approach to all-optical processing applications.

The remainder of this section provides a more detailed introduction into phenomenology and basics of SDS. We will also introduce a set of "standard equations", which will be repeatedly used in following sections. In Sec. 2 a detailed treatment of the bifurcation structure of SDS is given and the phenomenon of *homoclinic snaking* which is at the heart of the complexity behind the multistability of SDS and clusters of SDS, is analyzed. This research is of strong interest to the Applied Mathematics community – illustrating the universality of the phenomena related to SDS in Nonlinear Science – but the results are also highly relevant for applications. In Sec. 3, we will explore the specifics of SDS in lasers, i.e. systems with the additional symmetry of phase invariance. Here, the last years witnessed tremendous progress in semiconductor-based photonic devices driven by a recent European project FunFACS (Fundamentals, Functionalities and Applications of Cavity Solitons). Photonic crystal structures or, more generally, periodic refractive index modulations provide powerful tools to provide control over light propagation. Sec. 4 explores their application to control self-organization and SDS. Sec. 5 deals with specific mechanisms how SDS are stabilized and will demonstrate how the dynamics of fronts between

spatially extended states can lead to SDS. Sec. 6 gives an account of possible and realized applications of SDS and the material challenges needing to to be tackled to make SDS applications viable. Finally, Sec. 7 provides a short summary and outlook on the field.

This article draws mainly on the work of ourselves and collaborators. This is primarily for convenience, because (although still quite young) the field is already too large to be completely covered in a single review. We have tried, however, to present a fair and reasonably comprehensive list of relevant references. We already mentioned some reviews of earlier work: more recent relevant reviews, monographs and special issues include (Staliunas and Sánchez-Morcillo (2003); Drummond et al. (2004); Mandel and Tlidi (2004); Akhmediev and Ankiewicz (2005a); Weiss and Larionova (2005); Residori (2005); Akhmediev and Ankiewicz (2008)). Some information can be also found on the website of the FunFACS project (IST-STREP 004868, 2005-2008). Most of the effects we treat (with some exceptions in Sec. 5) can be understood in the framework of frequency-degenerate $\chi^{(3)}$-nonlinearities, or saturable nonlinearities where the third order term is the leading one. There is a rich phenomenology and literature on optical SDS – though no experiments – relying on coupling between fields with very different frequencies, e.g. by a $\chi^{(2)}$ nonlinearity. This has been shown in mean-field models to support SDS in both second-harmonic-generation (SHG) (Etrich et al. (1997); Michaelis et al. (2003)) and optical parametric oscillator (OPO) (Longhi (1997); Staliunas and Sánchez-Morcillo (1997); Oppo et al. (1999); Le Berre et al. (1999); Skryabin et al. (2000); Tlidi et al. (2000); Oppo et al. (2001); Etrich et al. (2002); Gomila et al. (2003)) configurations. In addition, we do not cover the rich literature on temporal dissipative solitons though it is highly relevant for modern ultra-fast mode-locked lasers, at least in some operating regimes. We can refer to the contributions in (Akhmediev and Ankiewicz (2005a, 2008)) here.

1.2 Phenomenology of optical SDS

An archetypical example for a cavity system sustaining SDS is the vertical-cavity surface-emitting laser (VCSEL) Wilmsen et al. (1999). These are high-finesse semiconductor microcavities which are closed by high-reflectivity distributed Bragg reflectors (DBR). The active medium consists typically of quantum well structures which can be absorbing or – with electrical or optical pumping – provide gain. The inner cavity is typically only one wavelength thick and the effective cavity length (including the penetration in the DBR) on the order of 1-2 μm. However, they can be produced with an aperture size of 100-200 μm, realizing a system in which the transverse boundaries can be "far" from the interesting self-localized structures. In the key experiment, illustrated in the left panel of Fig. 2, a VCSEL is operated as an amplifier but

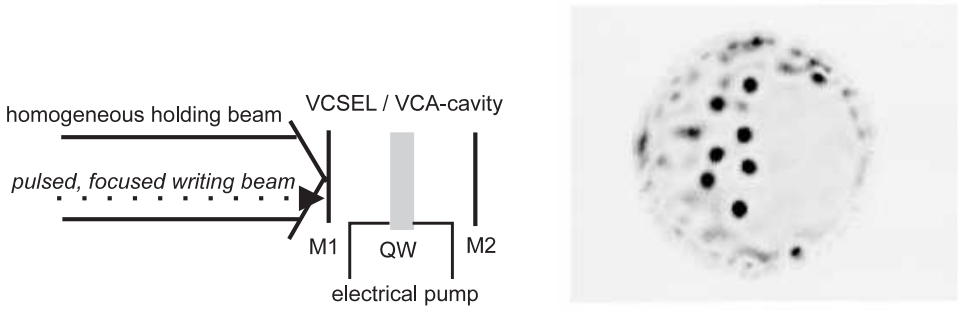

Fig. 2. Left: Scheme of an experiment in a vertical-cavity amplifier (VCA) operating around 980 nm. M1, M2 plane mirrors, QW quantum wells. The system is driven by a homogeneous cw broad-area holding beam. A pulsed focused writing beam can be used to control the SDS. Right: Typical intensity distribution of the output field in a vertical-cavity amplifier showing the presence of seven SDS. [Reprinted figure with permission from Hachair et al. (2004). Copyright 2004 by the American Physical Society.]

remains below the threshold for laser oscillation Barland et al. (2002); Hachair et al. (2004). Then a broad-area holding beam (HB) is added. At certain biasing conditions of the HB, SDS structures like those depicted in the right panel of Fig. 2 are observed. Similar observations were made later in a scheme where the the electrical injection was replaced by an optical pumping beam Barbay et al. (2006).

The fundamental SDS usually is a bright spot of light on some low amplitude background (see Figs. 2-4). It is self-localized in the two spatial dimensions *transverse* to the main propagation axis (e.g. the cavity axis). The decay of energy in the wings is asymptotically exponential, as can be shown by the method of "spatial dynamics" Coullet et al. (2000). Close inspection shows that spatial oscillations can be superimposed on this decay, see Figs. 3, 4. These are important for understanding interaction of SDS (e.g. the formation of the clusters shown in Fig. 3) and the locking of fronts (Sec. 5).

In the propagation or longitudinal direction, typical SDS are localized by the boundary conditions, e.g. the cavity mirrors (Fig. 1b, c). Along the longitudinal direction a SDS can show "trivial" changes – e.g. due to linear optical propagation Schäpers et al. (2000, 2003) – but at any particular plane it stays constant in time (after the transients have died out).

Fig. 4b illustrates another very important property of SDS. Over a considerable parameter range (here the HB intensity) they coexist with a background state (in the simplest case a homogeneous state) which is linearly stable against weak perturbations. This implies that SDS can be present or absent under the same conditions. This makes them natural "bits" for parallel processing of optical information. As beautifully demonstrated in Fig. 4a, they can be excited

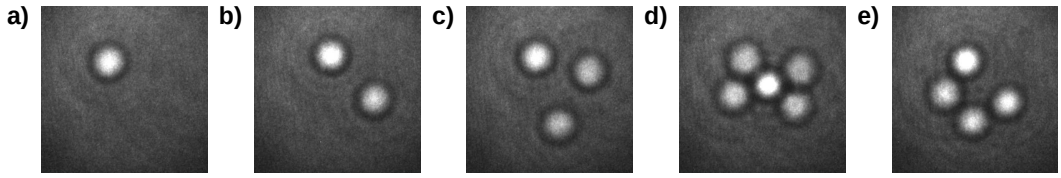

Fig. 3. Stable clusters of localized structures at different pumping levels in a single-mirror feedback system based on sodium vapor in a nitrogen buffer gas atmosphere as the nonlinear medium. Power: a) 131 mW, b) 133 mW, c) 133 mW, d) 135 mW and e) 138 mW. The images (transverse size 2.6 mm) are partially overexposed in order to emphasize the diffraction fringes surrounding each localized structure [Reprinted figure with permission from Schäpers et al. (2000). Copyright 2000 of the American Physical Society.]

by a writing beam (WB), a focused optical pulse derived from the same laser as the HB (see also the left panel of Fig. 2). For pulse amplitudes above a certain threshold, the SDS switches on. Below the threshold value, the system returns to the stationary state, i.e. "hard" excitation is required. The threshold marks a separatrix, which turns out to be an unstable SDS branch connecting the stable background state and the stable SDS branch (Fig. 4b). We will discuss this further in Sec. 1.4 and in Sec. 2. Whereas switch-on is initiated by a local increase of intensity due to constructive interference between the HB and the WB, the SDS can be erased again by injecting the WB with opposite phase Brambilla et al. (1996). This provides the basis for an optically controllable memory.

Finally, Fig. 4b indicates that the SDS branch is unique, i.e. the SDS has a defined amplitude and width for a given set of parameters. This is due to the fact that SDS are attractors of the dissipative dynamics, a feature that separates them from solitons in conservative systems, which exist as one-parameter families.

Note that in Fig. 2 SDS seem to exist only in parts of the device, and there are additional low amplitude states. This is related to device inhomogeneities and imperfections, an issue we will encounter repeatedly in our discussion. In order to demonstrate the solitonic nature of experimentally observed "spots", it is an established procedure Barland et al. (2002) to demonstrate that several (at least two) can be switched on and off independently, demonstrating their independence from each other and from boundaries or other structures in the device. We will discuss a specific example below (see Fig. 18 in Sec. 3). Note that this is an operational definition of an optical SDS, suitable for most experiments. However, switching and independence might be demonstrated by other means than optical injection.

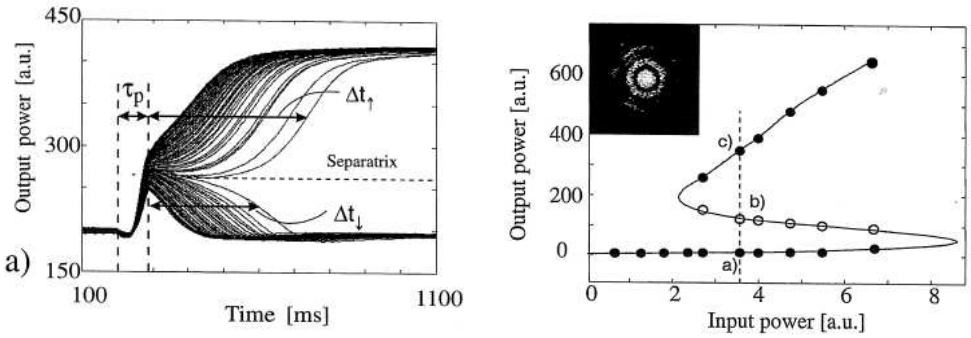

Fig. 4. SDS in a liquid-crystal light-valve (LCLV), a hybrid electro-optical system allowing the implementation of a single-mirror feedback situation (Fig. 1d) within a large transverse area Neubecker et al. (1995). a) Switching dynamics for different amplitudes of the WB (varying between sub-threshold and super-threshold excitation) and a constant pulse length of $\tau_p = 100$ ms. b) Steady-state characteristics of the LCLV: a) background state (no SDS), b) SDS branch (see inset for contrast-enhanced spatial structure), c) unstable branch reconstructed from measuring the separatrix as indicated in panel a). [Reprinted figure with permission from Schreiber et al. (1997). Copyright 1997 of Elsevier.]

1.3 Basic equations

Conservative solitons in Kerr media are described by the well-known Nonlinear Schrödinger Equation (NLS). The NLS assumes an *infinite* nonlinear medium (Fig. 1a). Real nonlinear optical media have finite dimensions and (except in glass fiber) solitons can rarely propagate more than a few centimeters before running out of material. To increase the propagation length it is therefore convenient to place mirrors at the ends of the medium, thus confining the soliton into a finite slab of material (Fig. 1b). With perfect reflection and zero absorption, one could indeed confine a soliton in such a "box" Firth and Harkness (1998). Real mirrors and materials are lossy, but we can make good the loss by "feeding" the caged soliton with an input field. We are thus led to consider a perturbed NLS:

$$i\frac{\partial E}{\partial t} + \frac{\partial^2 E}{\partial x^2} + |E|^2 E = i\varepsilon(-E - i\theta E + E_I) \tag{1}$$

The terms on the left are standard NLS terms, describing respectively evolution, diffraction and (Kerr) nonlinearity. Note that use of adimensional units for both space and time is implied. The three terms on the right side are perturbations of the NLS, all small if ε is. The first is just a linear loss (assuming $\varepsilon > 0$), and the last is the driving field E_I needed to sustain E against that loss. The middle term, in θ, is less easy to understand, but we must remember that coherent light confined between mirrors lies within an optical cavity, and so the response to the driving field will strongly depend on whether or not it

is in resonance with the cavity. Hence, therefore, the presence of θ, the *cavity mistuning*. If we ignore the left side of (1), then $E = E_I/(1 + i\theta)$, showing that the cavity has a resonance Lorentzian in θ. This is appropriate for a high finesse cavity, where just a single longitudinal mode may be considered. There is one further change from the usual spatial-soliton NLS: propagation (in z) is replaced by evolution (in t). This is natural: the soliton is now in a box, and not going anywhere.

We now set $\varepsilon = 1$, which is equivalent to a re-scaling: in particular it implies that time is scaled to the decay time of the cavity. This yields the Lugiato-Lefever (LL) equation, which was originally introduced Lugiato and Lefever (1987) as a model for pattern formation. The NLS limit is recovered as $\theta \to \infty$. The LL equation is a mean-field model. The term 'mean-field" arises because such models are usually derived by assuming a high finesse, so that the cavity field is approximately constant along the cavity axis. The high finesse allows the Airy function response of the cavity to be approximated by a single longitudinal mode, giving the Lorentzian resonance mentioned above. In practice, mean-field approaches apply much more widely, and usually provide a suitable description of the system evolution at any suitably-chosen reference plane. In most cases, a plane within or at the boundary of the nonlinear medium is a suitable reference plane (Figs. 1c, d).

Although some experiments can be described by the LL-equation, at least to some extent, most experiments with cw driving utilize a resonant or near resonant nonlinearity. Then higher order nonlinearities than the third are important, and the situation is better described by a saturation term than by a series expansion. In addition, absorption and gain might play a role. Early analysis of SDS formation in a two-level model with a mixed absorptive and dispersive nonlinearity is given in Tlidi et al. (1994), and for the purely absorptive case in Rosanov and Khodova (1990); Firth and Scroggie (1996); Brambilla et al. (1996). In addition, the medium response might be slower than the dynamical variation of the intra-cavity field, calling for an explicit equation of motion describing the dynamics of the medium. We are going to deal mainly with semiconductor models, where the dynamical variables are the intra-cavity optical field E in the VCSEL and the carrier density N. However, the level of description is such that N can be also thought of as the inversion in a two-level model (after suitable rescalings). Obviously, this model does not capture all peculiarities of the semiconductor nonlinearities (e.g. Chow et al. (1994)) but has proved to be suitable to describe the experiments in Barland et al. (2002); Hachair et al. (2004) (see Fig. 2) as well as other cases we will encounter in this review. The complete system is described by the following system of coupled partial differential equations Spinelli et al. (1998); Barland et al. (2002); Michaelis et al. (1997):

$$\partial_t E = -(1+i\theta)E + i\nabla^2 E - i\sigma(\alpha+i)(N-1)E + \frac{2\sqrt{T_1}}{(T_1+T_2)}F$$
$$\partial_t N = -\gamma\left[N - J + |E|^2(N-1) + D\nabla^2 N\right] \quad (2)$$

Here, σ is a coupling constant (a differential gain factor), α is the linewidth enhancement factor describing phase-amplitude coupling in a semiconductor. It corresponds to a detuning in a two-level situation. Typical measured values for α are in the range 1.5-8 Henry (1982) ($\alpha = 5$ is assumed in many simulations, here and elsewhere Hachair et al. (2004)). $\alpha = 0$ corresponds to a purely absorptive nonlinearity, $\alpha >> 1$ to the dispersive limit. T_1 and T_2 are the transmittivities of the VCSEL mirrors. The parameter J represents the injection current, normalized to the value at transparency. Time is scaled to the VCSEL cavity lifetime, and γ is the ratio of cavity lifetime to carrier response time in the VCSEL ($\gamma \approx 0.01$). The term $D\nabla^2 N$ describes carrier diffusion but will generally be omitted in what follows.

In the context of the amplifier experiment (Fig. 2) F denotes the external injection due to the HB. It can be $F = F(x, y, t)$ in order to describe spatial modulations of the HB (see mainly Sec. 6) and the action of the WB. In many formulations of the model, e.g. in (1), the internal value E_I of the driving field is used directly instead of the extra-cavity field amplitude F. In the context of the laser with feedback discussed in Sec. 3.3.3, F will represent the feedback field, $F = F(E(x, y, t))$.

Obviously, single-mirror feedback systems and LCLV are not described by these equations though the medium equation can be quite similar. We refer to the specialized literature here D'Alessandro and Firth (1991); Neubecker et al. (1995); Ackemann and Lange (2001); Ackemann et al. (2001).

1.4 Bistability and Multi-stability of SDS

A cavity soliton or SDS is a stable, self-localized optical excitation sitting on a uniform, or quasi-uniform, background, and substantially independent of transverse boundary conditions. A key property is that it can be present or absent under the same external conditions, i.e. it exhibits bistability between "off" and "on" states. In this introductory discussion we sketch some basic features which follow from these properties, both for a single isolated SDS and, importantly for practical applications, for multiple SDS. In Sec. 2 we will develop these properties in more detail, and for specific systems. We will discuss scenarios generic for dissipative solitons, such as *homoclinic snaking*, but also the limitations and modifications to such scenarios in the context of SDS in real systems.

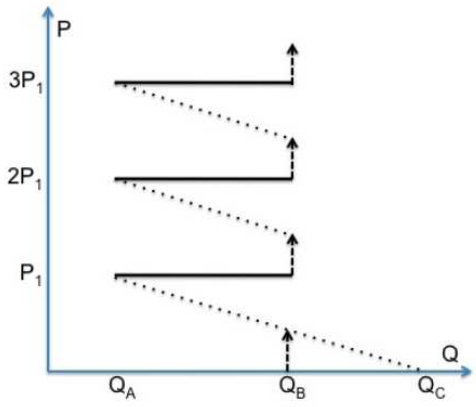

Fig. 5. Schematic existence diagram for excitation of independent SDS, each of "power" P_1 in an optical cavity, as a function of the parameter Q (see text). Solid lines are stable structures, dotted lines indicate the separatrix for switch on and off of each SDS, dashed arrow the minimum power perturbation needed to create a SDS within the stable range.

To begin, we consider the existence, stability and excitation of a single SDS. By assumption, for any suitable externally-controlled parameter Q there is a range of values over which both the one-SDS and no-SDS states are stable. For definiteness, assume that small values of Q correspond to weak nonlinearity. Since a SDS is an intrinsically nonlinear object, there will be a minimum value, say Q_A, below which no SDS exists. We also expect that there will be a maximum value Q_B, above which either no SDS exists or any SDS which does exist is unstable. Since all SDS are identical, and distinguishable from the background, we must be able to define a "power" measure P, such that a single SDS has power P_1, and n have power nP_1. We have set the background "power" to zero, which can always be done by subtraction. We will assume P_1 positive, though the physical power of a dark soliton would actually be negative. We thus arrive at a schematic P *vs* Q diagram (Fig. 5) consisting of a set of parallel lines, spaced by intervals P_1 and extending from Q_A to Q_B, the first rung corresponding to a single SDS, the second to two, and so on. In a real system, of course, the rungs would be neither exactly horizontal nor exactly straight (Fig. 4b), but that does not matter in the present context of a qualitative discussion.

We now consider the dynamics of excitation and erasure of SDS, beginning with the latter. Since the SDS ceases to exist at Q_A, it is reasonable to suppose that a small negative perturbation to its power will cause its decay when Q is only just above Q_A. At any value of Q in this neighborhood, one can envisage finding the minimum perturbation necessary to kill the SDS, and tracing the power of this minimally-perturbed SDS as a function of Q. Since the required perturbation is infinitesimal at Q_A, but increases with Q as the SDS becomes more stable, this "switch-down" power curve will have the general form of the dotted line falling away from the lowest rung of the "ladder" in Fig. 5. In fact, exactly such a curve was traced experimentally in an LCLV system, as

discussed earlier and shown in Fig. 4b. As mentioned, the dotted line in Fig. 5 tracks a *separatrix* between the basins of attraction of the no-SDS and one-SDS states, and the state lying exactly on the separatrix is another, unstable, SDS. It can be observed experimentally, as we have seen, but is also easily found numerically in model systems Firth and Harkness (1998); McSloy et al. (2002). In both cases the unstable SDS is actually metastable, in the sense that the decay times of structures close to it increase dramatically the closer they approach the exact unstable SDS – see Fig. 4a and (Schreiber et al. (1997); McSloy et al. (2002)). It is also found that, just as a structure with slightly lower power than the unstable SDS will decay into the background, conversely one with just slightly greater power will grow to form a stable SDS. The separatrix thus plays a key role in creating, as well as erasing, SDS.

Next, consider the behavior of the separatrix as Q is increased. At some point it will generally cross the line $P = 0$, at Q_C, say. At Q_C, therefore, any infinitesimal perturbation of the background state will grow. It follows that Q_C cannot be less than Q_B, since by assumption the single SDS, including its background, is stable up to Q_B. Normally Q_C is finitely greater than Q_B or, equivalently, at Q_B the separatrix lies at a finite power P_S above zero. In such a case, in order to create a stable SDS one must perturb the system strongly enough to induce a suitably-shaped structure with power at least P_S. Hence stable SDS should *not* appear spontaneously on increasing a control parameter such as Q. In addition, if one or more well-separated SDS are present in the system, then $Q_A < Q < Q_B$, and so creation of an additional independent SDS again requires a finite minimal perturbation equivalent to P_S. Nor, therefore, should SDS multiply, simply on increase of a control parameter. On this scenario, therefore, the bifurcation diagram for multiple independent SDS should be a kind of "disjointed snake", as sketched in Fig. 5, with the gaps indicating the need for "hard excitation" to jump upwards from rung to rung.

The form of Fig. 5 naturally prompts one to ask what happens outside the range $Q_A \leq Q \leq Q_B$. Below Q_A there are no SDS, and so the background seems to be the only candidate state, and it is stable. Above Q_B the same applies, but we already mentioned that the background is necessarily unstable above Q_C. We can't conclude anything about that region from the present outline model, but note there are many possible states which lie outside its scope, such as regular patterns.

How does this sketch compare with experiment, and with more quantitative theoretical models? We will address this question in some detail in Sec. 2, but it is worthwhile to have an initial discussion at this point. Considering models first of all, our picture is essentially confirmed, except that model studies do not usually consider excitation of well-separated SDS, but rather what might be regarded as close-packed clusters of SDS (Coullet et al. (2000); Burke and Knobloch (2006)). On the experimental side, our sketch scenario again

corresponds to some observed features, see, e.g., the single-SDS hysteresis loops in Fig. 4b, and also (for stable branches only) Fig. 17 in Section 3 and Tanguy et al. (2008a); Barbay et al. (2008). Perhaps the main issue is that SDS in experiment often appear spontaneously, on increasing a control parameter, multiplying on further increase. Again, detailed discussion is deferred to Sec. 2, but it is worth listing some possible reasons for this discrepancy. First, and most obviously, experimental systems have finite size and limited uniformity. Gradients and fluctuations in Q can be reduced as far as possible, but can never be wholly eliminated. If the range of variation exceeds $Q_C - Q_B$, one might envisage spontaneous appearance of SDS occurring. It is not enough, however, that Q_C locally drops below the average Q_B: Q_B will presumably also be affected by the gradient or fluctuation. Spontaneous appearance of stable SDS can only be enabled if Q_B is reduced significantly less than Q_C or, better still, Q_B actually increases as Q_C decreases. This cannot be ruled out, but such behavior would clearly be strongly dependent on both the system and the control parameter used. Thus parameter gradients and fluctuations are not *per se* an explanation for spontaneous generation of SDS, and have to be investigated on a case-by-case basis. Other possibilities ought to be considered also. For example, if there is a long-range inhibitory interaction between SDS, it will be harder (in a finite domain) to induce each additional SDS: sequential spontaneous appearance of SDS on parameter variation might then be possible (Firth et al. (2007a,b)).

Whatever the cause, we note that in any application in which each SDS acts as a "bit" of information, or the "on" state of a binary image pixel, any spontaneous generation of a SDS constitutes an error. The mechanisms for spontaneous generation (or decay) must thus be understood and controlled in any application. In fact, a functional system should behave just like in Fig. 5, with stable existence of (0,1,2,3,...) SDS over a single (broad) range of control parameter, coupled with the need for a finite, fairly large, perturbation to create a new SDS/bit. An operating point midway between Q_A and Q_B would ensure that existing SDS are also robust against perturbations, while the system can be "wiped" (all SDS destroyed) by sweeping Q below Q_A and back again.

2 Existence, Bifurcation Structure and Dynamics of Single and Multiple SDS.

The existence and basic properties of SDS in driven optical cavities is discussed in this Section. As a starting point, the link between SDS and patterns, in particular so-called homoclinic snaking, is outlined. In the theory, SDS should exist only below the threshold of a subcritical modulational instability, but in experiment they often appear spontaneously on parameter variation. Among

the possible reasons are experimental imperfections and limitations, and so we briefly discuss how finite system size, stray spatial gradients, and fluctuations of parameters might affect snaking. To do so requires a discussion of the response of SDS to the "forces" exerted by such parameter variations, and we show how the neutral or "Goldstone" mode related to translational invariance dominates the dynamics of the solitons. As mentioned in 1.4, spatial imperfections do not necessarily account for spontaneous generation of SDS, and we discuss alternative explanations, such as an additional nonlocal nonlinearity, for the observed "tilted snakes".

The bifurcation structure and dynamics of SDS in lasers is, in several respects, qualitatively different from that in driven systems, and is reviewed in Sec. 3.

2.1 Patterns, Dissipative Solitons and Homoclinic Snaking

As mentioned in Sec. 1, pattern formation is a widespread consequence of nonlinearity in spatially-extended systems. When a parameter is varied in model simulations, typically a pattern appears spontaneously at the modulational instability (MI) threshold. The pattern may grow smoothly from small amplitude, but sometimes there is an abrupt switch into a large-amplitude pattern. This persists as the parameter is reduced back below the switching threshold, until an abrupt collapse to the unpatterned state at a saddle-node (SN) bifurcation. In such *subcritical* cases (Cross and Hohenberg, 1993), both patterned and unpatterned states are stable over a finite parameter range, between SN and MI. In this review we are concerned with nonlinear optical systems, and we will base our discussion on the typical VCSEL model (2) introduced earlier. In the first instance we are primarily interested in systems driven by a monochromatic input field, ideally homogeneous in the transverse direction, and in steady-state or slowly-varying system responses. We therefore simplify our system by (crudely) eliminating the population dynamics so as to obtain a single field equation:

$$\frac{\partial E}{\partial t} = -(1+i\theta)E + i\nabla^2 E + \frac{\mu(1-i\alpha)}{1+|E|^2}E + E_I, \tag{3}$$

where $\mu = \sigma(J-1)$ and E_I is the effective driving field.

This equation has one or more homogeneous steady-state solutions E_0. For many purposes the intensity parameter $I = |E_0|^2$ is a more convenient drive parameter than the input field E_I itself, and we will often use it as such below. For a localized state, I is just the intensity of its homogeneous background field. For some purposes it is convenient to define a zero-background field A by $E(\mathbf{r},t) = E_0(1+A(\mathbf{r},t))$. Then, for example, MI occurs when the linearized

equation for A has net gain at some transverse wave vector. The so-called critical wavevector k_c is that which becomes unstable at the MI threshold, i.e. the smallest value of I for which MI occurs. Pattern formation will thus, at least initially, occur at k_c, but as I is increased beyond threshold all wavevectors in a band around k_c become unstable. Note that for $I >> 1$ the nonlinear term in (3) becomes small as the nonlinearity saturates, and so there must be an upper MI threshold at which E_0 stabilizes. The associated critical wave vector need not equal k_c.

Pattern formation in this model has been studied in detail in two important limits. Expanding the saturation denominator and truncating at the first nontrivial term, and also neglecting the nonlinearity of gain/loss, essentially yields Eq. (1). We will examine this "Kerr cavity" limit later, but first we consider a different limit, in which the dispersive nonlinearity is dropped, i.e. we set $\alpha = 0$ in (3). The equation then models a saturable amplifier or absorber in a cavity, depending on whether the gain μ is respectively positive or negative.

The absorber case ($-\mu = 2C > 0$) has been extensively investigated in relation to patterns and cavity solitons Firth and Scroggie (1994, 1996); Brambilla et al. (1996); Harkness et al. (2002)). State diagrams for stripe and hexagon output patterns are shown in Fig. 6 as a function of the intensity parameter I and relative wavevector k/k_c. An attractive feature of this model for numerics is that the critical wavevector is simply given by $k_c^2 + \theta = 0$, which means that the system compensates for the detuning of the cavity by tilting the intracavity wave. Of course this is possible only on one side of the cavity resonance: for positive θ there is no MI, only plane-wave optical bistability Lugiato (1984). Further, because there is no nonlinear index change, the cavity resonance frequency is independent of intensity. This simplifies numerical work, since there is no need to change computational parameters like space-step and box-size to adapt to changes in the critical wavevector. The dynamics also tends to be rather simple, with no Hopf bifurcations, which means that homoclinic snaking is not masked by other dynamical instabilities. This is illustrated in Fig. 6, where the patterns are stable over a large range of both intensity and wavevector (the white regions, termed "Busse Balloons"). Instability arises only for wavevectors too different from k_c, or where a pattern of different symmetry becomes more stable, e.g. on the curve labeled I_{rh} in Fig. 6a, where rolls (stripes) transform into hexagons. (In 2D, all wavevectors on a ring of radius k_c become unstable at threshold, leading to competition between patterns of different symmetry.)

System (3), with the parameters of Fig. 6, i.e. $C = 5.4$, $\theta = -1.2$, shows MI to patterns with wavevector k_c with threshold I_{MI}, the smaller root of $(I+1)^2 = 2C(I-1)$. For these parameters I is a single-valued function of E_I. Our present interest is not patterns themselves, but localized states such as SDS, including states which resemble finite domains of regular patterns sitting

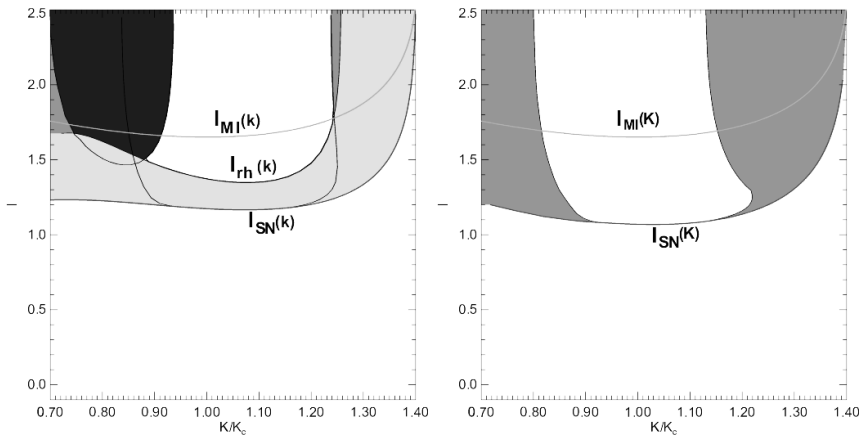

Fig. 6. Existence diagrams for (left) stripes and (right) hexagons for a saturable absorber in an optical cavity, as a function of the intensity parameter I and relative wavevector k/k_c, where k_c is the critical wavevector. $C = 5.4$, $\theta = -1.2$. In each case the MI threshold line is labelled. Between its minimum and the saddle-node (SN) lines (lowest curves) the pattern is subcritical. Shading indicates various instabilities: hexagons are stable over a broad band of wavevectors; stripes are less stable, and hexagon-unstable below the I_{rh} curve. [Reprinted figure with permission from Harkness et al. (2002). Copyright 2002 of the American Physical Society.]

on a smooth background with intensity I. Such states can be stable only if that background is stable, whereas arbitrarily-large domains of pattern cannot be expected to be stable if the infinite pattern is not. Hence we are naturally led to consider the case of a subcritical pattern, where both patterned and unpatterned states can exist and be stable for the same parameters and the same input field. As Fig. 6 shows, this happens over a considerable range of input fields lying below the MI threshold. Here, as is typical, the lower end of the coexistence range is marked by a saddle-node bifurcation (SN), at which the patterned state collides with a third state, an unstable pattern, and ceases to exist.

The obvious next question relates to competition between the patterned and unpatterned states in the same spatial domain. At their common boundary there will be a *front*, a localized structure which asymptotes to the flat state in one direction, and to the patterned state in the other. Two such fronts "back-to-back" would resemble the sort of localized state we have in mind (in one transverse dimension), while in 2D a front which closes around on itself to form a loop would resemble an "island" of pattern. The smallest such island would be a single spot of a hexagonal pattern, and this, in essence, is a cavity soliton (SDS).

There is a potential problem, however, in that fronts between coexistent states tend to move. As discussed in detail in Sec. 5, the more stable state typically invades and destroys the less stable one, so that the front is stationary only at the "Maxwell point" where the two states are equally stable. In the next

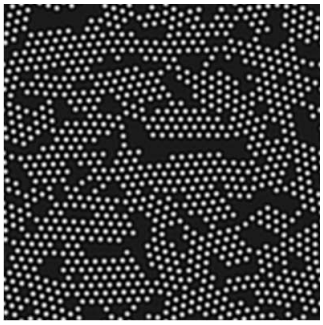

Fig. 7. "Cracked" hexagon pattern showing existence of large scale locked fronts between the patterned configuration and the flat background. [Reprinted figure with permission from Harkness et al. (2002). Copyright 2002 of the American Physical Society.]

subsection 2.1 we will see that the pattern-flat front behaves differently, and is typically stationary over a "Maxwell range". Further, localized states are closely associated with this parameter range, throughout which the patterned and unpatterned states can stably coexist. Fig. 7 illustrates such coexistence for the saturable absorber model Harkness et al. (2002). It was found that hexagons invade the flat state whenever I exceeds about 85% of its MI threshold value. For a range of smaller I a "cracked" hexagon pattern, i.e. islands of hexagons with flat-state between, was found to be stable, clearly illustrating stably locked fronts (Fig. 7). Note that there are one or two cases of single-spot islands, i.e. SDS.

The rest of this section is organized as follows. In subsection 2.2 we introduce the phenomenon of homoclinic snaking, which is the typical scenario for the occurrence of sequences of SDS in systems showing subcritical pattern formation. In subsection 2.3 we outline some of the general properties of SDS, including their dynamical response to perturbations of various kinds. Then in subsection 2.4 we present and describe specific cases of homoclinic snaking as found in several basic optical models related to (3), and discuss the applicability or otherwise of homoclinic snaking to real, finite and imperfect, photonic systems. In particular, we will discuss the fact that experimental "snakes" tend to be tilted, rather than vertical. In other words, localized states with different numbers of peaks tend to exist over staggered parameter ranges, rather than all existing within the same range as the theory of homoclinic snaking implies. In subsection 2.5 we show that augmenting the usual models with a nonlocal (in our example, global) coupling can induce a tilt in the homoclinic snakes. Such a nonlocal effect might perhaps explain the occurrence of SDS, rather than a pattern, as the first nonlinear structures to appear when the system is driven beyond MI threshold. We also discuss the effect of finite-range nonlocality, mediated by a symmetric kernel, which favors the appearance of well-separated simple solitons, rather than soliton complexes. We finally consider some physical mechanisms for the sort of nonlocal or quasi-global

nonlinearity which could account for the spontaneous appearance of SDS in experiments.

2.2 Homoclinic Snaking

Localized states in models where a pattern is in competition with a homogeneous state have been the subject of intense recent interest, for example in (Akhmediev and Ankiewicz (2005a); Champneys (1998); Nishiura and Ueyama (1999); Coullet et al. (2000); Firth et al. (2002); McSloy et al. (2002); Coullet et al. (2004); Clerc and Falcon (2005); Kozyreff and Chapman (2006); Burke and Knobloch (2006); Gomila and Oppo (2007); Burke and Knobloch (2007); Lloyd et al. (2008); Dawes (2008)). Key to this work is Pomeau's demonstration (Pomeau, 1986) that the interface between a pattern and a flat state can be stationary over a finite parameter range, the "locking range". To see why this should be so, consider the asymptotic approach of a stationary front to the flat state. Dropping the time derivative, and linearizing Eq. (3) around the homogeneous solution, we obtain a second-order differential equation in E, E^*, which yields a quartet of complex spatial eigenvalues $\pm\gamma \pm iK$. We must therefore expect that a front emerging from the flat solution in, say, the $+x$ direction will have components growing like both $e^{(\gamma+iK)x}$ and $e^{(\gamma-iK)x}$. Interference of these two components then implies that the front's field magnitude will oscillate around the flat-solution field with wavevector $2K$, with exponentially-growing amplitude, eventually matching (nonlinearly) on to the patterned state (Coullet et al. (2000); McSloy et al. (2002)).

Motion of such a modulated front is clearly going to be quite different from simple translation. It essentially involves nucleation of a new peak (for the case of invading pattern) or destruction of a peak (invading flat state). As a result, there is a *finite* parameter range around the Maxwell point, within which a modulated front remains at rest (Pomeau, 1986). For a system exhibiting a locked front between patterned and unpatterned states, Coullet et al. (Coullet et al., 2000) proved the appearance, around the locking range and hence between SN and MI, of a multiplicity of localized states, which resemble subsections of the pattern. Similar scenarios were previously identified for localized buckling Champneys (1998) and self-replicating patterns (Nishiura and Ueyama, 1999). The proof uses "spatial dynamics", dynamical systems theory applied to the spatial domain. It has two key ingredients. Firstly, there should be at least two spatial eigenvalues with positive real part, which we have seen is satisfied in driven–cavity optical systems. Secondly, patterns with a range of wavevectors should exist. This is normally satisfied throughout the pattern-existence range, except exactly at the MI and SN points. This is important because, as the control parameter is varied, the effective wavevector of the localized pattern has to vary to maintain the exact matching on to the

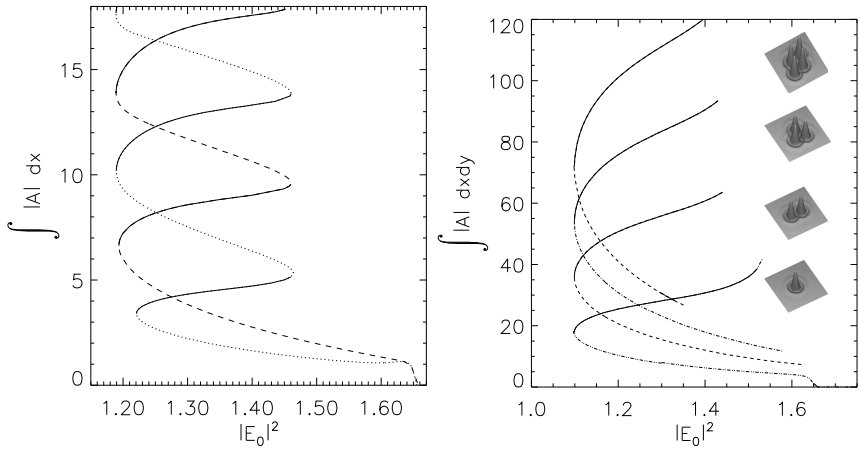

Fig. 8. Bifurcation diagram of 1D (left panel) and 2D (right panel) SDS. Displayed is the integral norm of localized structures against intra-cavity background intensity $I = |E_0|^2$. Inset on the right are examples of 2D SDS clusters corresponding to the positive stable branches. [Reprinted figure with permission from McSloy et al. (2002). Copyright 2002 of the American Physical Society.]

flat state. It follows that these "pieces of pattern" do not, in general, have period $2\pi/k_c$.

In one spatial dimension (1D), there are typically two sequences of SDS, with respectively even and odd numbers of peaks. The left panel of Fig. 8 demonstrates this phenomenon for the saturable absorber model of Fig. 6. Within each sequence the energy (or other norm) characteristically "snakes" upwards, zig-zagging to and fro across the locking range, adding a pair of peaks on each positive-slope "zig", while the connecting negative-slope "zags" are always unstable. Because all of these SDS are homoclinic to the flat state, the phenomenon illustrated in Fig. 8 is often termed *homoclinic snaking*. (See Burke and Knobloch (2006) for a comprehensive account of homoclinic snaking in a Swift-Hohenberg model.)

Note the general similarity to the "proto-snake" diagram, Fig. 5, conjectured in Sec. 1.4. The main difference (two snakes, not one) arises because our earlier discussion related to widely-separated, non-interacting solitons, whereas the theory of homoclinic snaking is for close-packed, and thus interacting, soliton complexes. Suppose we have two well-separated solitons. While we could attempt to switch off just one, as we discussed, we could also apply a perturbation to each, and switch off both. The latter is nicely symmetrical, and furthermore is well-defined as the two solitons are brought closer together and so into interaction. Symmetric addition of a pair of solitons is similarly insensitive to separation. Thus a proto-snake based on switching *pairs* of well-separated solitons goes over, as separations are decreased, into the "even" homoclinic snake instanced in Fig. 8. The "odd" snake is similar, except that one obviously can't remove two solitons when there is only one left.

Is there an equivalent in close-packed structures of adding or removing just one peak? Indeed there is: Burke and Knobloch (2007) recently showed that the two snakes are connected by a "ladder" of symmetry-broken states. The associated bifurcations all lie on the negative-slope parts of the snakes, however, which are unstable. As a consequence these symmetry-breaking switches are not commonly observed in the usual models. As we will see, however, addition of a global or long-range nonlocal interaction can shift the symmetry–breaking bifurcations onto the positive-slope branches, so that direct one-peak to two-peak switching becomes observable (Firth et al., 2007b).

As the number of peaks increases up the snake, the SDS resembles the coexistent patterned states ever more closely, and its approaches to the flat state on each wing asymptote to the pair of stationary fronts which characterize the locking range between the flat state and one of the patterned states (Coullet et al. (2000); Burke and Knobloch (2006)). In this regime, the snaking can be quantified by asymptotic theory (Clerc and Falcon (2005); Kozyreff and Chapman (2006)). Our main interest here, however, is in the few-peak SDS clusters forming the lower portions of the snakes. In the model systems to which the above theory (Coullet et al., 2000) applies, their existence range is smaller than, and lies wholly within, the range (SN,MI) over which both patterned and unpatterned states are stable: see Figs. 6, 8, for example. To observe such SDS it should therefore be necessary to place the control parameter within the snaking range, and apply a local excitation in the form of an address pulse. Under appropriate conditions, the system will evolve during and after the address pulse in such a way as to end on the desired "zig" of the snake. (To generate the SDS and multi-SDS shown in Fig. 8 the system was initialized with a structure similar to that being targeted, and a Newton method used to converge to the nearest stationary state, which somewhat resembles the address-pulse procedure (McSloy et al., 2002).)

If the localized states which form the snakes are domains of pattern embedded in the flat state, it is should be no surprise that there is a dual scenario for defect states, i.e. that there are localized islands of the flat state embedded in an infinite extended pattern (Coullet et al. (2004); Burke and Knobloch (2007)). The dual of the isolated SDS is a single missing cell of the pattern, and there are a pair of snakes corresponding to even- and odd-numbered clusters of defects. Coullet et al. (2004) conjecture that if there is a parameter range within which both the SDS and the single defect exist and are stable, then all possible defect structures exist and are stable. By this is meant that such a periodic pattern can be regarded as a close-packed array of SDS, and, further, that any or all of these SDS can be removed without destabilizing the remaining structure. If so, then the lattice has a full binary memory function, with each of its sites able to be independently set to "1" (one SDS), or "0" (no SDS).

It is necessary to remark that the theory of homoclinic snaking is strictly applicable only in one spatial dimension (1D), because it is built on the powerful methods of reversible dynamical systems theory, using the "spatial dynamics" analogy between time and 1D space. Nevertheless, localized states sitting on a flat background can only be stable if that background is stable, regardless of spatial dimensionality. Equally, a locking range between a flat solution and a co-existent pattern (e.g. hexagons) can also be expected in 2D if the pattern is subcritical, as already illustrated in Fig. 7.

It is therefore no surprise that 2D SDS are found in such model systems, in association with a locking range, and existing only well below MI. The right panel of Fig. 8, again for the saturable absorber model, shows the low-order bifurcation structure of 2D localized states. These include structures with a single peak (SDS), and also linear, triangular, and rhombic clusters which look like bound states of SDS units. There is increasing interest in the theory of 2D snaking, in particular Lloyd *et al* have studied snaking of localized hexagonal patterns in a Swift-Hohenberg model (Lloyd et al., 2008). This exhibits whole families of snakes, in contrast to the comparatively simple two-snake structure in 1D. Even so, localized hexagons are still a special and rather simple case compared to the random 2D assemblies of 1s and 0s which are possible in the functional-memory regime. While snaking bifurcation diagrams could in principle be constructed in such a case, it seems improbable that any worthwhile insight could be gained from doing so.

2.3 Basic Properties and Dynamics of SDS

At this point it is appropriate to look in a little more detail at the structure and basic properties of these cavity solitons, whose behavior is in fact typical of a wide class of dissipative solitons. As for the case of a front, their spatial decay to the flat solution has to be a superposition of two complex exponentials with the same real part, and so exhibits spatial modulation. In 1D the envelope of this modulation is roughly, though usually not exactly, a sech function. In 2D the SDS is asymptotically a generalized Bessel function, and the modulation takes on the appearance of a set of rings around the central peak: see, for example, Fig. 3 and the insets of Figs. 4b and 8b.

Turning now to dynamics, by definition a stable SDS has no linear perturbation eigenmode whose eigenvalue has positive real part. However, an ideally homogeneous broad-area device possesses translational symmetry. Hence a SDS can be placed anywhere, and no energy is needed to move it around. Mathematically, this is manifested by the fact that the SDS always has linear mode, $\vec{u}_0$, with zero eigenvalue. This eigenvector is proportional to the *gradient* of the SDS profile. Such symmetry-related neutral modes are also

referred to as "Goldstone" modes. Note that translational (and rotational) Goldstone modes, and many aspects of the effects of drift and pinning discussed later in Sec. 6, are not confined to SDS but apply to any self-organized patterns which spontaneously break the translational symmetry (Haelterman and Vitrant (1992); Grynberg (1994); Seipenbusch et al. (1997); Dawes et al. (2005)).

As mentioned, in a laser there is also a phase symmetry, which gives rise to a Goldstone mode proportional to the SDS itself, which we will discuss further in Sec. 3. For a stable SDS in a driven cavity system, however, all other eigenvalues have negative real part, by definition. This means that, as $t \to \infty$, the amplitude a_0 of the neutral mode dominates over all other a_i. Thus the dynamical effect of any perturbation $\vec{p}$ to a stationary stable state is primarily determined by its projection on to the neutral mode. The field equation linearized around the SDS is not usually self-adjoint, so its modes are not mutually orthogonal, but are *biorthogonal* to the modes of the adjoint equation. Hence $\vec{v}_0$, the adjoint of the neutral mode, acts as the projection operator on to the neutral mode, because it is orthogonal to all other linear modes of the SDS. The projection operation is equivalent to the usual inner product, which yields the equation Maggipinto et al. (2000):

$$\frac{\mathrm{d}a_0}{\mathrm{d}t} = \frac{1}{< \vec{v}_0 \mid \vec{u}_0 >} < \vec{v}_0 \mid \vec{p} > . \tag{4}$$

The denominator makes this equation normalization-independent. Like $\vec{u}_0$, its adjoint is an odd function of space, and so only perturbations which are asymmetric at the SDS position couple to the neutral mode. In particular, at any extremum of the perturbation the coupling vanishes.

Because the neutral mode is just the gradient of the SDS, physically $\mathrm{d}a_0/\mathrm{d}t$ is the translational velocity of the SDS under the influence of the perturbation. Obviously the motion of such a SDS under the influence of an external force is not Newtonian, but overdamped (Aristotelian). It is also clear that the motion under this dynamics is simple and limited: the SDS moves up (or down) any finite gradient, at a speed proportional to that gradient. Thus it can asymptotically approach, but never pass, a point where the gradient vanishes. In particular, it cannot oscillate around such a point. In essence, it acts like a particle with no inertia.

Perturbations to the SDS can be classified into three main types: (i) intentional or unintentional parameter variations, (ii) spatial or spatio-temporal noise, and (iii) perturbation of one soliton by another. Important examples for case (i) are phase and amplitude gradients or modulations of the driving field, which can be used to control SDS motion and positioning (Rosanov, 1991; Firth and Scroggie, 1996; Rosanov, 1996; Spinelli et al., 1998; Maggipinto et al., 2000). Such situations are discussed in detail in Sec. 6. The device

inhomogeneities already mentioned, if they are large-scale perturbations, can be thought of as parameter gradients, and thus belong also to this class. Small-scale inhomogeneities are a kind of disorder, and so can be thought of as 'frozen spatial noise', and thus of type (ii). Typical dynamics in case (i) will consist of SDS drift on the gradient until the gradient falls to zero, and the drift stops. If there is spatial noise, the SDS may encounter a fluctuation large enough to cancel the parameter gradient, and be trapped. (In 2D, material defects can deflect SDS, not just trap them.) Spatio-temporal noise, for example input-field fluctuations, will couple to the neutral mode and lead to an erratic motion of the SDS, even in an otherwise ideal system Firth and Scroggie (1996); Spinelli et al. (1998). If the noise spectrum is white, the motion is diffusive.

For case (iii), we noted that the asymptotic field amplitude of a SDS is modulated, so that the "force" it exerts on a nearby SDS oscillates as a function of separation, with maxima and minima. It follows that there is a discrete set of separations at which two SDS can be stably at relative rest, i.e. 2-SDS bound states. These have been observed in the Na-vapor feedback system (Schäpers et al., 2000), see Fig. 3. Since the modulation depth decays exponentially with distance, the binding rapidly weakens, and will become unobservable once the inter-SDS force becomes smaller than the typical values of the forces of types (i) and (ii).

2.4 Snaking in other optical models

We now consider snaking in other variants of (3), comparing and contrasting with the saturable absorber model already examined (Scroggie et al. (1994); Firth and Scroggie (1996); Brambilla et al. (1996); Harkness et al. (2002); McSloy et al. (2002)). As a second variant, we consider the Kerr cavity problem of Eq. (1) already mentioned (Lugiato and Lefever, 1987).

For the saturable absorber, we examined homoclinic snaking only in one parameter (I), but snaking also occurs *vs* θ, or indeed combinations of these parameters. The full picture for the Kerr cavity is illustrated in Fig. 9, where we reproduce the projections on to the (I, θ) plane of the SN lines lines corresponding to low-order localized states (Gomila et al., 2007). Since these SN lines are the signature of snaking, this diagram is a reminder that homoclinic snakes are in fact one-dimensional sections of a multiply-folded surface in a parameter space which in general has several dimensions (here, for the Kerr cavity, two).

As a third example of snaking in an optical model we consider a broad-area VCSEL, driven by an external coherent field and containing a bulk layer of GaAs as the active medium Tissoni et al. (1999a). The dynamical equations

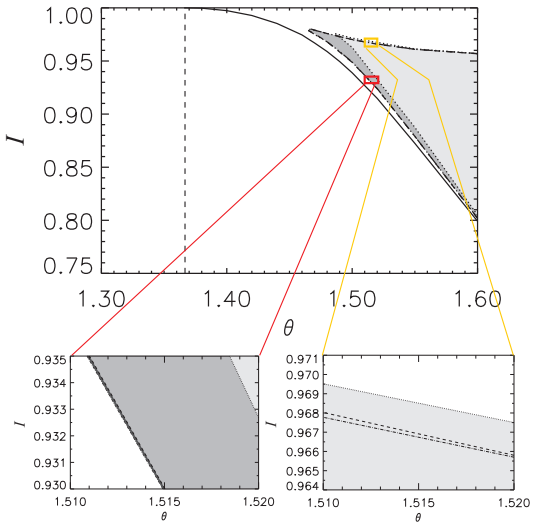

Fig. 9. Projection in the (I, θ) plane of the saddle-nodes for low-order localized states found in the Kerr-cavity. [Reprinted figure with permission from Gomila et al. (2007). Copyright 2007 of Elsevier Science.]

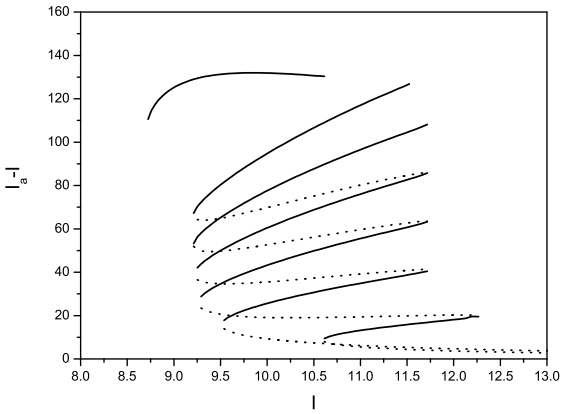

Fig. 10. Homoclinic snaking in a bulk semiconductor microresonator model Firth et al. (2007a). Against the intensity parameter I is plotted the excess spatially-averaged intensity for the various localized states. The uppermost curve represents a coexistent roll pattern, see Maggipinto et al. (2003). [Reprinted figure with permission from Firth et al. (2007a). Copyright 2007 of the American Institute of Physics.]

governing the electric field inside the cavity and the carrier density of the active material are very similar to Eq. (2).

This model has been extensively analyzed both in $1D$ and $2D$ Tissoni et al. (1999b); Maggipinto et al. (2000, 2003); it exhibits plane wave instability and MI for a wide range of parameter choices and injection frequencies. For the parameters of Fig. 10 the steady state curve of the homogeneous solution is bistable, and there is a branch of stable SDS asymptotic to the lower stable homogeneous solution, and associated with a band of subcritical pattern

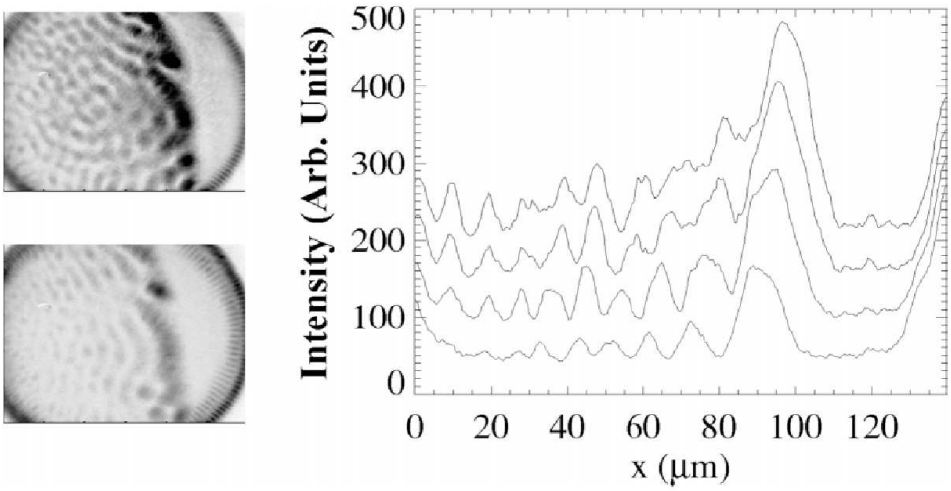

Fig. 11. Pattern front shifting as the injection intensity is increased, in a VCSEL amplifier. J=180 mA, P_{inj} from 1 mW (lowest in the graph) to 8 mW (highest). The different curves have been offset for clarity. [Reprinted figure with permission from Hachair et al. (2004). Copyright 2004 of the American Physical Society.]

solutions. This is the only full VCSEL model for which multi-peak localized states have been studied in detail. Fig. 10 shows typical homoclinic snaking, strongly suggesting that snaking and related theory is robustly applicable to semiconductor cavities, including VCSELs.

We will now examine the experimental situation with regard to patterns and snaking in broad-area VCSEL amplifiers. Since snaking theory depends heavily on the locking of the front between a stable flat solution and a coexistent stable pattern, we first consider experimental evidence on front behavior. Hachair et al. (2004) present a rather impressive sequence of stationary fronts (Fig. 11), corresponding to several different values of the ampltitude of the driving field. There is a well-defined front, which moves across the VCSEL aperture as the input field is increased. At first sight this is unexpected. In an ideally homogeneous VCSEL, we should expect MI on suitable variation of any parameter, such as input field. Once the MI threshold is reached, pattern should form, and should invade the whole of the VCSEL area, because the MI threshold lies well outside the locking range of the front between the pattern and unpatterned outputs. However, the VCSEL used in these experiments had an unintended detuning gradient, so that the detuning θ, and thus the MI threshold, had a roughly linear variation across the active area of the VCSEL. Hence, for fixed current and input field frequency, MI should be reached first at some point near the perimeter of the active area. Furthermore, as the front moves away from that point, the local detuning changes, because of the gradient, and the front's motion will slow down. At some point the detuning will correspond to the upper locking point between patterned and unpatterned outputs, and the front will stop there, giving a stable state in which part of the VCSEL is patterned, and part unpatterned, just as observed in Fig. 11. Changing the

input field changes the location at which the front comes to a halt, and thus explains the sequence of front locations in Fig. 11. Similar front behavior was observed when the wavelength, rather than intensity, of the input field was varied, and corresponding model simulations in the same work confirm this scenario (Hachair et al., 2004).

Turning now to SDS (in this case specifically cavity solitons), the theoretical expectation is that they should exist in association with the locking range, and hence in the unpatterned region adjacent to the front in Fig. 11. Again this is in rather good accord with experiment: the seminal experiment in Barland et al. (2002) involved writing and erasing CS in exactly this region (Fig. 2), with further confirmatory observations and simulations in Hachair et al. (2004).

We remark, however, that the nature of a broad-area VCSEL amplifier somewhat blurs the distinction between MI and the upper locking point. Even in the absence of material gradients, the VCSEL's active aperture is inhomogeneous due to the fact that one electrode is a ring, to allow efficient injection and emission of light. As a result, the current injection is transverse to the active region, leading to "current-crowding", and thus enhanced gain, on the perimeter. This is clearly visible in Fig. 11 as a ring of emission around the boundary. Because of current-crowding, the MI threshold is much lower on the periphery, and therefore pattern formation inside the VCSEL disc should occur by invasion from the perimeter, rather than local MI, even in the absence of a parameter gradient across the disc. Another experimental example of this "front invasion" can be seen in Richter and Barashenkov (2005), which shows patterns and SDS in a magnetic fluid.

Not all SDS systems have a "pattern reservoir" at the boundary. In an optically-pumped VCSEL or amplifier, for example, the gain is typically highest in the center, and drops off at the boundary. Then patterns should only appear when the MI threshold is reached, usually centrally. Conversely, any stationary pattern is always surrounded by non-pattern, and thus by a stationary front. Switch-off of the pattern should thus occur by invasion, not decay. In parameter space, this means at the lower locking-point, not the saddle-node.

Turning from fronts to solitons, we already mentioned that SDS can be written and erased in just the expected area of the current-pumped VCSEL amplifier, close to the front on the unpatterned side. Similarly, SDS have been created (and extinguished) by local perturbations in other optical systems, e.g. in Schäpers et al. (2002), and elsewhere, e.g. in a ferrofluid by Richter and Barashenkov (2005). The story does not end there, however, because solitons sometimes seem to appear spontaneously, i.e. without addressing, on parameter variation. Examples from optics, adapted from (Menesguen et al. (2006); Pedaci et al. (2006)), are illustrated in Figs. 12. This should be forbidden, according to snaking theory.

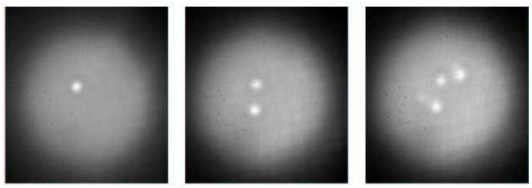

Fig. 12. Inverted contrast images showing sequential appearance of localized states (intensity spots on a flat background) in an optically-pumped VCSEL amplifier as the pumping rate is increased, leading eventually to a pattern-like state. *Courtesy of S. Barbay*, adapted from Menesguen et al. (2006); Firth et al. (2007a).

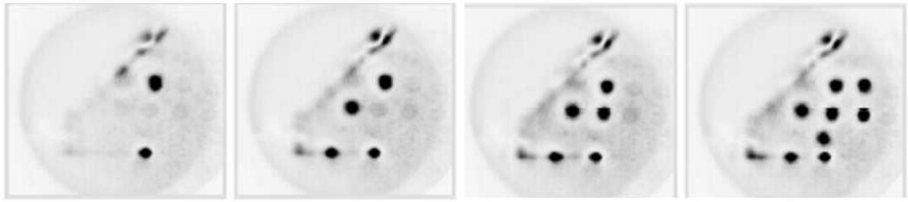

Fig. 13. Sequential appearance of localized states with increasing current in an electrically-pumped VCSEL amplifier. (The input beam phase is structured to trap SDS on an array, see Sec. 6.) [Reprinted figure with permission from Firth et al. (2007a). Copyright 2007 of the American Institute of Physics.] Adapted from Pedaci et al. (2006).

Following on from Menesguen et al. (2006), Barbay et al. (2008) undertook an experimental investigation of SDS appearance and hysteresis in an optically-pumped VCSEL amplifier. They used a broad, essentially homogeneous, input beam but the gain distribution was spatially limited by the size and shape of the short-wavelength pump beam. By ramping the pump beam power up and down over an appropriate range, they found spontaneous appearance in the reflected input beam of localized states with one, then more, main peaks as the gain was increased. Reducing the gain, peak numbers reduced, with hysteresis, until the reflection was once more at a low level across the whole pumped region. They thus sampled snaking bifurcation diagrams for SDS in this system, in both 2D (circular pump) and quasi-1D (stripe pump) cases. Both geometries showed evidence of a strongly-tilted snake.

A possible explanation for this tilted-snake discrepancy between theory and experiment is experimental imperfection. We already saw that, for VCSEL amplifiers, front dynamics is strongly affected by unintended gradients in material properties, and so we should consider possible effects of material gradients and spatial noise on SDS appearance, disappearance, and dynamics.

We note, first, that some sort of trap is probably necessary for SDS observation. According to the basic dynamics discussed above, even a very tiny gradient would sweep the SDS out of the system, probably so fast as to be unobservable by the slow imaging detectors typically used. So we must suppose

that the stationary SDS actually observed in VCSELs are probably trapped at some sort of local imperfection. Indeed it has been demonstrated (Tredicce (2004); Tanguy et al. (2008b)) that it is possible to move a cavity soliton away from its location by applying a perturbation in the form of a narrow laser beam. Turning the beam off results in the CS returning to its original location, at least if it has been moved only one or two diameters away. Of course, given traps which attract solitons, there should also be anti-traps which repel them. The use of cavity solitons themselves to identify and investigate the nature of such traps and imperfections is discussed further in Sec. 6.

Can SDS form spontaneously in traps? One could perhaps envisage that MI threshold is reached locally in the trap, while the surroundings remain below threshold. However, we already pointed out that locally exceeding the MI threshold should result in pattern invading the surrounding region, stopping only at the "locking point". Rather strong inhomogeneities would be needed for this expansion to halt when only a single spot has formed, as in Figs. 12 and 13. Recall also that the extended pattern may actually appear through invasion, rather than MI, placing strong requirements on trap depth, as well as size, for local MI.

Perhaps more likely is that inhomogeneities can affect front dynamics in such as way as to generate SDS. As a simple example, consider the decay of an extended pattern in a current-pumped VCSEL as the drive parameter is reduced. The strongest anti-trap present will presumably nucleate the process by reaching the SN point before other regions. This will give rise to a moving switching front, invading and destroying neighboring pattern. A deep enough trap may be able to retain a piece of pattern, i.e. a SDS – like a rock pool left by the receding tide. Such behavior has been observed at INLN on decreasing the VCSEL current (Barland, 2008). This scenario is made more plausible by the fact that the pattern, at the lower end of its existence range, behaves much more like an array of SDS than a coherent, correlated structure (see above discussion and (Taranenko et al., 2001)).

More generally, the front marks a region where a pattern is in quasi-equilibrium with the flat state. It seems plausible that it should be somehow easier to create a SDS by moving it across the front than by direct creation from the background. A local gradient transverse to the front could pull a spot from the pattern, which would then drift away, forming itself into a SDS, eventually falling into a trap and remaining as a stable isolated SDS.

The optically-pumped VCSEL amplifier case is somewhat different, with a fairly pronounced gain profile (Barbay et al., 2008), which tends to attract the SDS to the center of the pump. These authors also find some evidence of trapping on defects, however. A second key difference is that there can be no front invasion in this case, so that spontaneous appearance of structure should

only occur beyond the MI threshold.

In summarizing this subsection, we remark that certain features of the homoclinic snaking scenario, and related but more general features of subcritical pattern formation, are well observed in broad area VCSELs and other systems. Inevitably-present material imperfections and fluctuations, however, have important effects on the detailed behavior of real systems. Some of these are actually (or potentially) beneficial for the observation and understanding of SDS phenomena. Some, like the spontaneous appearance of SDS, are not fully understood, and are indeed harmful from an applications point of view.

2.5 "Tilted" Snaking due to Nonlocal Coupling

From the foregoing it is clear that SDS, and clusters thereof, should exist only below the MI threshold, and should appear only by localized addressing, whether in 1D or 2D. Certainly SDS exist as addressable, subcritical structures in at least some experiments. The spontaneous appearance of SDS-like objects on parameter variation (as in Fig. 12) is, however, inconsistent with the bifurcation structure found in 2D models like that of the right panel of Fig. 8.

We discuss above, and elsewhere in this review, possible explanations based on material imperfections. While plausible, these are somewhat *ad hoc*, and quite strongly system-dependent. In this subsection we analyze a less obvious, but perhaps a more fundamental explanation, namely that there is some intrinsic feature of the experiments not accounted for by the standard models. Suppose, for example, that the presence of one SDS inhibits the formation of a second in its neighborhood. There would be no effect on the overall MI threshold, because it assumes a SDS-free system. The development of a pattern in the neighborhood of a SDS would be inhibited, however, over some effective range. Then isolated SDS would form, coalescing to form a pattern only if and when the MI dynamics becomes strong enough to overcome the inhibition mechanism. Such effects, which could obviously account for at least some experimental data, are shown below to arise when a long-range (quasi-global) coupling is added to typical optical models.

As a theoretical basis for the above behavior, we add on the right of the model equation (3) a nonlocal coupling term G having the following form:

$$G(x,y,t) = i\gamma \left(\frac{1}{S} \int_S |E(x',y',t)|^2 K(x,y,x',y') dx' dy' \right) E(x,y,t) \tag{5}$$

$$= i\gamma I_a E(x,y,t) \tag{6}$$

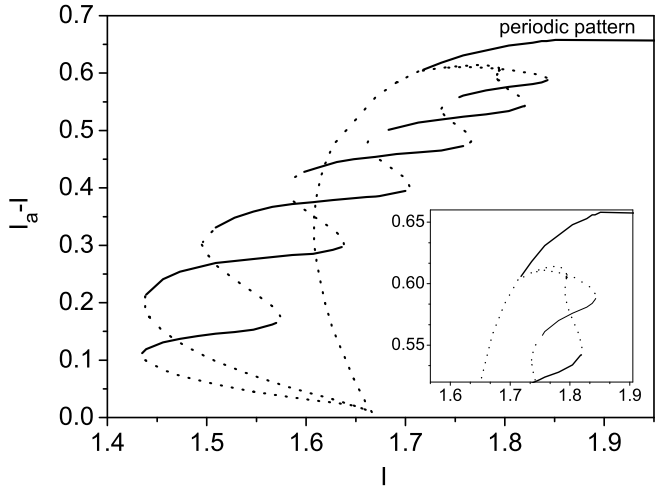

Fig. 14. "Tilted" snaking diagram showing solid and dotted lines denoting respectively stable and unstable multi-peak configurations for the 1D case of global coupling in the saturable absorber model. The inset is an enlargement of the diagram's upper part. The maximum number of peaks is linked to the dimension of the spatial box chosen for the numerical simulations. $\gamma = 0.25$, other parameters $C = 5.4$, $\theta = -1.0$. Compare Fig. 8. [Reprinted figure with permission from Firth et al. (2007a). Copyright 2007 of the American Institute of Physics.]

where S is the measure of the spatial integration domain and γ is a real constant coefficient. We suppose in the first instance that the kernel K is a real constant equal to 1, so the term G is purely imaginary and represents a global, nonlinear term whose action is to effectively change the cavity detuning θ. For the case of interest here, $\theta<0$, G further detunes the cavity if $\gamma>0$, hence raising the MI threshold for a given input field E_I.

Global coupling is, of course, physically unrealistic, but should provide a good guide to the effects of a nonlocal coupling with a nontrivial kernel of range larger than the size of the SDS considered. Should the range be larger than the effective system size, then the global-coupling approximation should be a very good one.

Adding such a global coupling, we study the existence, and stability with respect to spatially modulated perturbations, of stationary solutions to the previously–mentioned saturable absorber model using a Newton method (Firth and Harkness, 1998). In Fig. 14, we report the results obtained in 1D for $\gamma = 0.25$, $\theta = -1.0$, $C = 5.4$ together with the SDS existence branches, both stable and unstable. We plot the difference $I_a - I$ against I, assuming that the contribution to G arising from I is incorporated into θ. Analogously to Figs. 8 and 10, localized structures still form two intertwined snakes, bifurcating from the point of modulational instability ($I_{MI} = 1.66$ for parameters in Fig. 14)

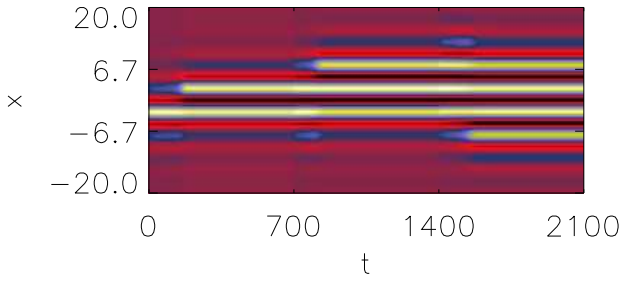

Fig. 15. (Color online) Time plots showing the sequential switching of localized structures when the input field (parametrized by I) from is ramped linearly with time from $I = 1.547$ to $I = 1.713$ (left to right). We start from a single-SDS initial condition. The gray-scale used goes from dark to light for increasing intensity values (in color from red via blue, yellow to white). Parameters: $\theta = -1.0$, $C = 5.4$ and $\gamma = 0.25$. [Reprinted figure with permission from Firth et al. (2007a). Copyright 2007 of the American Institute of Physics.]

and associated with even or odd numbers of intensity peaks. The global coupling has, however, tilted the snakes so as to overhang the MI threshold. This means that SDS (or clusters of SDS), rather than a system-filling pattern, should be the final state of the system just beyond the MI threshold.

We confirm this behavior by numerical integration of the full partial differential equation with a global coupling term. Adding noise to a stationary stable state on the homogeneous branch brings the system on to the single-SDS state, then increasing E_I induces a switching sequence which progressively adds one peak to the previous configuration (see Fig. 15). Following the tilted snake upwards we reach the roll pattern branch where it ends. As expected on the basis of the previous considerations, and contrary to what happens for $G = 0$, the roll pattern is stable only well beyond the MI point.

The stability of the states in Fig. 14 is, as usual, indicated by full lines for stable states, dotted for unstable ones. Note that part of some positive-slope branches are actually unstable. This is an interesting consequence of the introduction of global coupling. An additional effect of the distortion and tilting of the snakes is that some of the "ladder" states which link the even and odd snakes are shifted, so as to terminate on the positive slope branches. These bifurcations correspond to "odd" or (symmetry breaking) eigenmodes. This odd mode changes the peak number by one unit only, inducing a lateral spatial shift of the centroid of the structure, as is evident in the simulation in Fig. 15.

There are a number of physical mechanisms which could give rise to nonlocality in relevant optical experiments. These include transverse carrier diffusion (Wright et al., 1985), thermal effects, and energy balances. Thermal inhomogeneities arising from the presence of localized states can be expected to induce long-range effects, and are perhaps the strongest candidate to induce tilted snaking. In the optically-pumped VCSEL amplifier experiment (Bar-

bay et al., 2008) the authors point out that creation of SDS will create a temperature perturbation, over a range determined by the thermal transport properties of the VCSEL system. It is not yet clear whether the these effects would be such as to induce the observed tilting. The use by Barbay et al. (2008) of circular and stripe pumping provides an interesting test, because there were noticeable differences in the snaking and tilting in the two cases. Clearly thermal nonlocality would be sensitive to the pumping geometry, and it will be interesting to see whether it can explain the observations.

Some other candidates have a quasi-global character, such as boundary-induced constraints. Dawes (2008) have shown independently that systems with a conservation law (a global constraint) can show tilted snaking. In the SDS experiment in a magnetic fluid (Richter and Barashenkov, 2005) there is global constraint, relating to conservation of fluid volume.

In summary, subcritical homoclinic snaking is predicted by a powerful and attractive theory, but experimental evidence is limited and some observations are in contradiction with the theory. An additional nonlocal, or quasi-global, coupling could resolve some of these contradictions, and tilted snakes have been found in several implementations of such an approach (Firth et al. (2007b,a); Dawes (2008)). An alternative "local" explanation has been proposed, based on "ghosts" of higher-order patterns in an *ad hoc* model (Bortolozzo et al., 2008). It deals only with single, separated SDS, not clusters or snaking.

Since a significant part of this review deals with SDS in lasers, prompted by recent experimental advances, some comment on snaking in SDS laser systems is required. Perhaps the first thing to say is that the conditions for homoclinic snaking, in the formal sense (Coullet et al., 2000), do not apply. In Sec. 3 we show an example of a bifurcation diagram for a 1D SDS in a laser model which begins and ends at the "off" state, with no saddle-node bifurcations to multi-peaked structures (Paulau et al., 2008). That said, clusters of laser cavity solitons (LCS) have been found in recent experiments (Radwell et al. (2008); Genevet et al. (2008)) and have been studied in models of a laser with a saturable absorber (see, e.g., (Rosanov, 2005) and *op. cit.*). The latter clusters seem to be related to fronts between homogeneous solutions (see Sec. 5).

From an applications perspective, snaking is not really relevant – multi-stability and controllability of SDS are the key requirements. As mentioned in the Introduction, independent SDS in a homogeneous system naturally give rise to a multi-stable snake-like bifurcation diagram. Similarly, inhomogeneities and interactions will inevitably distort and tilt this generalized snake, reducing the degree of multi-stability. The focus, therefore, should be diagnosis and elimination or compensation of these effects, rather than semantics.

3 Cavity soliton lasers

3.1 Attractive features of a cavity soliton laser and bistable laser schemes

Up until now we concentrated on driven bistable systems, i.e. schemes where a nonlinear cavity or optical feedback system is driven by an external beam, the holding beam (HB), of high spatial and temporal coherence. For applications, it seems to be attractive to remove the necessity of the HB and to draw all the energy from an inexpensive incoherent source like an electric power supply or high-power laser diodes of low coherence. This implies going from a driven system to a laser, i.e. an active device where emission is self-sustained. Whereas in driven systems SDS are "slaved" because their phase, polarization and frequency is locked to the one of the HB, such a *cavity soliton laser (CSL)* – as any laser – has the freedom to choose its phase because it originates from a spontaneous symmetry breaking. Assuming that the cavity is sufficiently isotropic and broadband, polarization and frequency of its output is also undetermined including the possibility of multi-frequency operation which could result in irregularly or regularly self-pulsing SDS. In a CSL, actually every single SDS within the laser aperture should have the freedom to chose between all these possibilities. This gives exciting new opportunities for fundamental studies as well as applications. For example, the relative phase between CS is expected to affect their dynamics and interaction properties (Rosanov et al., 2005) and it will be interesting to compare the effects of phase-sensitive interactions of laser cavity solitons with the wealth of phenomena known for propagating spatial solitons (Stegeman and Segev, 1999). Another intriguing aspect of interactions between laser SDS is the possibility of frequency and phase locking known to be generic in laser physics for coupled lasers or different modes in the same laser (Jiang and McCall (1992); K. S. Thornburg et al. (1997)) and, more generally, coupled nonlinear oscillators (Pikovsky et al., 2001). Since all demonstrated laser SDS exist in a cavity, we will refer to them as *laser cavity solitons (LCS)* in the following.

Having argued that a CSL would be interesting one needs to caution that a simple free-running laser won't support SDS because the bifurcation at laser threshold is supercritical (i.e. continuous) and not subcritical. Hence there is no bistability, a prerequisite for SDS. However, there are several well-known options to enhance the complexity in a laser in order to allow for a subcritical start-up. In the laser with an injected signal (LIS), the laser with frequency-selective feedback (FSF) and the laser with a saturable absorber (LSA) SDS were demonstrated already experimentally. We will discuss each of these schemes in the following subsections.

A ring laser without non-reciprocal elements can show bistability between the

counter-propagating waves. Pérez-Arjona et al. (2007) and Columbo et al. (2008) predicted that this can form the basis of LCS and it is intriguing to imagine localized lasing in different directions, but an experimental implementation does not seem to be in sight. Equally interesting, but probably far from a realization, are LCS based on bistability in a two-photon laser (Vilaseca et al., 2001).

Polarization effects are an additional option to obtain bistability in a laser and indeed VCSELs are promising candidates because the ideal VCSEL cavity and the matrix elements for light-matter coupling are polarization degenerate. In small-area devices (and plane-wave models) bistability due to an interplay between spin-dynamics and phase-amplitude coupling (Miguel et al. (1995); Sondermann et al. (2003); Ackemann and Sondermann (2005); Mori et al. (2006)) is well known under conditions where the intrinsic symmetry is only weakly broken by uncontrolled fabrication anisotropies. One localized state in the center of a VCSEL with injection orthogonal to its principal polarization was reported recently (Hachair et al., 2009). A passive system showing polarization SDS will be discussed in Sec. 5.

We remark that there is some similarity regarding the phase symmetry between the laser case and the non-degenerate optical parametric oscillator (OPO) (Skryabin et al. (2000); Santagiustina et al. (2002); Esteban-Martín et al. (2006)), whereas in the case of the degenerate type-I OPO only two phase states are possible. Systems of the latter kind and the resulting front dynamics are discussed in Sec. 5. At present, there is no experimental confirmation of SDS in OPOs to our knowledge.

3.2 Cavity solitons in lasers with optical injection

The case of a laser with injection is somewhat in between the one of a driven system and a "true" free-running CSL because the injection breaks the phase invariance and frequency, phase and polarization of the SDS core are slaved to the one of the HB. The mechanism of bistability is similar in the laser and the driven absorber/amplifier case: Initially the HB is detuned from the cavity resonance and hence the intra-cavity intensity is low. However, there will be a threshold at which the driving field can cause a change in carrier density strong enough to drive it into resonance due to the refractive index change resulting from phase-amplitude coupling (Henry, 1982). This in turn leads to an increase in intra-cavity intensity and thus to a feedback effect destabilizing the low amplitude state. As a result, a high-amplitude state with low carrier density and high refractive index (in an amplifier) and a low-amplitude state with high-carrier density and low refractive index can coexist. This mechanism is usually referred to as *dispersive optical bistability* (Lugiato, 1984).

LCS were investigated in a VCSEL biased above threshold with an external HB by Hachair et al. (2006) and the findings were indeed quite similar to the amplifier case discussed in the sections before by Barland et al. (2002). However, the "laser" property manifests itself in one distinct difference, which is that the background of the LCS might be temporally varying. This is due to the fact that the lower branch of the bistability cycle does not necessarily correspond to an injection locked state but might be oscillatory due to a beating between the free-running laser emission and the injected field. These regular or irregular spatio-temporal oscillations of the background can be observed directly in the temporal domain in simulations and were confirmed experimentally indirectly by spectral measurements. For details we refer to (Hachair et al., 2006) and the review (Lugiato et al., 2008).

The modeling of this situation is surprisingly demanding because the standard adiabatic elimination of the dielectric polarization leading to the class-B equations given in Sec. 1.3 is no longer valid. After the adiabatic elimination, the gain and loss curves are flat and hence there is no selection mechanism for frequency and spatial wave number leading to spurious instabilities in the laser case ((Oppo et al., 1991; Jakobsen et al., 1992)). Keeping the equation for the polarization, (Rössler et al. (1998); Hachair et al. (2006)), is numerically very resource demanding because the resulting equations are stiff, spanning a time scale of about 10^4 between the decay rates for the dielectric polarization and the carriers. The action of a gain-line can be semi-phenomenologically included in the class-B equations by adding a filter in frequency space (Loiko and Babushkin, 2001). Reduced equations were derived via advanced adiabatic elimination schemes (Coullet et al. (1989); Oppo et al. (1991); Lega et al. (1994)) but were only valid under restrictive limitations. Recently, a great step forward was achieved by deriving a reduced set of equations with broad applicability and a 400fold increase in computational efficiency compared to a code incorporating the polarization equation (Oppo et al., 2009). This enabled systematic numerical investigations of the properties of LCS with injection and is expected to be fruitful for investigating and understanding spatio-temporal laser dynamics in general.

3.3 Cavity solitons based on frequency-selective feedback

3.3.1 Scheme and mechanism of bistability

Figure 16a shows a scheme, which is suitable for obtaining LCS via frequency-selective feedback. A broad-area laser with a plano-planar cavity (in the realization discussed below a VCSEL) is coupled to a self-imaging external cavity, i.e. a cavity containing a telescope with two lenses adjusted to infinity. The

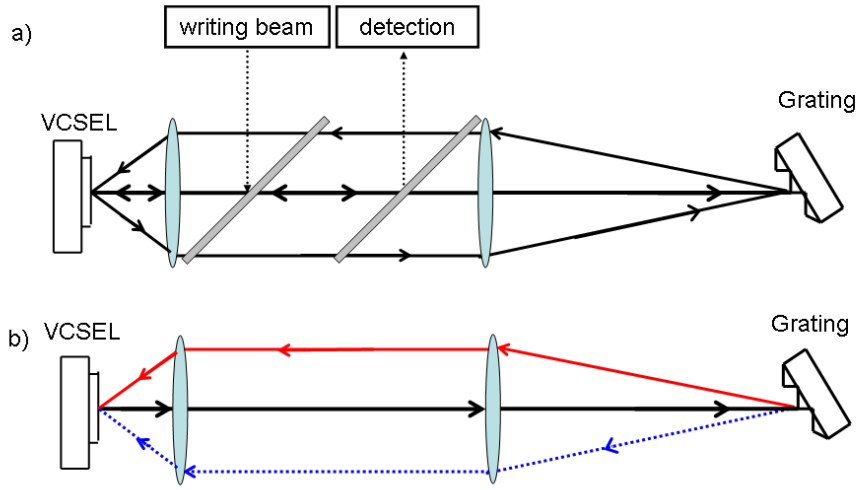

Fig. 16. (Color online) Scheme of a VCSEL with frequency-selective feedback by a diffraction grating in a self-imaging cavity and schemes of ray trajectories in the external cavity. The scheme in Tanguy et al. (2008a,b) used a 62 cm long cavity with a telescope magnification of 38. a) The path of a ray at the Littrow wavelength closes into itself independent from its propagation angle with respect to the optical axis. b) A ray with a wavelength different from the Littrow wavelength propagating towards the grating along the optical axis (black lines) is coming back at the same location but at a different angle. The sign of deviation depends on whether it is blue-detuned (blue lines, dashed) or red-detuned (red lines, solid) with respect to the Littrow wavelength.

ABCD-transfer matrix of the system is $\begin{pmatrix} 1 & 0 \\ 0 & 1 \end{pmatrix}$. This configuration can support arbitrary field distributions; any ray originating from somewhere within the laser aperture at some emission angle returns to exactly the same position with the same angle after one round-trip. Hence there is no diffraction in the external cavity and the high Fresnel number of the broad-area laser is preserved. The cavity is closed by a frequency-selective element. In the first realization reported (Tanguy et al. (2006, 2008a,b)) it was a diffraction grating in the so-called Littrow configuration, where the first order of the grating is reflected back into the VCSEL. Other options are volume Bragg gratings (Radwell et al. (2008); Ackemann et al. (2009)) or Fabry-Perot cavities and etalons (Fischer et al., 2000b).

There is one frequency, referred to as the grating frequency in the following, where an on-axis ray is exactly retro-reflected into itself. After one round-trip through the self-imaging cavity, this is also true for rays at arbitrary angles (see Fig. 16a), i.e. the grating behaves like a normal plane mirror. The frequency selectivity of the Littrow scheme stems from that fact that a ray with a wavelength detuned from the Littrow condition will return to the

VCSEL at a different angle than the one it originated from (Fig. 16b), though still to the same position. Fig. 16b shows an on-axis wave as an example but the same change in angle occurs for any off-axis wave. Hence, the returning ray is not matching the resonance condition of the VCSEL any more and is rejected (see (Schulz-Ruhtenberg et al. (2009)) for a detailed discussion).

The mechanism of bistability is a kind of dispersive bistability (as discussed above) due to the competition between two preferred frequencies in the system, the longitudinal resonance of the VCSEL cavity and the grating (or any other filter) frequency. Initially they are not aligned, the emission amplitude is low and the carrier density high. For the same parameter, there might be a state, in which the emission amplitude is high and the carrier density low as a consequence. Due to phase-amplitude coupling, the refractive index increases and hence the wavelength of the cavity resonance is red-shifted (Henry, 1982). This closes a feedback loop and the two resonances are roughly aligned in the upper state of the bistability loop. A detailed treatment of this effect for small-area VCSEL is given in (Naumenko et al. (2006, 2007)).

3.3.2 Experimental investigations in VCSELs

If the experiment is performed in a broad-area VCSEL, a bistability curve like the one in Fig. 17 is obtained if the current is ramped slowly up and down from a starting value well below the free-running laser threshold (Tanguy et al. (2008a,b)). The grating frequency is chosen to be lower than the VCSEL resonance at the start. After some low-amplitude shoulder, there is an abrupt switching to a high-amplitude emission state, which stays in some range even if the current is decreased again. Note that – though the scanning variable is nominally the current – in effect the x-axis in Fig. 17 corresponds to a wavelength axis due to the increase in resonance wavelength of the VCSEL with current due to ohmic heating. Hence, the detuning between the two resonances is decreased until the feedback effect discussed above is triggered. Experimentally, the resulting high-amplitude state is at a slightly higher frequency than the grating frequency.

Inspection with a CCD-camera shows that not the whole aperture of the VCSEL (diameter of 200 μm) switches on, but only a small localized spot with a diameter of about 10 μm FWHM (Fig. 17, right column). The angular width in far field is about 2.5°, which is indistinguishable from the diffraction limit within experimental resolution. The linewidth in single-mode operation is 10 MHz. Hence, these spots represent coherent emission: They are *microlasers*, stabilized by solitonic effects, within the larger pumped aperture.

This formation of LCS can take place at several locations in the aperture at different threshold currents. An example is shown in Fig. 18a, which shows

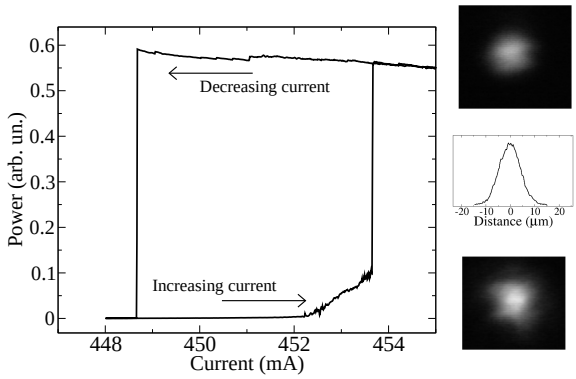

Fig. 17. Power versus current for a single laser CS in a VCSEL operating at 980 nm. In this case the comb filter (explained in the body of the text) was inserted in order to reduce the optical background of the spot and hence obtain a cleaner hysteresis. The panels on the right show, from top to bottom: the near-field intensity distribution around the spot, a transverse intensity profile through the center of the near-field distribution, the far-field intensity distribution. [Reprinted figure with permission from Tanguy et al. (2008a). Copyright 2008 of the American Physical Society.]

three LCS and some extended background states. The shoulder before the abrupt switch-on in Fig. 17 is also related to the excitation of these states. They are blue-detuned to the LCS and have a much broader linewidth than the LCS. They can be disfavored by introducing a suitable mask serving as a spatial filter at the near field image plane at the grating (Tanguy et al. (2008a,b)). The LI-curve obtained if the whole aperture of the VCSEL is monitored is very complex and consists of many interleaved hysteresis loops of the individual LCS. If the device is biased at a point where at least two LCS are simultaneously bistable, the experiment depicted in Fig. 18 can be performed. It demonstrates that an additional LCS can be written by an external WB (b) and stays if the WB is removed (c). Afterwards a second LCS is written (d, e) and erased again by applying the WB at a slightly different position (g, g). Then the first LCS is erased by the same means (h, i). This experiment demonstrates the crucial property of independence of two spatially well separated SDS stressed in Sec. 1 giving them solitonic properties. In a slightly different setup, all $2^3 = 8$ states of three simultaneously bistable LCS were demonstrated (Ackemann et al., 2009). From a photonics point of view, this establishes an all-optical manipulation of the emission state of parallel microlasers with possible applications in all-optical networks.

The switching is robust in the sense that it is "incoherent", i.e. it does not rely on a fixed phase relationship between WB and LCS. WB and the emerging LCS can even have quite different frequencies up to about 50 GHz. Furthermore, it works with a polarization of the WB parallel or orthogonal to the one of the LCS (which is linearly polarized due to the anisotropy of the diffraction grating). This hints to the fact that the main effect is mediated by the car-

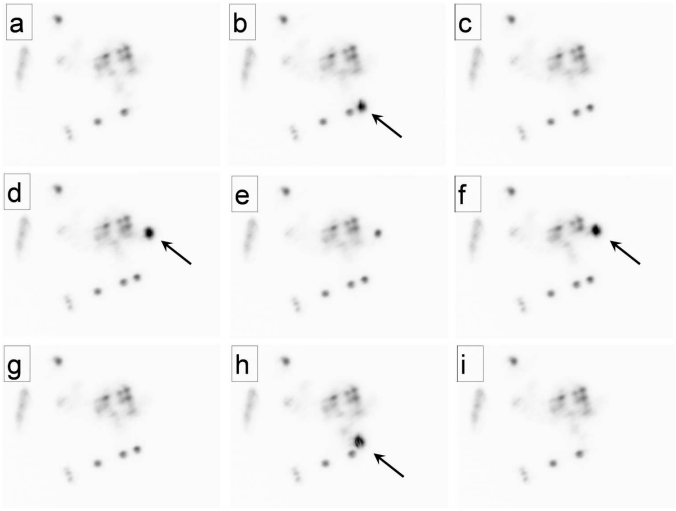

Fig. 18. Near-field intensity distributions showing the successive switching on and off of two LCS with an injected incoherent WB in a VCSEL with a diameter of 200 μm (brightest spots, indicated by arrows). Dark areas correspond to high intensities. The WB is derived from a tunable laser source, with wavelength tuned in the vicinity of the VCSEL cavity resonance. It is focused onto the VCSEL with a 12 μm spot diameter (FWHM) and a power in the mW range. Two sites where spontaneous spots could be observed were selected for WB injection, and the VCSEL was biased within their bistability range. a) Both spots are off, b) injection of WB, c) one spot is switched on and remains after the WB is blocked, d) injection of WB at second location, e) second spot remains on, f) WB injected beside second spot, g) second spot switched off and does not reappear (first spot unaffected), h) injection of writing beam to switch off first spot, i) both spots remain off. [Reprinted figure with permission from Tanguy et al. (2008a). Copyright 2008 of the American Physical Society.]

rier population. Switching was quantitatively studied in Tanguy et al. (2007). Minimal switching power and pulse duration were observed for a WB with a frequency about 8 GHz higher than the one of the emerging LCS, which seems to coincide with the (low-amplitude) longitudinal resonance of the VCSEL. The minimal pulse duration investigated was limited by the acousto-optical modulator (AOM) used to generate the pulses to 20 ns, which was sufficiently long to induce switching. The system settles down to an asymptotic state after about 40-50 ns.

Though "incoherent" switching was obtained before in driven cavity or feedback systems (Maywar et al. (2000); Schäpers et al. (2000, 2002); Taranenko and Weiss (2001); Pesch et al. (2005); Barbay et al. (2006)), the main route for control there is the phase of the WB with respect to the HB (and thus the CS) (Brambilla et al. (1996); Spinelli et al. (1998); Barland et al. (2002); Hachair et al. (2005)) leading to constructive or destructive interference and thus controlling locally the amplitude of the intra-cavity field. The insensitivity of the switching in CSL to phase is probably one of their major advantages

in applications though it is probably fair to say that many aspects of the switching process and potentials for optimization are not well understood at this point (see also Sec. 3.4.2). The results reported by Tanguy et al. (2007) are obtained by directly aiming the WB at the LCS. It turns out that the position of the WB with respect to the LCS is actually important, at least for quasi-cw control pulses. The effect can be seen in Fig. 18, where the location of the WB was slightly changed in between ignition and erasure. This difference is related to the symmetry breaking indicated in Fig. 16b. As discussed in more detail in Sec. 6.4, this asymmetry induces a preferred drift direction and hence an "upstream-downstream" asymmetry to the vicinity of any "trap" the LCS is residing in. Ignition of an LCS is possible from an "upstream" position, whereas "erasure" seems to be a result of a "downstream" perturbation of the trap by the WB (Tanguy et al. (2008a,b)). These "traps" are the result of disorder in broad-area photonic devices pinning the position of the LCS and leading to scatter in the limit points of their hysteresis loops. For example, a defect line with three LCS is clearly apparent in Fig. 18e in the lower part of the aperture.

Replacing the diffraction grating by a volume Bragg grating (VBG) as the frequency-selective element results in a much more compact and robust setup and a potentially much faster response time (Radwell et al., 2008). Indications for phase-locking between different LCS and of polarization effects due to the small polarization anisotropy of that setup were also found and are currently under systematic investigation (Radwell et al., 2008).

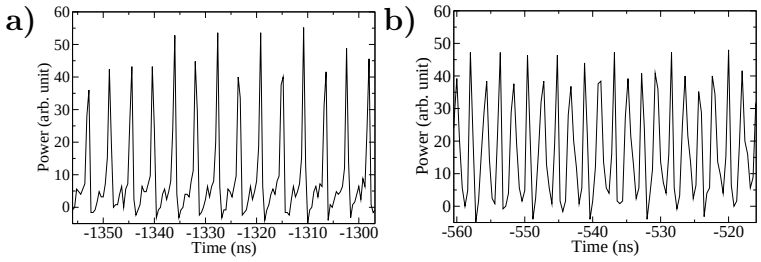

Fig. 19. Close-up of timetraces of a switch-on transient recorded with a fast avalanche photodiode located at the position of the stationary LCS. The zero of the time axis is arbitrary. a) is obtained in the beginning of the transient, b) later on. [Reprinted figure with permission from Tanguy et al. (2008a). Copyright 2008 of the American Physical Society.]

Finally, we mention that the freedom of a LCS to choose frequency might lead to the simultaneous operation on multiple-external cavity modes with the possibility of self-pulsing, especially during transients. Fig. 19 shows the transient dynamics of a LCS switching on spontaneously. The dynamics vary over the time before switch-on, beginning with regularly spaced large-amplitude pulses every round trip time of 4 ns, see Fig. 19a. Gradually, additional pulses appear in between two main pulses and the modulation depth decreases (Fig. 19b), until the modulation ceases almost completely at the end of the switch-on tran-

sient, though it might be still multi-mode. In that regime different longitudinal modes oscillate probably in anti-phase giving an almost constant envelope (Viktorov and Mandel, 2000). A transition between pulsing and anti-phase dynamics is a common scenario in transients of semiconductor lasers with feedback (Vaschenko et al. (1998); Sciamanna et al. (2002)). Alternatively, the laser can go into single-longitudinal mode operation after the transient.

Recent experiments with a cavity round-trip time shorter than the carrier lifetime demonstrate sustained self-pulsing (Ackemann et al., 2009), which opens an interesting path to *self-pulsing SDS* and possibly *3D-localization* by *mode-locking* of LCS operating on many external cavity modes.

3.3.3 Theoretical treatment

For the theoretical description of the VCSEL with FSF, Scroggie et al. (2009) developed a model which describes the coupled cavity dynamics by adding a suitable feedback term to the standard model for intra-cavity field E and carrier density N of a VCSEL (Eq. 2), which reads

$$F(t) = e^{-i\delta\tau_f}\hat{G}(t-\tau_f/2)\ \left[-r_1 F(t-\tau_f) + t_1 E(t-\tau_f)\right]. \tag{7}$$

Here, δ and τ_f denote the external cavity detuning and round–trip time, while r_1 and t_1 are the (real) amplitude reflection and transmission coefficients of the VCSEL output mirror. The operator $\hat{G}$ describes the frequency–selective filter and is taken to be

$$\hat{G}(t)\ [h(t)]\ = \frac{r_g}{2\beta}\int_{t-2\beta}^{t} e^{i\Omega_g(t'-t)}\ h(t')\ dt', \tag{8}$$

describing a sinc-shaped modulation in frequency space. The frequency $1/\beta$ determines the bandwidth of the filter, while Ω_g is its central frequency. The parameter r_g is an overall reflection coefficient. It should be noted that the term $r_1 F$ in Eq. (7) is not-included in the "standard"-description of semiconductor lasers with feedback, which takes only a single round-trip in the external cavity into account (so-called Lang-Kobayashi approximation, (Lang and Kobayashi, 1980)). The addition of the reflected feedback field after one round-trip allows to take into account all round-trips at essentially no extra computational costs (see also (Giudici et al., 1999)). This allows for a proper description of the regime of strong feedback used in the experiments. Note also that though the gain line and the (VCSEL internal) losses are flat, the external cavity provides frequency-selection and thus suppresses the spurious instabilities mentioned in Sec. 3.2.

Analytical and numerical analysis shows that there is a current range below the solitary laser threshold where both the nonlasing state and extended grating-controlled states are stable. In that range LCS are found with properties quite

similar to the experimental ones regarding asymptotic behavior as well as switch-on transients. Their size is about 8-10 μm.

Some insight in how these LCS form can be obtained by looking at single-frequency solutions, which are given in 1D by $E(x,t) = A(x)\exp(-i\omega t)$. It turns out that the solution can be cast into a form which involves a cavity part, Eq. (9a), and a soliton part, Eq. (9b), which need to be fulfilled simultaneously:

$$[-i\omega + (1 + i\theta) - S(\omega)]\, A = CA \tag{9a}$$

$$i\nabla^2 A + \frac{\sigma(J-1)(1-i\alpha)}{1+|A|^2} A = CA. \tag{9b}$$

Here, $S(\omega)$ represents the filter function. Eq. (9a) can be represented by a curve in the complex C–plane parameterised by ω and is depicted for a particular set of parameters in Fig. 20a. The different curves represent all possible external cavity mode where the envelope is due to the sinc-shape of the filter function.

Eq. (9b) represents a nonlinear eigenvalue problem for soliton solutions in which the complex parameter C corresponds to an effective loss and detuning. For a given set of parameters we can expect bounded solutions only on a null set in the complex C–plane, i.e. a curve at most. It is shown as a dashed line in Fig. 20b. As this curve is followed from left to right, the corresponding solutions become broader with lower peak amplitude. It eventually terminates, with infinite width and zero amplitude, on the straight line $C = \sigma(J-1)(1 - i\alpha)$, parametrized by current, defining low-amplitude spatially-homogeneous solutions to Eq. (9b).

Exact SDS solutions to Eq. (9b) are known in 1D, if the saturation denominator is expanded, and truncated at the first nontrivial term. These solutions are of chirped-sech form, and have been known in this context for many years (Paré et al., 1989). Normally, however, either the SDS or the non-lasing background state are unstable, so these solutions have had limited experimental relevance. Use of FSF can solve that problem by ensuring that the non-lasing state has no available resonances with positive gain under conditions where the soliton curve intersects one or more modal curves, as in Fig. 20a. The soliton curve for the chirped-sech SDS solutions is simply a straight line. As can be expected, that line is tangent to the soliton curve of the full model at its termination, where the amplitude of the SDS becomes small.

Fig. 20 shows that there can be many intersections between the cavity response and soliton solution curves, and hence many single–frequency soliton solutions. Indeed LCS with different frequencies were reported by Tanguy et al. (2008a). Moreoever, it can be seen that changing a system parameter will alter the soliton and cavity response curves, creating (or destroying) laser solitons in pairs through saddle–node bifurcations (at least one of such a pair is necessarily unstable). Since $Re(C)$ represents the net cavity loss we expect the system to

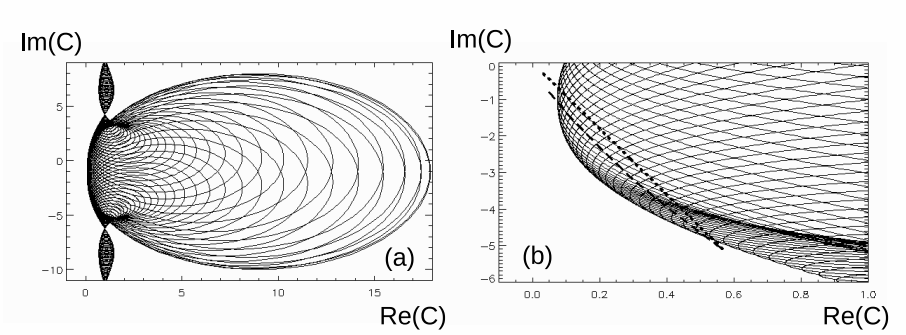

Fig. 20. (a) Effective cavity response (Eq. (9a)) for the coupled–cavity system plotted in the complex C–plane. (b) Blowup of (a) showing the LCS (dashed line) for a current $J = 1.63$ and plane–wave threshold (dotted line) solutions of Eq. (9a) [Reprinted figure with permission from Scroggie et al. (2009). Copyright pending with American Physical Society.]

favor the soliton which minimizes this quantity. Numerical simulation bears this out: as new LCS appear on changing a system parameter, the laser has a tendency to shift operation to the LCS with the smallest losses. The kinks in the LI-curve of Fig. 17 are a manifestation of that process.

Numerical simulations confirm also that simultaneous operation on several external cavity modes is possible and results in self-pulsing (Scroggie et al., 2009). More detailed investigations are necessary but the preliminary results support the notion that the VCSEL with FSF might be viable approach to mode-locked LCS and 3D light confinement.

A more detailed study of the bifurcation characteristics of LCS with FSF was given in Paulau et al. (2008). The model is simplified to a class-A description, i.e. the carrier equation is eliminated. This provides a proper description of the stationary solutions though the stability properties might be slightly different. Other simplifications are a Lorentzian filter profile and the adoption of the Lang-Kobayashi approximation. Fig. 21 shows that the nonlasing solution becomes unstable versus lasing of extended plane-wave solutions (dashed curves) between the points A and B. Between B and the threshold of solitary lasing (at higher currents, not shown) lasing coexists with a stable nonlasing state. From both A and B branches of localized solutions originate which merge in C. Some parts of the upper branch close to C correspond to stable LCS, the rest is unstable. The lower subfigure illustrates the statement made already for the more detailed model above. At the bifurcation points the size of the LCS diverges. Moving away from A and B they become more localized (and acquire a higher amplitude). In the stable range they are about 5 μm in rough agreement with experiments.

Having discussed homoclinic snaking in detail in Sec. 2 it is maybe surprising that the LCS does not snake: The branch of the 1-LCS solution reconnects to the homogeneous state on both sides. Obviously there might be islands

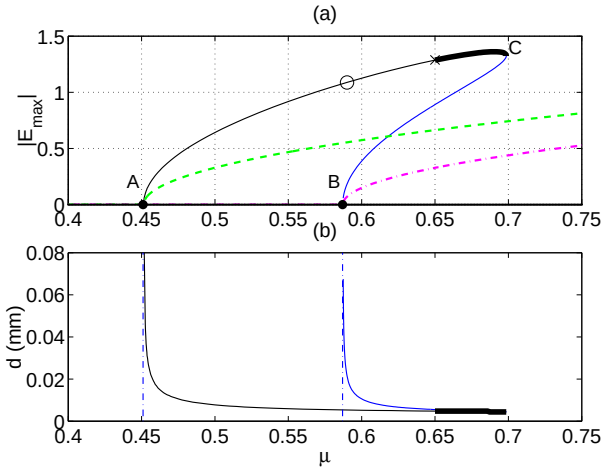

Fig. 21. Dependence of (a) maximum field amplitude, and (b) width of LCS on pump current. The solid lines denote the CS branches. The stable part is indicated by a thick line. The dashed (dash-dotted) line corresponds to the homogeneous external-cavity mode with maximal (minimal) gain. In between the circle and the cross, the LCS on the upper branch are spontaneously moving with constant speed. The points A,B,C are explained in the text. (*Courtesy of P. V. Paulau*, adapted from Paulau et al. (2008)).

in phase-space representing more complicated solutions and clusters but they were not explored yet. It is believed that the existence of the phase symmetry in the laser equations inhibits the "classical" snaking discussed in Sec. 2. In view of this result it is surprising that the hysteresis loops of single LCS to clusters observed in the VCSEL with FSF (Radwell et al., 2008) are quite similar to the ones observed in amplifier systems, which are expected to show snaking (Barbay et al., 2008). One possible explanation is disorder, possibly in both cases.

3.4 Laser cavity solitons due to saturable absorption

3.4.1 General theory and early experiments

The dominant mechanism of bistability in a laser with saturable absorber (LSA) is "absorptive" and not "dispersive", i.e. an effect on the cavity losses and not not due to a shift of resonances. The basic bifurcation scenario is illustrated in Fig. 22. Below threshold the nonlasing state is stable. It loses stability if the gain compensates for the non-saturable losses (outcoupling, background absorption) and the losses in the absorber (here at $\mu \approx 5.2$). If the laser starts, the intra-cavity field saturates the absorber, absorption drops, the losses are reduced and the laser switches abruptly to a finite amplitude. Reducing the pumping the laser can stay on as long as the field is able to sustain the saturation and the switch-off point is only reached where the gain

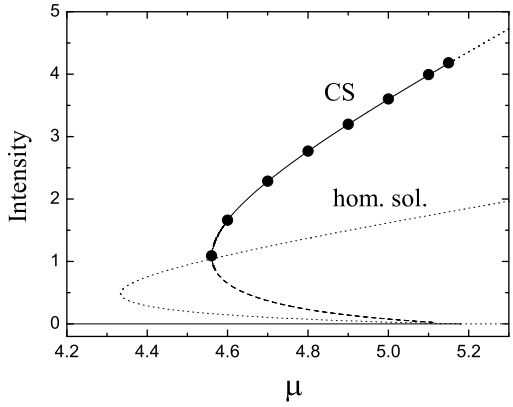

Fig. 22. Local intensity versus pumping parameter in gain section for a LSA. The characteristics are obtained for a semiconductor nonlinearity but serve to illustrate a more general phenomenology. Light dotted lines: homogenous state. Solid line: stable SDS branch. Dashed line: Unstable SDS branch. *(Courtesy of F. Prati*, adapted from Prati et al. (2007)).

can't compensate the non-saturable losses any more (here at $\mu \approx 4.25$). The corresponding hysteresis loop of a plane-wave emission state is depicted as the dotted line in Fig. 22. In broad-area LSA it turns out under quite general conditions (see below) that the homogenous lasing solution is unstable and stable LCS develop instead (dots on upper branch).

The field of LCS in LSA was pioneered by a theoretical suggestion of Rosanov's group (Fedorov et al. (1991); Rosanov and Fedorov (1992)) and confirmed experimentally soon afterwards (Bazhenov et al. (1991); Saffman et al. (1994); Taranenko et al. (1997)). The setups were based on dye gain media and bacteriorhodopsin saturable absorber or photorefractive nonlinearities. A review summarizing much of this nice work on non-semiconductor systems is given in (Weiss and Larionova, 2005).

Extensive and significant theoretical work on properties and dynamics of LCS in a LSA was done by Rosanov's group (Vladimirov et al. (1999); Fedorov et al. (2000); Rozanov et al. (2004); Rosanov et al. (2005)) and is reviewed in (Rosanov (2002, 2005)). We don't go into detail here because some issues are reappearing in the following subsection on semiconductor devices, in Sec. 6.4 (motion and spontaneous motion) and in Sec. 5 (front dynamics leading to SDS with different, but discrete width). We mention that LSA are also predicted to support dark solitons with topological charges, i.e. ring-shaped structures with zero intensity and a phase singularity (of different orders) in the center. The core is similar to the "optical vortices" in normal lasers (Coullet et al. (1989); Staliunas et al. (1997)) but they should be more prevalent in CSL (especially in higher orders) due the fact that the dark center is stabilized

by the additional unsaturated losses (Rosanov, 2002). LCS do not need to be circularly symmetric and very complex interaction and motion behavior is found (Rosanov (2002); Rosanov et al. (2005)).

Finally, the energy flow in LCS was analyzed giving some insight to the statement in the introduction that SDS are an attractor of the dissipative dynamics balancing not only diffraction and nonlinearity but also loss and gain. By analysis of the transverse Poynting vector, Rozanov et al. (2004) have shown that energy is injected in the wings of the structure and flows inwards towards the center and outwards towards the background (see also Akhmediev and Ankiewicz (2005b) for the case of temporal LCS and Oppo et al. (1999) for OPO SDS).

3.4.2 Modeling and design of semiconductor-based devices

Obviously, there is a strong drive to replace the rather bulky and slow schemes mentioned in the previous subsection by semiconductor amplifiers and absorbers, ideally in a monolithic microcavity. A model to describe semiconductor-based LSA was given in (Bache et al. (2005); Prati et al. (2007)). Compared to our "standard equations", Eq. (2), the interaction of the field E with the carriers n in the absorber needs to be added:

$$\dot{E} = \left[-1 + i\nabla_\perp^2 + (1 - i\alpha)N + (1 - i\beta)\right] E \tag{10a}$$

$$\dot{N} = \gamma \left[\mu - N(1 + |E|^2) - B_1 N^2\right] \tag{10b}$$

$$\dot{n} = \gamma_n \left[-\eta - n(1 + s|E|^2) - B_2 n^2\right]. \tag{10c}$$

Here, α and β are the linewidth enhancement factors of the gain and absorber sections, γ and γ_n represent the ratio of nonradiative carrier decay in the different materials to the field decay rate rate. μ represents the pumping parameter of the gain section and η background absorption in the absorber. s denotes the saturation parameter or better the relative saturation parameter between gain and absorption. B_1, B_2 represent bimolecular recombination due to spontaneous emission in the quantum wells. These are the only semiconductor specific terms, without them the semiconductor equations map exactly onto the two-level equations used in (Fedorov et al. (2000); Rosanov (2002)).

It should be noted that these equations do not contain a mechanism for wave vector, respectively frequency, selection. Any tilted wave with $E \sim \exp\left(i\vec{q}_\perp \cdot \vec{r} - i(\omega + q_\perp^2)t\right)$ is a solution and the thresholds are degenerate. Usually, the solution with $q_\perp = 0$ is analyzed. As discussed in Sec. 3.2, a more elaborate elimination procedure for the dielectric polarization is needed to remove this degeneracy leading to the appearance of a diffusion term or a forth order nabla-operator (depending on detuning) in the field equations (Coullet et al. (1989); Lega et al. (1994); Fedorov et al. (2000); Rosanov (2002)).

However, the results on LCS seem to be robust with respect to this degeneracy.

Fig. 22 stems from this semiconductor model (Bache et al. (2005); Prati et al. (2007)). If a WB is injected at the cavity frequency, LCS switch on and settle down to a stationary structure in the current range between $\mu \approx 4.45 \ldots 5.15$, after a transient reminiscent of spiking typical for class-B lasers. For $\mu \lesssim 4.45$, the LCS collapses to the off-state. Beyond $\mu \approx 5.15$, a filamentation instability sets in.

One crucial condition for the bistability and hence existence of LCS is $s > 1$, i.e. the absorber saturates more easily than the gain medium (Bache et al., 2005). This can be influenced by quantum and device design as well as a demagnification between gain and absorber section (in a non-monolithic realization).

The second important condition for the stability of LCS is that γ_n/γ is small enough (for $B_1 = B_2 = 0$) , i.e. the absorber is slower than the gain medium. Beyond some limit a Hopf bifurcation is found, which corresponds to self-Q-switching or passive Q-switching (Fischer et al., 2000a), and prevents the formation of LCS (Bache et al., 2005). In semiconductor devices, the bimolecular terms imply that the gain medium decays in tendency faster than the absorber because it operates at higher carrier densities. Prati et al. (2007) have shown that for typical values of B_1, B_2, bistability can exist already for $s = 1$ and $\gamma = \gamma_n$. This is an important result because it indicates that one can use the same material as absorber and gain medium.

Switch-on and switch-off of LCS were studied in detail in Mahmoud Aghdami et al. (2008). The authors studied incoherent injection which only enters the carrier equation via a local perturbation in μ (for example by optical pumping in high energy carrier states) and semi-coherent injection at the cavity and the LSA frequency entering the field equation in the way discussed before in Eq. (2). In all cases there was no fixed phase relationship between LCS and WB and the dynamics was mediated by the carriers. Hence typical response times are on the order of one nanosecond. The type of switching (on or off) can be controlled by choosing suitable values for pulse duration and amplitude.

A monolithic integration of gain medium and absorber is known for edge-emitters (Kawaguchi, 1994) and in a lesser extent for small-area VCSELs (Fischer et al., 2000a). The even more demanding task for broad-area devices was addressed in Barbay et al. (2005) by using optical pumping and employing special aperiodic designs of the Bragg reflectors and a suitable positioning of the quantum well within the standing wave field patterns to ensure that the absorber is only weakly pumped but still interacts with the lasing field. Based on such a design recently a bistable localized spot was obtained in device center (Elsass et al., 2008). These nice results indicate that the design is on

a good track, though the independent manipulation of two structures is still outstanding.

A very intriguing twist to the theme of a monolithic CSL with SA comes from a scheme with mixes propagational solitons and SDS: It unfolds the repeated encounter of gain and saturable absorption back into a propagational sequence of gain and absorber in an edge-emitting semiconductor structure (i.e. going back the path from Fig. 1a to Fig. 1b we took in Sec. 1 to introduce cavity solitons). The properties of these 1D SDS and their interesting, phase-sensitive interaction behavior was investigated in a sequence of papers (Ultanir et al. (2003, 2004, 2006)) and is reviewed in Ultanir et al. (2005).

3.4.3 Experimental realization using face-to-face VCSELs

Another possibility to combine an absorber with a gain medium is to couple them via an external cavity. This approach was used before to achieve mode-locking in vertical-cavity devices (Jasim et al., 2004). In Genevet et al. (2008) a cavity with two intra-cavity telescopes is used to image the active zones of two broad-area VCSELs onto each other with a magnification of 1. The resulting LI-curve is depicted in the left part of Fig. 23, where the current in the gain device is ramped up and down. For low current (region A), the laser is below threshold. In region B it lases due to feedback from the output facet of the passive VCSEL. The spatial patterns are complex and typically not stationary. Then the two lasers start to interact and the intensity drops due to the onset of absorption in the passive device (region C, note that changing the current also changes the detuning conditions due to Joule heating). At the end of the region, the intensity switches abruptly to a high value. This transition is hysteretic. In the near field localized bright spots form in the gain as well as in the absorber section (images on the right of Fig. 23). They can be switched on and off independently, confirming their solitonic nature.

This provides a nice second demonstration of a semiconductor-based CSL. Currently, properties and dynamics of the LCS are analyzed in detail. Obviously, the scheme is not simply described by Eqs. (10a-10b), but characterized by a quite complex coupled cavity situation, which needs to be captured in a refined treatment. In regime B, a feedback equation similar to Eq. (7) represents a starting point for an analysis. In regime C, the nonlinearity of the reflection from the passive device needs to be incorporated in addition.

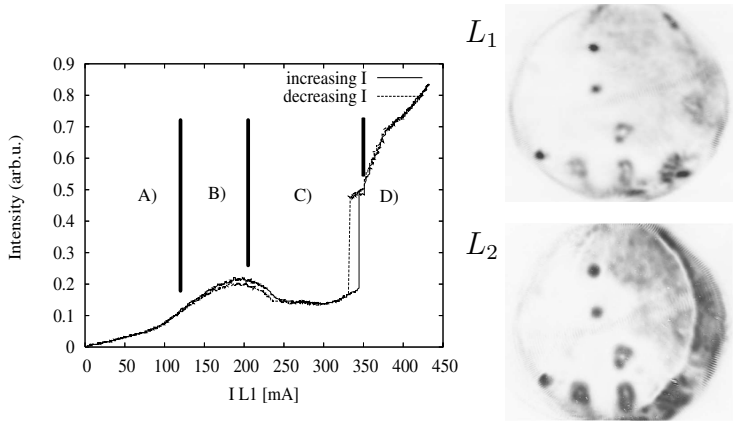

Fig. 23. Left panel: Local intensity output emitted by the system when the current I_{L_1} is scanned in the gain device for all the other parameters constant. A) below threshold, B) lasing by feedback, C) absorption by L_2, bistable behavior, D) pattern formation. Right panel: Examples of near field intensity distributions in both devices in region C showing LCS (upper one gain device; lower one absorber). L_2 is slightly shifted on the left. Dark areas correspond to high intensities. *(Courtesy of P. Genevet*, adapted from Genevet et al. (2008))

4 Spatial Dissipative Solitons due to Periodic Modulations

The effect of background modulations in the nonlinear dynamics of broad–area photonic devices leads to control and stabilization of spatial structures (Neubecker and Zimmermann (2002); Martin et al. (1996)). When describing the appearance of SDS in the presence of periodic modulations, two main approaches have been followed. On one side, continuous variables and modulations have been considered in models of intra-cavity photonic crystals (ICPC) while on the other discrete models have been used in the so called tight-binding limit. We provide first a review of SDS in photonic devices with ICPC with continuous variables and then those found in devices formed by separate, yet coupled, discrete elements.

4.1 Spatial Dissipative Solitons due to intra-cavity photonic crystals

Intra-cavity photonic crystals are described as periodic modulations of the material's refractive index. For appropriate values of the cavity detuning, the *linear* band-gap of the photonic crystal inhibits modulational instabilities that lead to the formation of periodic spatial structures (patterns) (Gomila et al. (2004); Gomila and Oppo (2005)). This phenomenon has been recently realized experimentally by Terhalle et al. (2008). These references are restricted to the case of supercritical bifurcations only. The effects of a periodic modulation of the refractive index on the formation of subcritical structures was studied by

Gomila and Oppo (2007). This case is especially relevant for the observation of stationary SDS.

The model considered is that of an optical cavity containing a self-focusing Kerr medium (Lugiato and Lefever (1987); Scroggie et al. (1994)) (see Eq. (1)) and a linear medium with a spatially modulated refractive index:

$$\partial_t E = -[1 + i(\theta + f(x))]E + i\partial_x^2 E + E_I + i|E|^2 E, \tag{11}$$

where θ is the average detuning between the frequency of the pump and the frequency of the cavity, $f(x)$ accounts for the modulated refractive index in the transverse direction of the photonic crystal, and E_I is the input field. $f(x)$ is a square function of amplitude α and wavenumber k_{pc}. This model is convenient for its simplicity but SDS induced by ICPC are expected in a variety of photonic devices such as saturable absorbers, optical parametric oscillators and lasers. In the absence of a photonic crystal ($\alpha = 0$) Eq. (11) has a homogeneous steady state solution implicitly given by

$$E_0 = \frac{E_I}{1 + i(\theta - I)}, \tag{12}$$

where $I = |E_0|^2$. Eq. (12) has a single-valued solution for $\theta < \sqrt{3}$ (see Sec. 2.4). The homogeneous solution is stable for $I < 1$ and becomes modulationally unstable at $I = 1$ with critical wavenumber $k_c = \sqrt{2 - \theta}$, leading to the formation of a stripe pattern.

Periodic modulation of the refractive index can inhibit the formation of patterns with $k_c \sim k_{pc}/2 = 2$, i.e. for values of the detuning around $\theta = -2$ (Gomila et al., 2004). In that case, the response of the system to the ICPC is very small, accordingly to the large and negative decay rate of perturbations at $k = k_{pc}$ (see Fig. 24a). Here, instead, we are interested in regimes where SDS exist. SDS are found above $\theta = 41/30$, where the critical wavenumber is small and the wavenumber $k_{pc} = 2k_c$ is only weakly damped (see Fig. 24b). In this case the system presents a strong response to the perturbation introduced by the spatial periodic modulation. A strong response to the ICPC enhances the amplitude of the fundamental solution, and induces a reverse subcritical bifurcation and patterns at large values of the input intensity. By increasing the amplitude of the spatial modulations the reverse subcritical bifurcation and associated patterns progressively move down to lower values of I until they collide with the upward directed instability of the fundamental solution (see Fig. 25).

When increasing the amplitude of the ICPC modulation α we observe a progressive stabilization of the fundamental solution at large values of I (see Fig. 25). The fundamental solution becomes stable through a locking with the periodic forcing introduced by the ICPC, similar to the case studied by

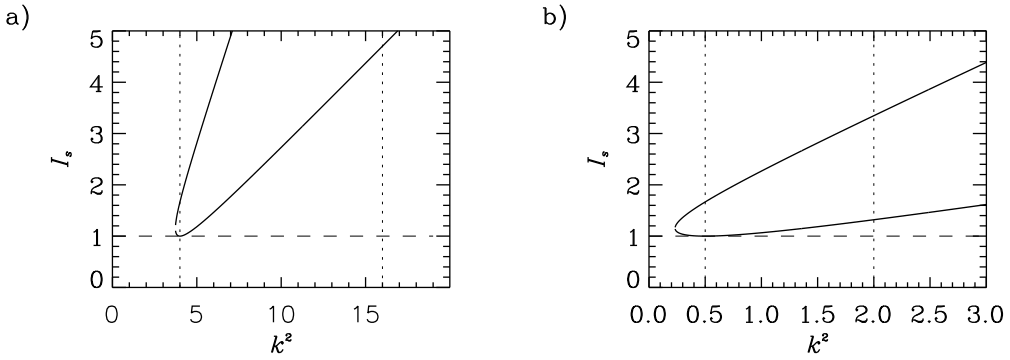

Fig. 24. Marginal stability curve of the homogeneous solution without photonic crystal ($\alpha = 0$) for a) $\theta = -2$ and b) $\theta = 1.5$. The horizontal dashed line shows the threshold for pattern formation. Here $I_s = I$ is the stationary intensity of the homogeneous solution. The two vertical dotted lines indicate the critical k_c and photonic crystal k_{pc} wavenumbers. The vertical distance from the marginal stability curve to the threshold line is an indication of the stability of perturbations corresponding to that wavenumber. [Reprinted figure with permission from Gomila and Oppo (2007). Copyright 2007 by the American Physical Society.]

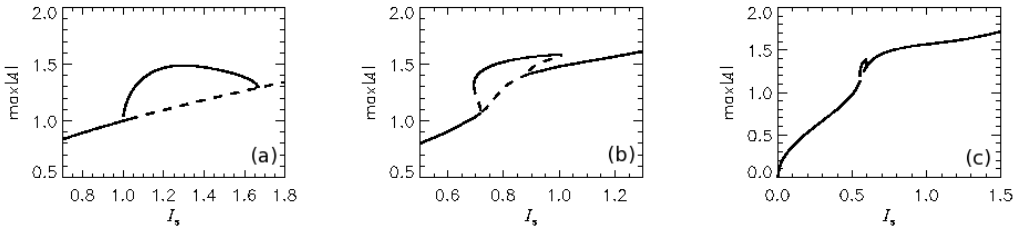

Fig. 25. Bifurcation structure of a pattern at the critical wavenumber in absence (a) and presence of a intracavity photonic crystal of amplitudes (b) 0.2 and (c) 0.4, for $\theta = 1.5$. Solid (dashed) lines correspond to stable (unstable) solutions. Here $I_s = I = |E_0|^2$ is the stationary intensity of the fundamental solution.

Neubecker and Zimmermann (2002). In our case, however, the modulation is in the refractive index instead of in the input pump. Eventually, the fundamental solution becomes stable for all values of the pump except those between two bifurcation points that lead to the pattern with $k = k_c$ (see Fig. 25(b) and (c)). Both bifurcations are subcritical and the fundamental solution stably coexists with the pattern in two different regions of the parameter space. Remarkably, the new region of coexistence between the fundamental and the pattern solution close to the reverse (second) subcritical bifurcation is much larger in parameter space than the first one. For instance, in the system without photonic crystal and for $\theta = 1.5$, pattern and homogeneous solution coexist and are stable for $0.938 < I < 1.0$ while with a gentle periodic modulation (such as with $\alpha = 0.2$) this region shifts to $0.6936 < I < 0.72$ and a completely new and broader region appears for $0.891 < I < 1.006$. We note that the size of the new subcritical region is 0.115 as compared with 0.062 in the case without

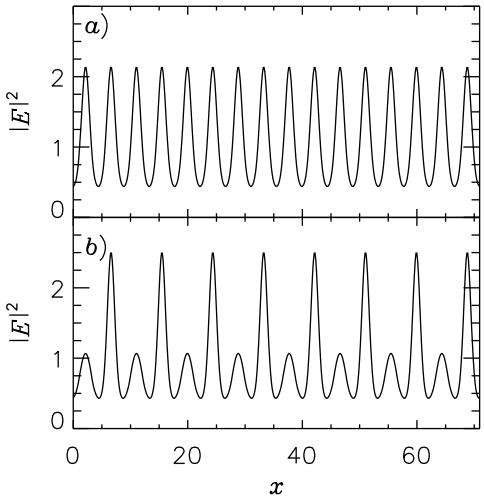

Fig. 26. Intensity profiles of the coexisting a) fundamental and b) pattern solutions for $I = 0.96$ and $\theta = 1.5$ in presence of a periodic modulation of amplitude $\alpha = 0.2$. [Reprinted figure with permission from Gomila and Oppo (2007). Copyright 2007 by the American Physical Society.]

photonic crystal. This is roughly an 85% increment, greatly enhancing the possibility to realize experimentally SDS in a novel regime of bistability due to the ICPC.

In the bistability region between fundamental and pattern solutions close to the reverse subcritical bifurcation, SDS are found. For example for $\alpha = 0.2$ and $\theta = 1.5$, fundamental, pattern and SDS solutions are found in the range $0.891 < I < 1.006$. Fig. 26 shows the intensity profiles of the fundamental and pattern solutions.

The fundamental solution is (trivially) modulated at the same periodicity $\lambda_{pc} = 2\pi/k_{pc}$ of the ICPC, while the pattern has a wavelength equal to $2\lambda_{pc}$ and consists of high peaks on top of a lower modulation at k_{pc}. The coexistence of a fundamental and a pattern solution often leads to the existence of localized solutions (the SDS) that consist of an oscillation of the pattern embedded in the fundamental solution. Fig. 27a shows the profile of a single and double peak SDS generated by seeding peaks of the pattern on the fundamental solution. In order to recover more familiar shapes of SDS, Fig. 27b displays the intensity of the difference between the SDS and the fundamental solution E_{FS}.

As for SDS in photonic systems with no background modulations, a family of (multi-peaked) localized states is found. The fundamental solution, however, is now periodically modulated in space so that the spatial reversibility typical of snaking (Woods and Champneys (1999); Coullet et al. (2000, 2004); McSloy et al. (2002); Burke and Knobloch (2006)) takes place only at some discrete positions. Steady state equations of systems with ICPC contain spatial pe-

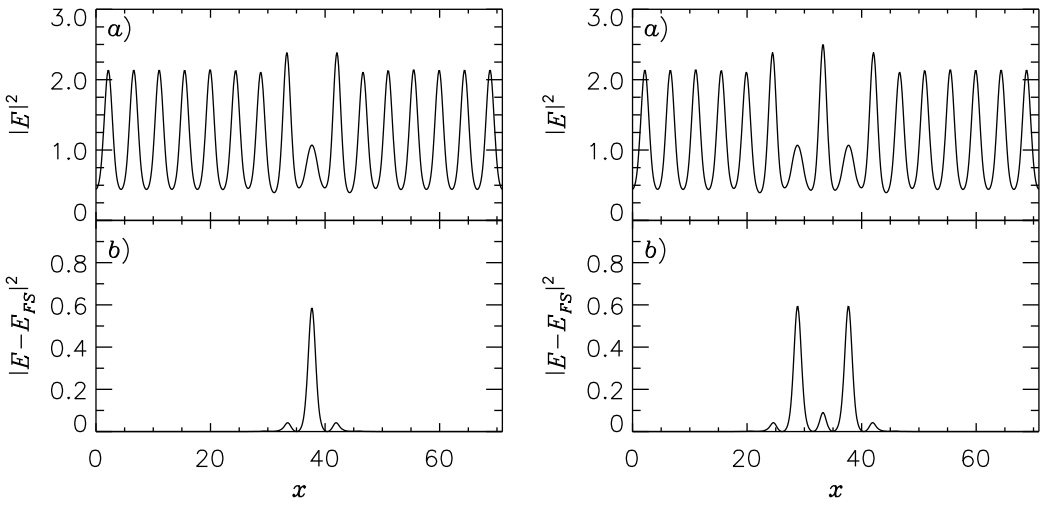

Fig. 27. **Left side:** a) Intensity of a single peak localized structure (SDS) and b) the intensity difference between the SDS and the fundamental solution in the new subcritical regime for large values of I. Here $I = 0.96$, $\theta = 1.5$ and $\alpha = 0.2$. **Right side:** The same but for a two-peaks SDS. [Reprinted figure with permission from Gomila and Oppo (2007). Copyright 2007 by the American Physical Scoiety.]

riodic forcing and are then non-autonoumous. A general theory of snaking describing these situations is still missing but there are strong analogies with standard snaking as described in Sec. 2. For example, the left and right sides of Fig. 28 show snaking-like diagrams of the single and two peak SDS with ICPC, respectively. Note that the single peak SDS does not connect directly with the three peak SDS as commonly observed in homogeneous systems (see left side of Fig. 28). In the ICPC case the line of single peak solutions (1) folds back first through a three unstable peak SDS (3u) and then through a two peak structure with a missing peak (hole) at its center (2a), i.e. a 2-homoclinic orbit. In homogeneous systems N-homoclinic orbits appear in separated bifurcation lines, while in the ICPC system they merge with the fundamental snaking of 1-homoclinic orbits. Similarly, on the right side of Fig. 28 the snaking of the two peak SDS entangles with a 2-homoclinic orbit consisting of two peaks with two holes in the middle (2b). Solutions with separated SDS peaks like (2a) and (2b) of Fig. 28 would have weak stability in systems with homogeneous fundamental solutions since the latter have spatial invariance. (2a) and (2b) acquire robustess in the presence of a spatially modulated fundamental solution like the ICPC system discussed here. The unusual properties and robustness of these and other SDS in photonic systems with ICPC require further generalizations of the snaking theory (see for example Woods and Champneys (1999); Coullet et al. (2000, 2004); Burke and Knobloch (2006)) and are the focus of present research efforts. We note that localized states between two periodic solutions, although of a different nature than the ones investigated here, have also been studied by Bortolozzo et al. (2006).

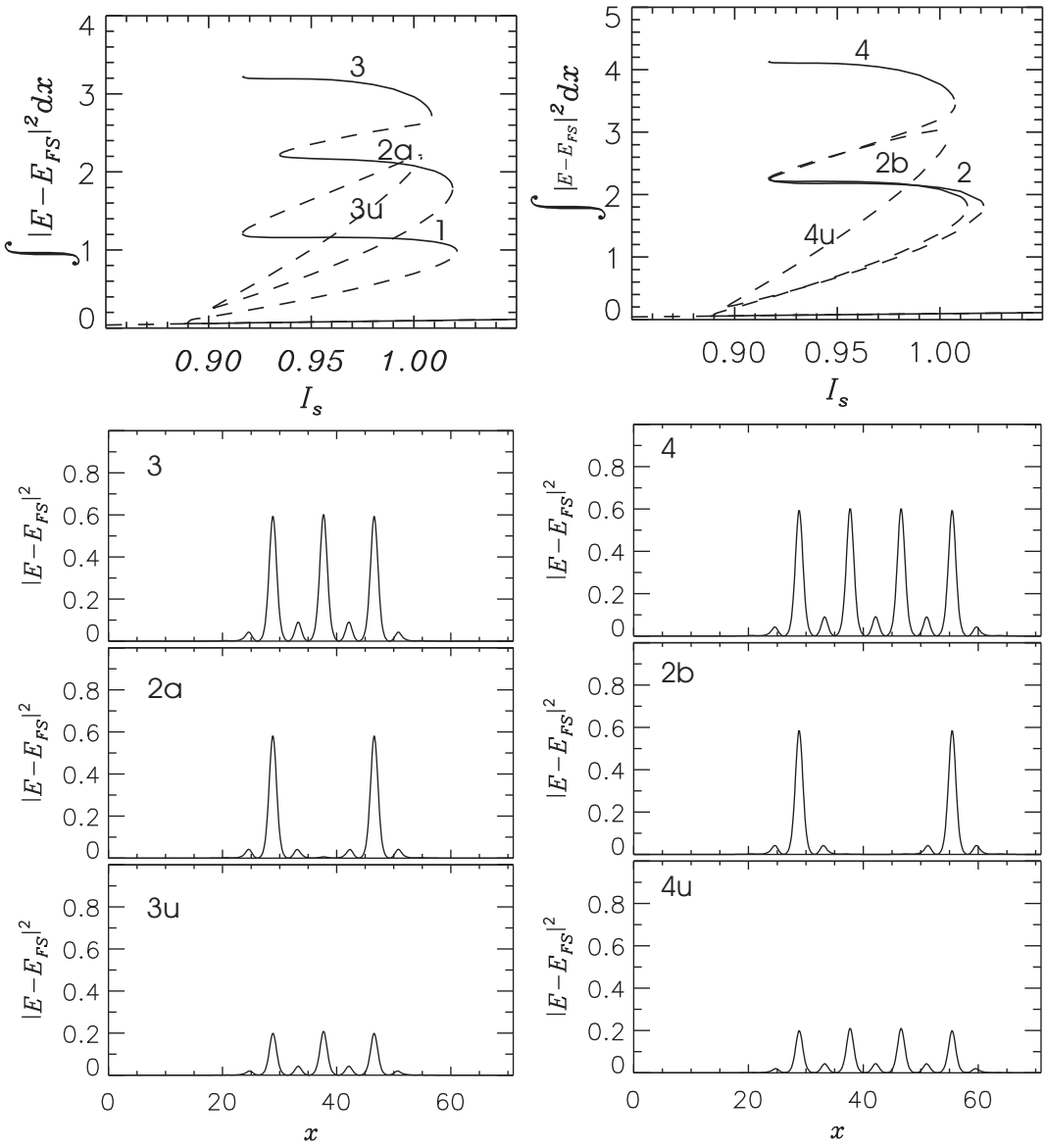

Fig. 28. **Left side:** (a) Snaking-like diagram of a single peak localized structure. Solid (dashed) lines indicate stable (unstable) SDS solutions. The lower panels show the transverse profile of the structures corresponding to lines labeled 3, 2a and 3u respectively. The localized structure corresponding to line 1 is the single peak SDS shown on the left side of figure 27. **Right side:** The same but for the two peaks SDS. In this case, line 2 corresponds to the right side of figure 27. [Reprinted figure with permission from Gomila and Oppo (2007). Copyright 2007 of the American Physical Society.]

SDS in photonic systems with ICPC may be of difficult detection in the near field intensity because of the limited excursion difference between the fundamental and pattern solutions. An easier way to detect the presence of a SDS in the modulated output of an ICPC device is to construct its far field (Fourier transform) distribution in the focal plane of a converging lens (Gomila and Oppo, 2007).

Present results of ICPC induced SDS (see (Gomila and Oppo, 2007)) have been obtained in a prototypical model for optical pattern formation but their validity should extend to other photonic devices more relevant for practical applications such as models for semiconductor absorbers and lasers with feedback. Recent generalizations of ICPC induced SDS have also considered modulations in the longitudinal direction (Staliunas et al., 2008). Finally, remarkable control of the conservative counterparts of SDS in photonic lattices has been recently demonstrated in photorefractive crystals (Fischer et al., 2006)

SDS, snaking, and subcritical bifurcations induced by periodic modulations of parameters are universal features in the study of complex systems and should also be observable in a variety of scientific disciplines outside optics and photonics.

4.2 Discrete Spatial Dissipative Solitons

The most studied discrete model in photonics is the discrete nonlinear Schrödinger (DNLS) equation that describes arrays of optical waveguides. Localized solutions of the DNLS (often referred to as discrete solitons (Christodoulides and Joseph, 1988)) correspond to self-trapped states, have been known for some time (Eilbeck and Johansson, 2003) and have been observed experimentally in semiconductor waveguides (Eisenberg et al., 1998).

The introduction of dissipation in optical DNLS is due to Peschel et al. (2004) who derived a model of spatially coupled cavities obtained by placing mirrors at the open ends of the waveguides (see left panel of Fig. 29) .

The model that they have obtained is given by:

$$\left(id_t + \Delta + i + \alpha|A_n|^2\right) A_n + C\left(A_{n+1} + A_{n-1}\right) = A_{in} \tag{13}$$

where A_n is the normalized complex amplitude of the field in the n-th waveguide, Δ is the detuning from the cavity resonance, $\alpha = \pm 1$ describes a focusing or defocusing nonlinearity, C is the spatial coupling parameter, and A_{in} the driving field. The main difference from the DNLS is the presence of losses due to the partially transmitting mirrors (see the third term in Eq. (13)). Eq. (13) can also be seen as a discretized version of the model by Lugiato and Lefever (1987) and the discrete counterpart of Eq. (11).

The stationary response of a single cavity to the driving field displays bistablity over certain ranges of the input power (see the grey curve in the right panel of Fig. 29). Numerical schemes for the determination and stability of spatial solutions (Firth and Harkness (1998); Harkness et al. (2002); McSloy et al.

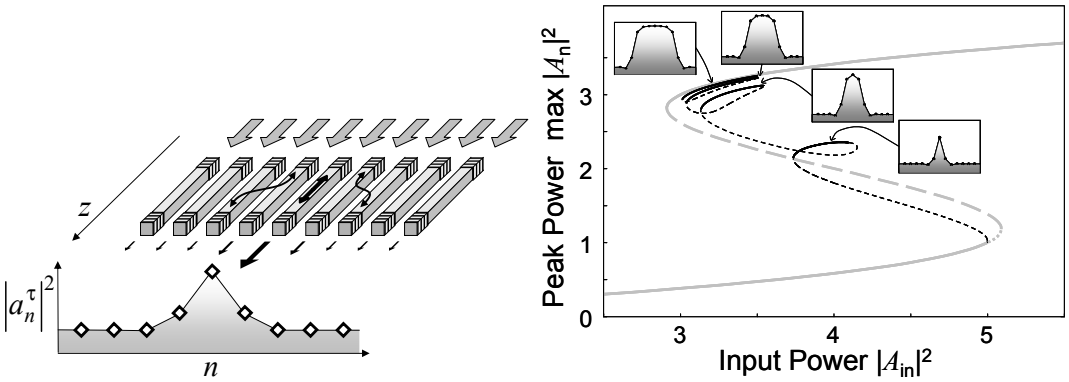

Fig. 29. **Left side:** Coupled cavities formed by a waveguide array with mirrors on each end facets. **Right side:** Stability range of discrete SDS for the defocusing case. Homogeneous solution (grey curve, solid for stable, dashed for unstable, dotted for modulationally unstable), peak power of discrete SDS (black curve, solid for stable and dashed for unstable). The insets show discrete SDS of different orders. Parameters are $\alpha = -1$, $\Delta = 2.5$ and $C = 0.25$. [Reprinted figures with permission from Peschel et al. (2004). Copyright 2004 by the Optical Society of America.]

(2002)) can be used to find discrete SDS at generic values of the coupling C and within the single cavity bistability (see the right panel of Fig. 29). In particular, families of bright discrete SDS of increasing width, dark discrete SDS and even oscillating discrete SDS can be found and tracked in parameter space (Peschel et al., 2004).

Recent work has extended discrete SDS to quadratic nonlinearities (Egorov et al. (2005a); Egorov and Lederer (2008)) and tilted input beams (Egorov et al. (2005b, 2008)). Finally, it is intriguing to note that localized dissipations in the DNLS equation lead to the formation of self-trapped states with strong similarities to the conservative discrete solitons (Livi et al., 2006).

5 Phase Fronts and Locked Spots

In this section, we present a diffractive effect on phase fronts that leads to the formation of SDS in the shape of localized spots due to their locking in space. The presence of spatial oscillations in the front's tails is a prerequisite for locked spots that belongs to the broader universal class of SDS. We will show that diffraction is the mechanism responsible for such oscillations thus making locked spots a universal feature in broad-area nonlinear optics and photonic devices.

Stationary and moving fronts separating two different phases have been at the centre of research in spatio-temporal structures of non-equilibrium systems for a long time (Gunton et al. (1983); Bray (1994)). In systems with non-conserved

order parameters (such as chemical reactions, anti-ferromagnets and optical absorbers), phase separation coarsens with a $t^{1/2}$ power law (Allen and Cahn, 1979) and has been studied via Monte-Carlo simulations (Gunton et al., 1983), coupled map systems (Kapral and Oppo (1986); Oppo and Kapral (1987)), and the integration of partial differential equations (Bray, 1994).

In photonics, locking of moving fronts (labelled as "switching waves") have been introduced by Rosanov and collaborators (Rosanov and Khodova (1990); Rosanov (1991); Fedorov et al. (1991); Rosanov (1996, 2002)) in a saturable absorber system described by:

$$\partial_t E = i\frac{v}{2k}\nabla^2 E - \frac{v\alpha E}{2(1+|E|^2/I_s)} - \frac{v(1-Re^{i\Delta})}{L}E + E_i \tag{14}$$

where E is the intracavity field, v the group velocity, k the wavenumber, α the linear absorption coefficient, I_s the saturation intensity, Δ the detuning, L the cavity length and E_i the input amplitude. A simple renormalization of time, space and field variables leads to the mean field model of a saturable absorber (Lugiato and Oldano (1988); Firth and Scroggie (1996))

$$\partial_\tau E = -(1+i\theta)E - \frac{2C}{1+|E|^2}E + E_I + i\nabla^2 E \tag{15}$$

where $C = \alpha L/4(1-R)$ is the cooperative parameter. Eq. (15) is nothing but Eq. (3) with $\alpha = 0$ and $2C = -\mu$, and has been presented in Sec. 2.1 to discuss the snaking of SDS with (or close to) bistability between a homogeneous and a pattern state for θ different from zero (Firth and Scroggie (1996); Harkness et al. (2002); McSloy et al. (2002)). At resonance ($\theta = 0$), a bistability between two homogeneous states corresponding to high and low absorption respectively, can be found. Fig. 30(a) and (b) (Fig. 30(c) and (d)) show the 1D evolution of the amplitude $|E|$ of Eq. (15) for an initial domain of the low (high) absorption state on a high (low) absorption background, for $C = 10$ and $|E_I|^2 = 0.33$ ($|E_I|^2 = 0.35$). In both cases we observe a rapid formation of traveling fronts between the two stationary states. Since the fronts are sharp spatial structures, diffraction produces spatial oscillations in the approaching of the homogeneous states. The temporal evolution of these domains does not end in a coalescence of fronts which is typical of purely diffusing systems but in the formation of SDS. In particular Fig. 30(b) (Fig. 30(d)) shows a stable peak (trough) on the high (low) absorption background.

From the dynamical point of view, the presence of the fronts' oscillatory tails is a non-trivial spatial feature since it is through their interaction that an entire family of SDS is generated (Coullet et al. (1987); Coullet (2002); Rosanov and Khodova (1990); Rosanov (1996, 2002); Oppo et al. (1999, 2001)). The interaction force between two fronts with oscillatory tails is spatially modulated with attractive (repulsive) locations where its minima (maxima) are located

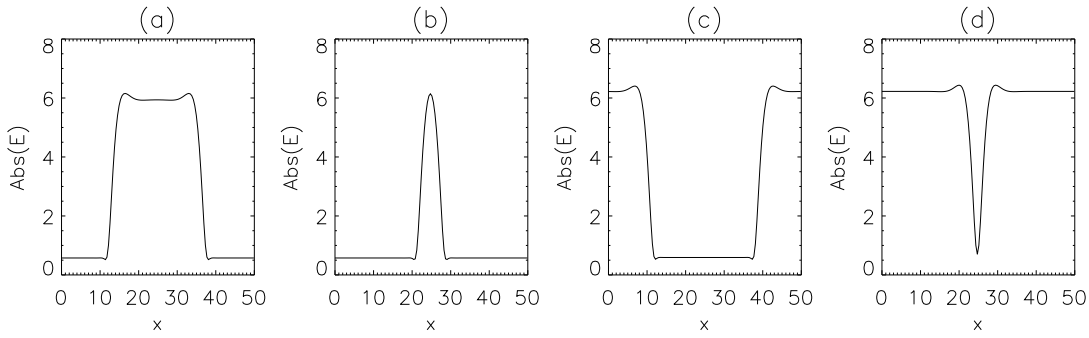

Fig. 30. **Panels (a) and (b):** Dynamical evolution of the field amplitude $|E|$ of a 1D domain of low absorption on a high absorpiton background for the nonlinear absorber equation (15). Parameters are $C = 10$ and $|E_I|^2 = 0.33$. Panel (b) shows the final asymptotic state. **Panels (c) and (d):** Dynamical evolution of the field amplitude $|E|$ of a 1D domain of high absorption on a low absopriton background for the nonlinear absorber equation (15). Parameters are $C = 10$ and $|E_I|^2 = 0.35$. Panel (d) shows the final asymptotic state.

(Coullet et al. (1987); Coullet (2002)). The depth (height) of these minima (maxima) increases the shorter the distance between the fronts.

The dynamics of 2D fronts differ from that in 1D in that curvature effects become important. In order to understand better 2D front dynamics in photonics and to compare it with phase separation in other fields of science, it is essential to maintain full equivalence (in energetic terms) of the two phases in order to avoid nucleation phenomena. For the saturable absorber case of Eq. (15) this is achieved only for a single value of the external amplitude E_I corresponding to the Maxwell construction of the bistable regime. There are however three examples of photonic devices where the equivalence of the bistable states is maintained by symmetry and not by the (single value) choice of a control parametrer. These are the Degenerate Optical Parameric Oscillator (DOPO), the Vectorial Kerr Cavity (VKC) and the model for a Sodium Cell with Feedback Mirror and $\lambda/8$ plate (SCFM). We review here the main features of fronts and locked SDS in these models with a specfic aim of their 2D experimental realization in the SCFM system.

We start with the DOPO model of Oppo et al. (1994) at resonance where fronts and locked spots are easier to discuss:

$$\begin{aligned} \partial_\tau A_0 &= \Gamma\left(-A_0 + E_I - A_1^2\right) + i\nabla^2 A_0 \\ \partial_\tau A_1 &= -A_1 + A_0 A_1^* + 2i\nabla^2 A_1 \,. \end{aligned} \tag{16}$$

These equations describe a pump field A_0 that generates a signal field A_1 at half its frequency via parametric down conversion in a Type-I crystal inside an optical cavity. In Eqs. (16) Γ is the ratio between the cavity decay rates at the pump and signal frequencies and E_I is the (real) amplitude of the input

pump. Eqs. (16) admit three spatially homogenous solutions:

$$A_0^s = E_I - (A_1^s)^2 \qquad A_1^s = 0, \;\; \pm\sqrt{E_I - 1} \tag{17}$$

with the zero solution being stable for $E_I < 1$ and unstable otherwise, while the two-phase solution exists and is stable for $E_I > 1$. The two-phase solutions are mirror images of each other, differ by a phase π and have the same intensity $|A_1^s|^2$. For large values of Γ, Eqs. (16) reduce to a single parametrically driven Ginzburg-Landau equation for the signal field (Oppo et al., 2001) that admits two stationary (Ising) front solutions

$$A_1^f = \pm\sqrt{E_I - 1}\tanh\left(\sqrt{(E_I - 1)/2}\;\; x\right) \tag{18}$$

where x is a generic direction in the 2D transverse plane. Such fronts connect the two homogeneous phase solutions and correspond to straight lines of darkenss since the signal intensity is zero at the core of the front (Trillo et al., 1997). For generic values of Γ, Eqs. (16) are non-variational and an explicit form of the front solution is not available. Accurate numerical methods for the determination of stationary (and travelling) spatial solutions have however found stable fronts of more complicated shape than a simple hyperbolic tangent, over a wide range of values $E_I > 1$ for, for example, $\Gamma = 1$ in Eqs. (16) (Oppo et al., 2001). Decreasing values of Γ from, say, 100 to 1, make the fronts steeper and steeper in space. Narrow optical features diffract and develop oscillatory tails typical of Airy functions. In Fig. 31 oscillatory tails of two (interacting) fronts are clearly visible. Fig. 31 shows six locked SDS for the DOPO system with $E_I = 2$ (Oppo et al., 2001). All these solutions are stationary, stable and coexist with their counterparts obtained by reflection around the horizontal x axis (top-bottom exchange).

In 2D the solutions of Fig. 31 correspond to parallel stripes of alternating phases separated by fronts with "locked" tails. We will refer to them as "locked fronts" although, to be precise, the solutions of Fig. 31 are not exactly locked Ising fronts since the "topological" constrain of zero real and imaginary parts at the core of the front has been removed, the shift from zero being the smaller the broader the spatial soliton is. In 2D it is also natural to consider the evolution of one phase surrounded by the other and the phenomenon of phase separation where domains of the two phases are dynamically equivalent. Since the order parameter is not conserved, we are in the presence of phase separation and not of spinodal decomposition. This has importance when determining the appropriate growth law for the dynamics of the phase domains. In phase separation dynamics, the final state can be homogeneous in one of the two phases or formed by linear stripes of alternating phases.

Fig. 32(a) and (b) show the long term evolution in 2D of the real part and intensity of the signal field of Eqs. (16) for $\Gamma = 1$ and $E_I = 1.5$. Domains of

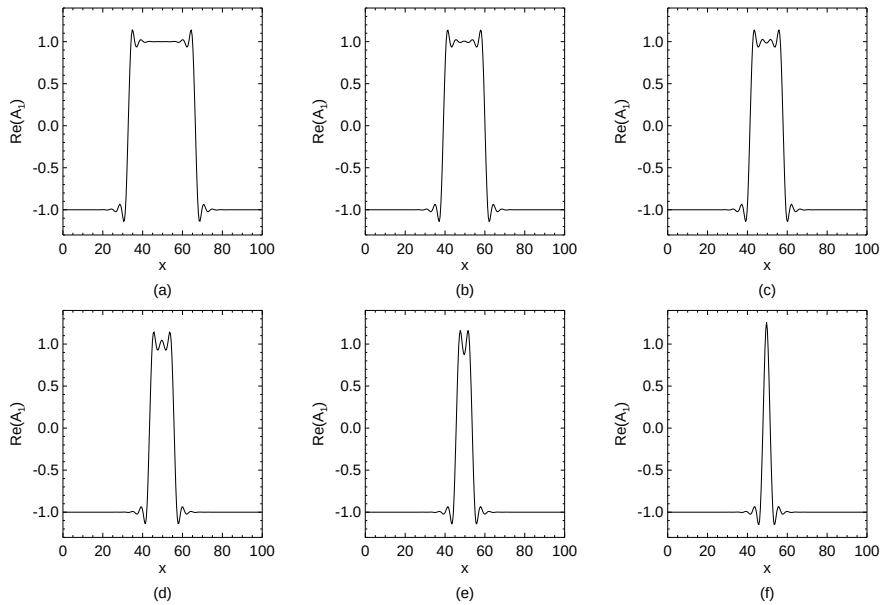

Fig. 31. Stable SDS formed by locked fronts' tails in the DOPO for $\Gamma = 1$ and $E_I = 2$. [Reprinted figure with permission from Oppo et al. (2001). Copyright 2001 by the American Physical Society.]

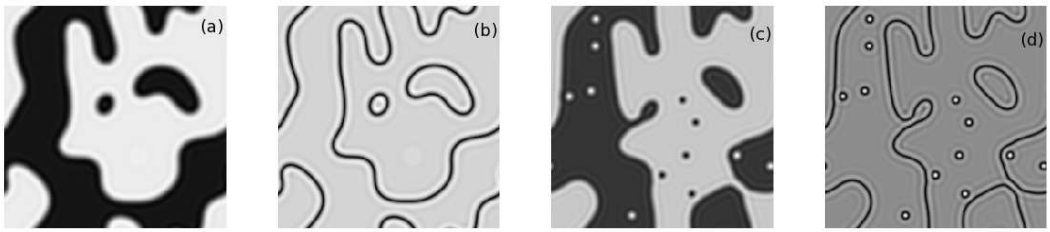

Fig. 32. Snapshot of the 2D evolution of the real part ((a) and (c)) and intensity ((b) and (d)) of A_1 for $\Gamma = 1$ and $E_I = 1.5$ ((a) and (b)) and $E_I = 2.4$ ((c) and (d)).

one phase embedded in the other are clearly visible while the dark lines in the intensity plots correspond to the core of fronts where the signal intensity is close to zero.

It is possible to demonstrate that the dynamics of the phase domains of the DOPO follows the $t^{1/2}$ power law of the Allen and Cahn (1979) coarsening by evaluating the structure factor, i.e. the Fourier transform of the two-point correlation function of the front dynamics. The scaling of the structure factor with $t^{1/2}$ was verified for DOPO fronts by Le Berre et al. (2000); Oppo et al. (2001). We note however that other coarsening laws different from $t^{1/2}$ and observed in some numerical experiments (Le Berre et al. (2000); Tlidi et al. (2000)) are due to boundary and finite size effects. The $t^{1/2}$ Allen-Cahn coarsening law demonstrates that the motion of the fronts in 2D is due to local

curvature, the dynamics of a circular front of radius R being ruled by:

$$d_t R(t) = -\frac{\gamma}{R}\,. \tag{19}$$

The long-term dynamics of DOPO fronts is however modified when the input pump amplitude E_I exceeds a critical value (equal to 2.21 in our simulations). Stable locked fronts of circular shape appear (see Figs. 32(c) and (d)) (Oppo et al. (1999, 2001)) and interrupt the coalescence of closed domains. The theory of locked fronts developed in 1D by Coullet et al. (1987); Coullet (2002) can in fact be generalised to the radial variable (Vladimirov et al., 2002). Stable circular SDS or "locked spots" due to the locking of a front's tail with itself have been observed in numerical simulations of several 2D optical systems (Rosanov and Khodova (1990); Rosanov (1996); Ouchi and Fujisaka (1996); Staliunas and Sánchez-Morcillo (1997); Oppo et al. (1999); Sánchez-Morcillo and Staliunas (1999); Oppo et al. (2001)). When locked spots exist, domains of one phase embedded in the other no longer shrink to zero but collapse onto these SDS solutions. The dark ring of DOPO locked spots is what remains of the circular Ising domain wall separating the two phases. Since localized SDS with circular symmetry have a zero eigenvalue (marginal stability) for translational motion (Firth and Scroggie, 1996), it is possible to move and pin these structures to maxima (or minima) of appropriate spatial modulations of the input pump beam (Scroggie et al., 2005). Arrays of circular locked spots can thus be arranged and manipulated by the operator at will by using background modulations (Scroggie et al., 2005). This procedure represents a first step in the control of fronts separating two phases.

A second system where the symmetry between bistable homogeneous states is maintained is the Vectorial Kerr Resonator (VKR) studied for example by Geddes et al. (1994); Hoyuelos et al. (1998); Gallego et al. (2000):

$$\partial_t E_\pm = -(1+i\theta)E_\pm + i\nabla^2 E_\pm + E_I - \frac{i}{4}\left[|E_\pm|^2 + \beta|E_\mp|^2\right]E_\pm \tag{20}$$

where $E_\pm$ are the circularly polarized field components, E_I is the pump, θ the detuning, and β the cross coupling of the susceptibility tensor. Considering $\theta = 1$ and $\beta = 7$ as in Gomila et al. (2003), it is possible to find bistability between two homogeneous solutions for pump values E_I above 1.5. These two solutions are perfectly equivalent apart from the orientation of the polarization ellipse. Again, fronts connecting these two solutions exist and have oscillatory tails. Oscillatory tails can lock in 1D and 2D leading to locked fronts and SDS of the locked spot kind (Gallego et al. (2000); Gomila et al. (2003)). The relevance of the VKR model is that it demonstrates that polarization domains can display the front phenomena described in the DOPO and be used to characterize phase separation in systems driven by diffraction instead of diffusion.

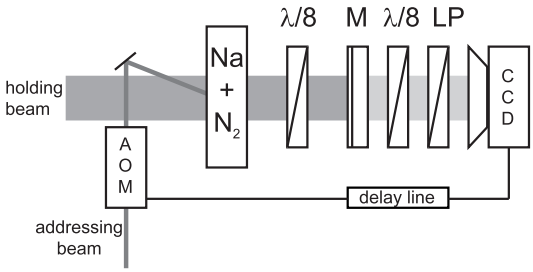

Fig. 33. Schematic experimental setup. $\lambda/8$: $\lambda/8$ retardation plate, M: mirror of high reflectivity, LP: linear polarizer, CCD: charge-coupled device camera, AOM: acousto-optic modulator

Recent experiments performed with a cell of optically pumped sodium vapor in front of a single feedback mirror (see Fig. 33) have used polarization domains as equivalent but separate phases (Pesch et al. (2005, 2007)).

Experimental investigations of moving fronts in 2D are rare. In Pesch et al. (2007) the $t^{1/2}$ growth law for coarsening dynamics between two equivalent homogeneous states as well as its modifications due to SDS formation with locking fronts is observed and investigated in the optical setup of Fig. 33.

The system is formed by a sodium vapor cell injected by a linearly polarized laser that is reflected by a feedback mirror. A $\lambda/8$ retardation plate induces a coupling between the circularly polarized componenets of the light field. This system exhibits a bifurcation leading to two homogeneous states of the orientation (Yabuzaki et al. (1984); Große Westhoff et al. (2000)). There is a broad range of input powers where the two states are coexisting and homogeneous.

The system is initially prepared in a state with negative polarization rotation. Then an addressing beam of circular shape and opposite polarization is switched on by means of an acousto-optic modulator (AOM). A domain of one of the bistable unstructured states embedded into a background of the other state, i.e. a circular front, is thus created. The insets on the left side of Fig. 34 show some sample frames of the time sequence (Pesch et al., 2007). The continuous shrinkage of the domain finally leads to its disappearance within a time period of 4 ms and the initial background state is recovered (see the left side of Fig. 34).

In agreement with Eq. (19) the dynamics is given by $R(t) = [{R_0}^2 - 2\gamma t]^{1/2}$ describing a $t^{1/2}$ law of the Allen and Cahn (1979) type . The experimental shrinking of circular domains shown on the left side of Fig. 34 is described very well by curvature-driven dynamics. This is also confirmed by numerical simulations of a microscopic model of the system with the inclusion of the action of the $\lambda/8$-plate (Große Westhoff et al. (2000)). Numerical data obtained from this model agree very well with the experimental measurements (see the open circles on the left side of Fig. 34).

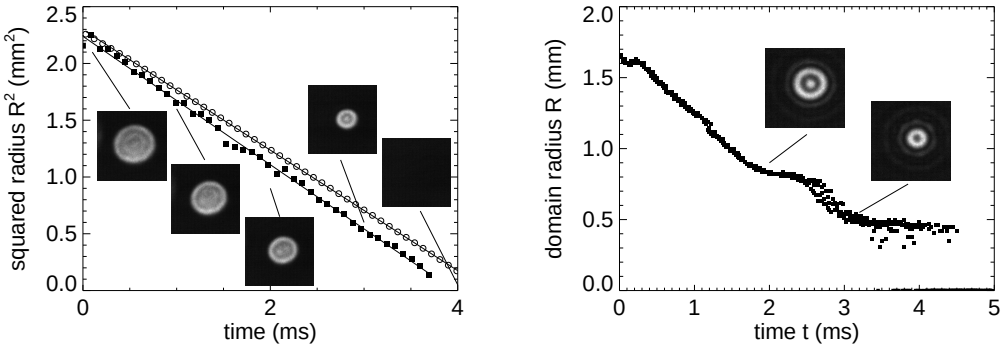

Fig. 34. Contraction of a circular domain (radius squared versus time). **Left side:** Solid squares denote experimental measurements and open circles results from numerical simulations. Straight lines correspond to a linear fitting. The insets show the shape of the beam at different times in a grey-scale ('bright' denoting high intensity). **Right side:** Contraction of a circular domain close to the locking region. Insets show images of the domain at the plateaus of the contraction curve. [Reprinted figure with permission from Pesch et al. (2007). Copyright 2007 by the American Physical Society.]

At higher values of the input power, there is a qualitative change in the dynamical behavior of the domains. The right side of Fig. 34 shows the temporal evolution of a domain at high input powers in an overlay of three sampling sequences at equal values of the parameters. While the monotonic decrease of the domain radius persists, the contraction curve shows a large amount of modulations and two main plateaus. The insets on the right side of Fig. 34 show images of the domains at the radii of the plateaus (Pesch et al., 2007). These structures display pronounced radial oscillations. With increasing input power, the oscillations become more pronounced. If the input power is increased again, stable SDS are observed. The states at which the dynamics nearly stops are interpreted as precursors of the stable SDS due to locking of the fronts (Pesch et al., 2005).

As a result of the tail interactions a discrete family of SDS of different sizes (see the insets on the right side of Fig. 34 for a qualitative example of two SDS of different size) is observed in parameter regions where front velocities are low and locking is promoted by the appearance of pronounced spatial oscillations. The regions of existence of SDS obtained from the experiment and from numerical calculations using a Newton method are presented in the left and central panels of Fig. 35. In contrast to 1D systems where the curvature-driven dynamics is absent, the thresholds for the existence of each SDS have a cusp shape. Above the cusp thresholds, broad regions of SDS existence with large overlaps are observed. Multistability between SDS of different orders and sizes is commonplace.

The main features of the locking phenomenon can be captured phenomeno-

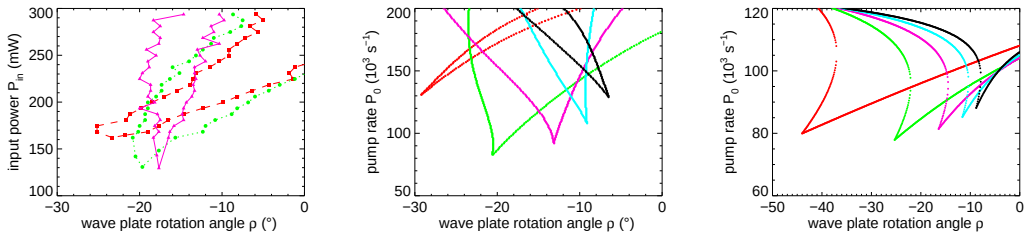

Fig. 35. (Color online) Regions of existence of SDS of different orders and sizes (from first to fifth order: squares (red), circles (green), up-triangles (magenta), down-triangles (cyan), diamonds (black)). Left Panel: experiment. Central Panel: Newton method of the modified model of Große Westhoff et al. (2000). Right Panel: analytic solution of Eq. (21). [Reprinted figure with permission from Pesch et al. (2007). Copyright 2007 by the American Physical Society.]

logically by a modified equation for the radius dynamics. Coullet et al. (1987) have shown that the interaction of two fronts separated by a distance d and due to their oscillatory tails leads to a force of the type $f(d) = g\cos(\beta d)e^{-\alpha d}$. It is therefore reasonable to model the evolution of the radius of a circular domain wall using the following ansatz:

$$d_t R(t) = -\frac{\gamma}{R} + g\cos(\beta 2R)e^{-\alpha 2R}, \tag{21}$$

where α and β are calculated from the real and imaginary parts of the eigenvalues of the most undamped spatial modulations of the homogeneous solutions. β corresponds to the wavenumber of the modulations, α is the decay rate of the modulations and vanishes at the modulational instability point. For simplicity we assume a linear dependence of α with the pump. This simple eikonal equation qualitatively reproduce the bifurcation structure and region of existence in the parameter space of the SDS (see the right panel of Fig. 35). An important feature of this discrete family of SDS is that, at difference with 1-D systems, higher order SDS of larger size may have lower thresholds than the fundamental one (see Pesch et al. (2007)).

Finally, it is important to mention that locked SDS are not the lone circular structures that can be observed in photonic devices. Circular domains of one phase embedded into the other can be stabilised by a careful balance of the curvature shrinking of large droplets and an incipient modulational instability of a flat front that leads to the growth of small domains (Gomila et al. (2001, 2003)). Noise can also have non-trivial effects on locked fronts in space as demonstrated by Rabbiosi et al. (2002, 2003).

6 Applications of cavity solitons

6.1 Positioning of SDS and all-optical memories

As discussed in the previous sections, the single SDS is bistable and can be set and reset by an optical control pulse. Hence a SDS can represent an optical "bit". Due to the fact that they can exist anywhere in the transverse plane of a photonic device, there is, in principle, a multitude of parallel channels available in a single device, thus creating the prospect of controllable memory arrays. Pioneering work putting forward this application of SDS was done in (McDonald and Firth (1990); Rosanov (1991)).

As it was discussed already in Sec. 28, an ideally homogeneous broad-area device possesses translational symmetry (limited by the extent of its apertures, of course) so that spatio-temporal noise will couple to the neutral mode and lead to an erratic motion of the SDS (Firth and Scroggie (1996); Spinelli et al. (1998)). This random motion needs to be suppressed for applications. This can be achieved by introducing intentional parameter modulations that are larger than typical noise amplitudes. The SDS will move in the potential or "landscape" induced by the perturbation until they reach a local minimum where the coupling to the odd neutral mode vanishes (cf. Eq. (4)). In driven systems, this perturbations is most conveniently introduced by phase modulations in the holding beam as originally suggested by Firth and Scroggie (1996). In Fig. 36 a square matrix is defined by a phase modulation in the holding beam driving a cavity with a saturable absorber. A number of SDS is initiated (panel a) which drift in the direction of the local gradients until they reach a local minimum. Here, they form the letters "IT" (panel b). Obviously, the parameter modulation not only sustains the information "IT" against noise but also relaxes the requirements for the aiming accuracy of the WB. It is sufficient to hit the basin of attraction of the pixel sought after.

Trapping of a laser SDS in a phase trough obtained by the displacement of an intra-cavity lens was reported soon afterwards (Taranenko et al., 1997). The first realization of an array of SDS was achieved in sodium vapor with optical feedback (Schäpers et al., 2001). There, SDS were pinned on a 2×2-array by means of the phase and amplitude modulations induced by Fresnel diffraction from a square aperture placed in the holding beam just before the nonlinear medium.

It should be mentioned that though the HB is useful in controlling the position of SDS on the one hand, it can be also the origin of undesired spatial variations. Short-scale spatial noise can be minimized by spatial filtering but long-scale variations due to the spatially varying beam profile are more difficult to avoid

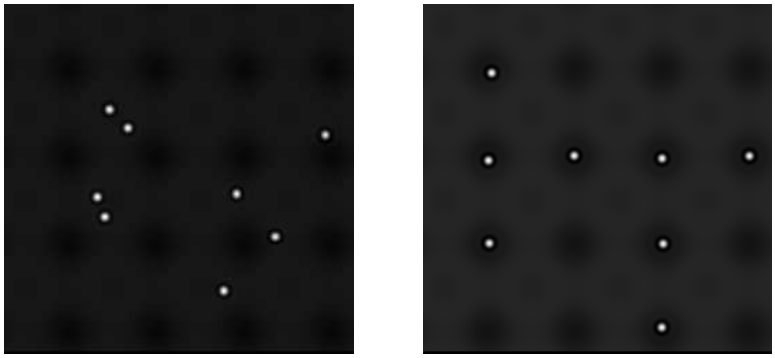

Fig. 36. Numerical simulation: Writing the letters IT in SDS on a square array of pixels created by a phase modulated pump. The real part of the field E is shown at (a) 20 and (b) 800 cavity lifetimes [Reprinted figure with permission from Firth and Scroggie (1996). Copyright 1996 by the American Physical Society.]

(Rosanov (1991); Taranenko and Weiss (2001); Schäpers et al. (2003)). In most experiments a Gaussian intensity profile is used, driving the SDS to the beam center in many cases (Taranenko and Weiss, 2001; Hachair et al., 2009; Elsass et al., 2008). This motion is not only due to the direct action of the amplitude gradient of the HB but also to the phase gradients indirectly induced because the HB creates carriers (or changes the atomic states) which in turn change the refractive index. As a result, the HB creates a background lensing effect, which can either enhance the tendency of the SDS to move towards the center (in a self-focusing situation) or push the SDS towards the beam wings (in a self-defocusing situation). For example, SDS in sodium vapor with single-mirror feedback were found to prefer an equilibrium location on a circle at a finite distance from the beam center due to an interplay of the background phase gradients (pushing outwards) and the amplitude gradients (pushing inwards) (Schäpers et al., 2003). This behavior is apparent for the clusters depicted in Fig. 3.

Forcing a large number of SDS on a pixel array was demonstrated in two independent LCLV experiments (Gütlich et al. (2005); Bortolozzo et al. (2005); Bortolozzo and Residori (2006); Gütlich et al. (2007)). Fig. 37a illustrates that the device as manufactured supports SDS only in a limited area of the aperture (lower left area for the bias conditions chosen) (Gütlich et al., 2007). In addition to this large-scale inhomogeneity there is disorder on small-scales which pins the position of the SDS and leads to the rather irregular positioning apparent in Fig. 37a. We discussed the relevance of disorder for pinning before for the semiconductor cavities. The relative position of SDS is also affected by mutual interactions, if they are close.

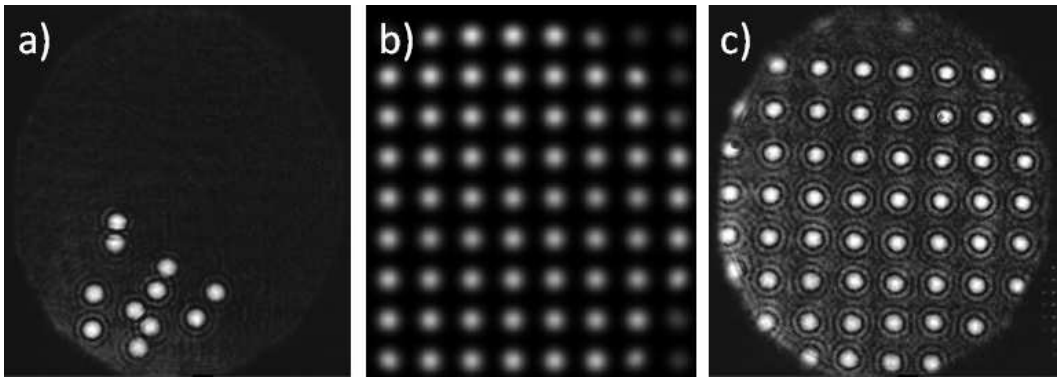

Fig. 37. Position control using an external incoherent amplitude control. a) Spontaneously appearing SDS in the uncontrolled system. b) The spatial distribution of the external control consisting of a square lattice with Gaussian shaped peaks at the lattice points (not exactly to scale with a) and c). c) Array of SDS pinned by the external control. *(Courtesy of C. Cleff*, adapted from Gütlich et al. (2007)).

Then a control signal is generated by a spatial amplitude modulation of an incoherent light beam via a spatial light modulator (SLM) and injected onto the writing side of the LCLV. A phase modulation, controllable in strength and spatial shape, is then added to the coherent beam reflected at the readout side. An example realizing the numerical suggestion of a square lattice in Fig. 36 is shown in Fig. 37b. Fig. 37c shows that an essentially perfect positioning of the SDS can be achieved by this method. Furthermore, the control signal can be dynamically reconfigured and thus the configuration of SDS changed. This degree of freedom is not available in arrays of bistable pixel created by micro-machining. Particularly important is that positioning control by phase modulation of the HB was also achieved in a semiconductor VCA (see Fig. 13, (Pedaci et al., 2006)).

It turns out, however, that it is still a challenge to ensure that all the SDS in these induced arrays are simultaneously bistable (Schäpers et al. (2001); Pedaci et al. (2006); Gütlich et al. (2007)). An interesting and challenging line of research is to compensate inhomogeneities by suitably matched perturbations as achieved for example in LCLV to a great extent (Gütlich et al., 2005). Corresponding experiments are underway for laser SDS (Radwell et al., 2009).

Although the control of the position of SDS has made tremendous progresses in recent years, a competitive optical memory based on SDS remains an objective difficult to achieve. This is due to the fact that the area of SDS is given roughly by a few times the diffraction parameter of a plano-planar cavity, i.e. the minimal area coupled by diffraction. It is given by

$$a = \frac{v_g \lambda_0}{4\pi n_b \kappa}, \tag{22}$$

where v_g is the group velocity of the light, λ_0 the vacuum wavelength, n_b the

background refractive index and κ the field decay rate in the resonator (Spinelli et al., 1998). For typical semiconductor microcavities it is about $(4.2\ \mu\mathrm{m})^2$ and a typical size of a SDS is 10 μm FWHM (Barland et al. (2002); Tanguy et al. (2008a)). SDS at telecommunication wavelengths are expected to be larger by 25%. Decreasing the size of SDS by decreasing the cavity finesse (and hence increasing κ) is an option but this will increase the pumping requirements. There are interesting suggestions to manage SDS size by applying the techniques discussed in Sec. 4, which might enable wavelength size SDS (Staliunas, 2003). Nevertheless, regarding the fact that current hard drives have a capacity of about 500 bits/μm^2 and holographic optical memories reach 800 bits/μm^2, it seems that a SDS memory is only viable if it is directly connected to some all-optical processing applications in a photonic network. The most promising attribute of SDS in terms of applications is their mobility, since it is a feature with which micro-machined pixels cannot compete.

6.2 Exploring the mobility of SDS

As stated above, it seems to be fruitful to exploit the mobility of SDS for applications. Eq. (4) shows that a SDS should drift across the aperture as long as it is not in an extremum of the perturbing potential (Firth and Scroggie (1996); Scroggie et al. (2005)). Indeed drifting SDS were observed in the earliest CSL due to a phase gradient introduced by tilting one of the cavity mirrors (Saffman et al. (1994); Taranenko et al. (1997)). Drift is also induced in feedback system if the feedback mirror is tilted (Schäpers et al., 2001). Both in the CSL and in the feedback system, it was demonstrated that SDS can be ignited at one side of the device aperture and drift across the aperture due to the mirror tilt until they disappear at the opposite side of the device (Taranenko et al. (1997); Schäpers et al. (2001)). This process can be repeated over and over again, if pulses from the WB are repetitively injected. We will show in the next section that this opens up the possibility of an all-optical delay line for an optical bit stream.

Quantitative investigations on SDS drift were recently performed in a LCLV (Gütlich et al. (2007); Cleff et al. (2008)). It was confirmed that the speed of the SDS is proportional to the strength of the imposed phase gradient as expected from Eq. (4), at least on "average". The erratic deviations from the expected ideal behavior in speed and direction of drift are due to background gradients related to imperfections of the device (Gütlich et al. (2007); Cleff et al. (2008)). A modulation in SDS speed can be induced by superimposing a modulation onto a gradient. Strong perturbations can be used to channel the motion of a SDS, also around corners. Barriers can be constructed obstructing SDS motion but leaving a gap open at some desired output port. Many of these features as well as the vectorial character of the projection described by

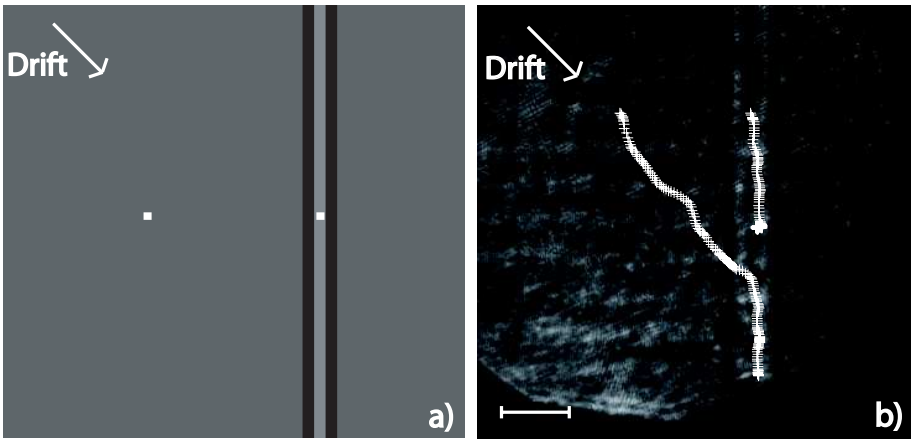

Fig. 38. a) Line structure geometry for a control signal to guide a SDS in a LCLV. b) Trajectories of two SDS. One is guided from the start and stopped by inhomogeneities. Another one moves into the line structure and is guided afterwards. The scale bar in panel b) corresponds to 1 mm. *(Courtesy of C. Cleff*, adapted from Cleff et al. (2008)).

Eq. (4) are nicely illustrated in Fig. 38. The scheme (panel a) illustrates the ideal situation: A phase gradient is introduced which should lead to a drift of SDS from the upper right towards the lower right of the aperture. In addition, a vertical channel is defined which channels SDS motion. Two SDS are positioned in the upper half of the aperture, one "free" to follow the gradient, one starting in the channel. As one can see in Fig. 38b, the "free" SDS follows the gradient with minor corrections due to the small-scale inhomogeneities of the background, whereas the other stays in the channel. Time resolved observations show that the two SDS are always at the same height, i.e. the vertical component of the velocity is the same. Further down the aperture, the channel has a defect at which the second SDS is stopped whereas the first one can enter the channels and is confined by it further downstream. These observations demonstrate very well the potential for controlling SDS via tailor-made external modulations as well as the effects of background inhomogeneities.

6.3 All-optical delay line

Future photonic networks will require all-optical routers (see, e.g., Boyd et al. (2006)) for high-speed switching of data packets. If new packets are arriving when a router is busy, they need to be buffered in an all-optical delay line. Hence delay lines or "slow light" are considered to be key elements of such networks (see, e.g., Boyd et al. (2006); Gauthier (2007); Editorial (2007)) and reference therein for a review). This delay should be continuously tunable. The state-of-the-art techniques for slowing light modify the *longitudinal* group velocity, i.e. they rely on *dispersion*. Nearly all proposed systems use some kind of resonance. The field is too vast to give a proper review here and we refer

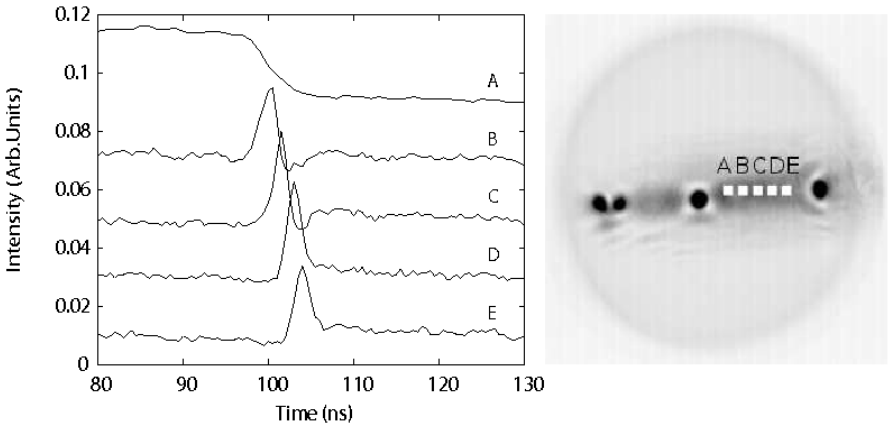

Fig. 39. Passage of a cavity soliton in front of a linear array of 5 detectors (A-E). Left panel: time traces of these detectors, displaced vertically by 0.02 units for clarity. Detector A monitors the point addressed by the writing beam, applied at time $t = 0$. Right panel: positions of the detectors in the transverse plane (indicated by squares). The area monitored by each detector has diameter less than 7.2 μm and the separation between neighboring detectors is 8.9 μm. Also shown is a time-averaged output image of the VCSEL during the CS drift. [Figure reprinted with permission from Pedaci et al. (2008a). Copyright 2008 of the American Institute of Physics.]

to Boyd et al. (2006); Gauthier (2007); Editorial (2007); Pedaci et al. (2008a) and references therein.

As indicated in the previous section, drifting SDS open a fundamentally different access to an optical delay line. Stationary SDS in a cavity can be considered as "stopped light". After a transient, the SDS lives in the cavity forever. By perturbing the symmetry, the SDS acquires a small, controllable *transverse* velocity component leading to a delay between injection and read-out at different positions within the aperture. The idea was probably first formulated by Kuszelewicz (1997) and worked out in Firth (2000). A demonstration of the feasibility of this scheme in a semiconductor microcavity was given recently in Pedaci et al. (2008a).

The system under study was a vertical-cavity amplifier (see Fig. 2). With the help of cylindrical lenses the HB was formed to channel the SDS to a line so that spatio-temporal dynamics can be resolved by a linear array of fast avalanche photodetectors (Fig. 39 right panel). Addressing takes place at point A in the presence of a phase gradient. After the WB is switched off, a SDS forms and drifts along the channel until it decays after some distance, presumably due to inhomogeneities. The drift distance is 36 μm, the delay 7.5 ns, so the average speed is about 4.7 μm/ns (supersonic). This drift speed is of the order of magnitude expected from numerical simulations (Pedaci et al., 2008a).

The performance of a delay line is commonly assessed by two criteria: the

delay-bandwidth product M or, for digital signals, the ratio between delay and the bit period (Tucker et al., 2005) and the maximal operating speed. M corresponds to the maximum number of bits which can be stored in the delay line (Tucker et al., 2005). For the single pulse, M varies but always lies between 2 and 2.5. In previously-described slow-light systems based on dispersion in the vicinity of electronic, vibrational or cavity resonances (Boyd et al. (2006); Gauthier (2007); Editorial (2007); Pedaci et al. (2008a) and the references therein) M is of order of one. This first demonstration of a SDS delay line already compares quite well with these numbers, although $M \approx 50$ was recently demonstrated using slow light in-between two absorptive atomic resonances (Camacho et al., 2006) (with some pulse distortion and significant absorption).

One issue affecting the operation speed of the SDS-based scheme is the possibility of a "traffic jam" at the injection point: Successively written SDS need to be sufficiently apart in order to avoid patterning effects due to interaction between SDS resulting in timing jitter. It turns out that a pulse-to-pulse distance greater than about ten carrier lifetimes is a safe timing leading to a total bandwidth limit of about 90 Mb/s or $M \approx 0.7$, expressed as delay/bit-window. A speed-up of the device can be achieved by shortening the carrier lifetime (Pedaci et al., 2008a).

Larger values of M can be obtained using resonators of larger transverse dimension and improved homogeneity. Although this is challenging (see the next section), there seems to be no barrier, in principle, whereas systems relying on linear resonances suffer from an intrinsic trade-off between the bandwidth of the slow-light transmission window and the steepness of the refractive index spectrum which determines the slowdown factor (Gauthier (2007); Khurgin (2005)). Cascading many devices, e.g. using microresonators, solves this issue for perfect devices (Xia et al. (2007); Notomi et al. (2008)) but in reality one can expect problems due to disorder like for the SDS-based scheme. Also systems operating close to a photonic band-gap (Mok et al., 2006) are sensitive to disorder. It hence appears that all-optical delay lines based on very different approaches share actually many common problems. The only exception seems to be a system which uses wavelength shifting to modify the group velocity (Okawachi et al., 2006). It achieves excellent M, around 1200, but at the cost of significant complexity in the setup. Further developments in this area of research are expected soon.

6.4 Delay lines in a CSL and spontaneous motion of LCS

The demonstration of several schemes of a CSL discussed in Sec. 3 opens interesting new opportunities for a delay-line. First, the fact that no HB is

necessary and hence no fixed phase relationship of the WB to the device simplifies the implementation in applications. Second, lasers can be faster than amplifiers, the relevant time scale is given by the relaxation oscillation or $1/\sqrt{\gamma}$. The absence of the HB is actually an obstacle to obtain drift because it is a convenient way to break the parity without affecting the existence region and properties of the SDS much. Luckily it turns out that CSL models seem to have robust regions in parameter space in which SDS drift spontaneously with a speed depending on parameters. This behavior occurs if an asymmetric internal perturbation of the SDS becomes degenerate with the translational Goldstone mode (Scroggie et al., 2002) and is a general feature of SDS (see, e.g., Bödeker et al. (2003) for reaction-diffusion systems).

In the class A case of a LSA (i.e. an instantaneous response of the medium), the equation of motion for the intra-cavity field has an additional symmetry with respect to a Galilean transformation (Rosanov (2002); Fedorov et al. (2000)). As a consequence, every stationary solution generates a family of moving solutions with arbitrary velocity, which can be selected, e.g. by tilting the WB with respect to the cavity axis. This symmetry is broken by a finite relaxation rate, but moving SDS survive in wide parameter regimes in two-level models (Fedorov et al. (2000); Rosanov (2002)). Moreover, solutions with a periodically modulated velocity and bistability between stationary and moving solutions are found (Fedorov et al., 2000). Spontaneously moving SDS were obtained recently also in the semiconductor model (Prati et al., 2007) discussed earlier (Prati et al., 2009). The speed is some μm/ns, similar to the amplifier case and can be tuned over a large range by changing the pumping of the active medium (Prati et al., 2009).

Spontaneous motion is also found in simplified models of the VCSEL with FSF (Paulau et al., 2008) (between the circle and the cross in Fig. 21). Indeed, drifting localized excitations were found experimentally in the scheme with feedback from a diffraction grating (Tanguy et al., 2008b), where the spatial symmetry is broken by a mechanism similar to a mirror tilt: As indicated in Fig. 16b, the wavefront of the returning beam will be slightly tilted with respect to the one of the emitted beam, if the frequency of the LCS is not exactly at the grating frequency, which is usually not the case (Tanguy et al. (2008b); Paulau et al. (2008); Scroggie et al. (2009)). As we have seen, the phase gradient in the tilted wavefront should induce a drift motion. This drift motion is usually pinned at device inhomogeneities (Tanguy et al. (2008a,b)) but parameters and locations in the device can be found, where a drift is possibly over a distance of 50 μm with an average velocity of about 1.4 μm/ns. These figures of merit are very similar to the amplifier case. During the drift, the tilt angle in far field changes to be slightly off-axis. This is probably an intrinsic feature of drifting LCS (Paulau et al. (2007, 2008)) but further experimental and theoretical studies might be helpful to establish that the drifting structure is a soliton indeed.

As mentioned already at several occasions within this article, the positioning and drifting behavior of SDS is strongly affected by spatial disorder which seems to be unavoidable in all solid-state materials. Though the situation is better in gases – the optical quality of atomic vapors is far superior (Schäpers et al. (2001); Ackemann et al. (2001)) – obviously these are not very attractive for applications for many other reasons. Given that these imperfections are ubiquitous and to a great extent phase perturbations – i.e. not straightforward to detect by simple intensity measurements – one can ask the question whether it is fruitful to turn the argument around and use the extreme sensitivity of SDS to disorder to characterize this disorder. For example, one might characterize the stiffness of a trap, i.e. the curvature around a local minimum of the potential, $\Phi(x) = bx^2/2$, by superimposing a known gradient, $\Phi(x) = ax$, by an external perturbation. The SDS will be displaced by this perturbation to a location where the gradient of the total potential, $(\mathrm{grad}\Phi)(x) = a + bx$ vanishes. From a measurement of the displacement of the SDS, $x_{eq} = -a/b$, the curvature parameter can be obtained (Firth and Ackemann, 2008). Due to the fact that it relies on the (non-Newtonian) force of the background on the SDS, one might refer to it as *soliton force microscopy (SFM)*. Alternatively, one could measure a gradient by injecting a small beam providing a circularly symmetric trap. The spatial resolution of the scheme is about the size of the SDS (i.e. about 10 μm in typical semiconductor microcavities). Atomic force microscopy (AFM) has a much better resolution but is is impossible or at least very tedious to scan areas with a size above one micrometer. Moreover, AFM can only probe surfaces. White-light spectrometers, which are used in many fabrication labs, have typically only a resolution of some hundreds of micrometer and also a spectral resolution not better than a few tens of GHz. Hence the SFM might provide a nice device for the intermediate range.

A variant of the idea sketched above was recently applied to a vertical-cavity amplifier (Pedaci et al., 2008b). The spontaneous emission of the VCSEL used looks fairly homogeneous except for some enhancement due to current crowding at the perimeter (Fig. 40 upper left). A fringe pattern covering the whole aperture is superimposed onto the HB. In the direction perpendicular to the fringe this will pin the SDS, but along each fringe the intensity is uniform, and the SDS are free to move. The system is initially prepared such that several SDS are present and distributed in the device. If a vertical fringe pattern is slowly shifted horizontally across the device, a pattern like the one displayed Fig. 40 (upper center) is obtained. The SDS do not follow a straight horizontal line but move up and down along the stripes during the shift because there are attracting and repelling defects in the device which deflect the motion. This procedure is repeated along the horizontal, vertical, +45, and -45 orientations in the two directions of motion. The video frames acquired for each position

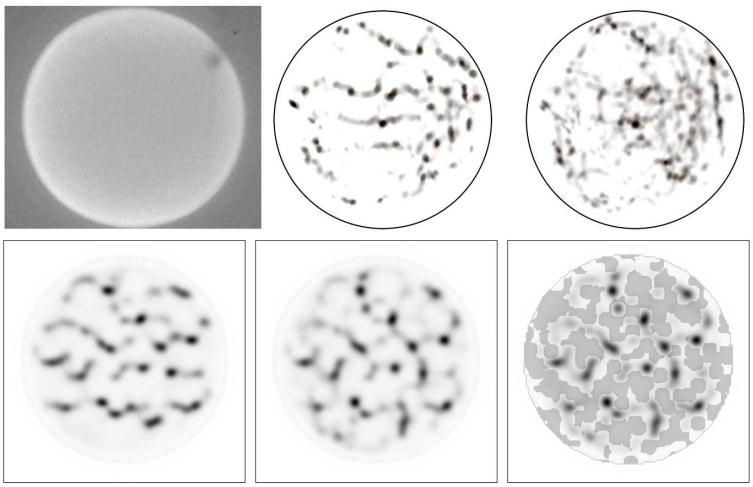

Fig. 40. Illustration of a SFM process in a vertical-cavity amplifier. Upper row: Experiment. Left: spontaneous emission profile of the VCSEL. Center: SDS trajectories when vertical fringes are dragged towards the left. Right: map of the defects in the VCSEL structure as the result of the superposition of several scans. Lower row: Simulations. Left: SDS trajectories in the case of vertical fringes adiabatically shifted toward the left. Center: map of the defects in the VCSEL structure as the result of the superposition of several scans. Right: superposition of the map and the surface defined by $\Theta(x, y) = -2.0$ (Reprinted with permission from Pedaci et al. (2008b). Copyright 2008, American Institute of Physics).

and orientation of the fringes are all added. The resulting image is a gray-scale map of the aperture where black (white) corresponds to high (zero) possibility to host a SDS, i.e., to attractive (repulsive) local inhomogeneities (Fig. 40 upper right). For an ideal defect-free medium, such analysis would result in a homogeneously gray map. The isolated dark points in the real systems correspond probably to local trapping defects (where the blackness gives an indication of its depth), whereas the grayish lines represent probably ridges which serve only as traps for certain orientations of the fringes. Note the contrast of this map to the homogeneous spontaneous emission pattern.

The procedure was repeated in numerical simulations where variations in cavity resonance conditions (total span about 10 GHz in optical frequencies) due to growth fluctuations in active zone, spacer layer or Bragg reflectors were assumed. The experimental observations were reproduced qualitatively (Fig. 40 lower left and center). Furthermore, the simulations allow for a direct comparison between the spatial distribution of the variations and the SFM-map giving support to the expectation that the most prominent inhomogeneities are fluctuations of the cavity resonance. Indeed, it is found that regions with a detuning $\Theta < -2$ are attracting and the others repelling. Also the trap and ridge hypothesis is supported by the simulations. Pedaci et al. (2008a) estimated that a resolution of the order of 300 MHz is reached, which is much better than typical grating spectrometers.

Obviously, one would like to compare the SFM-map with a map of the resonance and gain conditions obtained by linear reflection measurements for a further assessment of accuracy, sensitivity and cost-benefit of this method. In the amplifier scheme, a tunable laser is needed but that is not the case for the VCSEL with frequency-selective feedback making it potentially much simpler. Indeed, first measurements show that similar maps can be obtained also in that system (Radwell et al., 2007).

In any case these experiments illustrate that SDS are sensitive to detuning fluctuations, which translate to a sub-monolayer accuracy. One possibility to reduce this sensitivity is to reduce the finesse at the expense of increasing the driving power. This is to be explored in future studies.

7 Conclusions

In this review we have examined some of the many interesting features and potentially useful properties of spatial dissipative solitons, ranging from fundamental issues in nonlinear science and statistical physics to applications in state-of-the-art photonic devices.

In one transverse dimension a general bifurcation scenario for SDS – subcritical homoclinic snaking – is predicted by a powerful and attractive theory, but experimental evidence is limited and some observations appear to be in contradiction with the theory. From an applications perspective, detailed verification of homoclinic snaking is not really the most pressing issue since multi-stability and controllability of SDS are the real key requirements. In fact, independent (non-interacting) SDS in any homogeneous system naturally give rise to a multi-stable snake-like bifurcation diagram. Inhomogeneities and interactions will inevitably distort and tilt this generalized snake, reducing the degree of multi-stability. The focus, therefore, should be diagnosis and elimination or compensation of these effects. Understanding the interaction of disorder and nonlinearity is thus a key issue which needs to be addressed in semiconductor microcavities for applications. Nevertheless, we envisage that this quest will feed back to give fruitful impetus to fundamental theoretical considerations.

We conjecture that the early work on SDS in periodic media we have reviewed will develop significantly due to the tremendous possibilities in controlling light brought about by photonic crystals. On the fundamental side, the connection between SDS in discrete systems and in those with continuously modulated parameters needs to be worked out in more detail. In experiments, an important milestone will be the observation of discrete and photonic-crystal induced SDS.

We discussed the impressive recent progress in cavity soliton lasers and it is clear that the dynamics, stability, interactions and clustering of SDS in lasers will be important subjects in future years. For applications, robust schemes with monolithic integration of the gain element to the frequency-filter or absorber section need to be developed. There seems to be no obstacle in principle to the transfer of schemes based on 980 nm devices to telecommunication wavelengths. However, material issues are more demanding in that region, and so the implementation is a significant challenge.

Finally, mode-locking of LCS is an intriguing and important future challenge. The longer–term vision is to achieve three-dimensional or spatio-temporal localization (Wise and Di Trapani, 2002) by combining spatial localization in the transverse plane with mode-locking. This would lead to pulses shorter than the extent of the optical system in propagation direction (or shorter than the round-trip time in the temporal domain). We noted that the pulses in mode-locked lasers can be understood as temporal dissipative solitons, at least in some operating regimes (see the contributions in Akhmediev and Ankiewicz (2005a)). It seems likely, however, that mode-locked LCS could be obtained in VCSELs with FSF or with saturable absorption, operating on many external cavity modes. 3D SDS in a cavity (previously termed *cavity light bullets* (Brambilla et al., 2004)) could thus be achieved, at least in the "average–soliton" sense. Furthermore, telecommunication pulse rates (10 Gb/s and beyond) ought to be feasible in such systems.

Acknowledgements

We gratefully acknowledge funding from the European Union under the FunFACS IST-STREP project 004868, the Deutsche Forschungsgemeinschaft, the British Council and the Royal Society. Over the years we have benefitted from collaborations and illuminating discussions with many colleagues, research assistants and PhD students. Of these, contributions from A. Scroggie, D. Gomila, W. Lange, and, collectively, our FunFACS partners are gratefully acknowledged. Finally our special thanks go to all who have kindly supplied diagrams, figures and permissions.

References

Abraham, N. B., Firth, W. J., 1990. Overview of transverse effects in nonlinear-optical systems. J. Opt. Soc. Am. B 7, 951–961.

Ackemann, T., Aumann, A., Große Westhoff, E., Logvin, Y. A., Lange, W., 2001. Polarization degrees of freedom in optical pattern forming systems:

alkali metal vapor in a single-mirror arrangement. J. Opt. B: Quantum Semiclass. Opt. 3, S124–S132.

Ackemann, T., Lange, W., 2001. Optical pattern formation in alkali metal vapors: Mechanisms, phenomena and use. Appl. Phys. B 72, 21–34.

Ackemann, T., Radwell, N., Jäger, R., 2009. IEEE/LEOS Winter Topical Meetings, Innsbruck, Austria, Jan 12-14, 2009. Optically controllable microlasers and 3d light confinement based on cavity solitons in vertical-cavity devices. Paper TuB2. 2.

Ackemann, T., Sondermann, M., 2005. Polarization dynamics in vertical-cavity surface emitting lasers. In: Calderon, O. G., Guerra, J. M. (Eds.), Trends in Spatiotemporal Dynamics in Lasers. Instabilities, Polarization Dynamics, and Spatial Structures. Research Signpost, Keralia, pp. 82–110.

Akhmediev, N., Ankiewicz, A. (Eds.), 2005a. Dissipative solitons. Vol. 661 of Lecture Notes in Physics. Springer, Berlin.

Akhmediev, N., Ankiewicz, A., 2005b. Dissipative solitons in the complex Ginzburg-Landau and Swift-Hohenberg equations. In: Akhmediev, N., Ankiewicz, A. (Eds.), Dissipative Solitons. Lecture Notes in Physics. Springer, Berlin, pp. 1–17.

Akhmediev, N., Ankiewicz, A. (Eds.), 2008. Dissipative Solitons: From Optics to Biology and Medicine. Vol. 751 of Lecture Notes in Physics. Springer.

Allen, S., Cahn, J., 1979. A microscopic theory for antiphase boundary motion and its application to antiphase domain coarsening. Acta Metall. 27, 1085–1095.

Arecchi, F. T., Boccaletti, S., Ramazza, P. L., 1999. Pattern formation and competition in nonlinear optics. Phys. Rep. 318, 1–83.

Bache, M., Prati, F., Tissoni, G., Kheradmand, R., Lugiato, L. A., Protsenko, I., Brambilla, M., 2005. Cavity soliton laser based on vcsel with saturable absorber. Appl. Phys. B 81, 913–920.

Barbay, S., Hachair, X., Elsass, T., Sagnes, I., Kuszelewicz, R., 2008. Homoclinic snaking in a semiconductor-based optical system. Phys. Rev. Lett. 101, 253902.

Barbay, S., Ménesguen, Y., Hachair, X., Leroy, L., Sagnes, I., Kuszelewicz, R., 2006. Incoherent and coherent writing and erasure of cavity solitons in an optically pumped semiconductor amplifier. Opt. Lett. 31, 1504–1507.

Barbay, S., Ménesguen, Y., Sagnes, I., Kuszelewicz, R., 2005. Cavity optimization of optically pumped broad-area microcavity lasers. Appl. Phys. Lett. 86, 151119.

Barland, S., 2008. Personal Communication.

Barland, S., Tredicce, J. R., Brambilla, M., Lugiato, L. A., Balle, S., Giudici, M., Maggipinto, T., Spinelli, L., Tissoni, G., Knödel, T., Miller, M., Jäger, R., 2002. Cavity solitons as pixels in semiconductors. Nature 419, 699–702.

Bazhenov, V. Y., Taranenko, V. B., Vasnetsov, M. V., 1991. Transverse optical effects in bistable active cavity with nonlinear absorber on bacteriorhodopsin. Proc. SPIE 1840, 183–193.

Bödeker, H. U., Röttger, M. C., Liehr, A. W., Frank, T. D., Friedrich, R.,

Purwins, H. G., 2003. Noise-covered drift bifurcation of dissipative solitons in a planar gas-discharge system. Phys. Rev. E 67, 056220.
Bortolozzo, U., Clerc, M. C., Falcon, C., Residori, S., Rojas, R., 2006. Localized states in bistable pattern-forming systems. Phys. Rev. Lett. 96, 214501.
Bortolozzo, U., Clerc, M. C., Residori, S., 2008. Local theory of the slanted homoclinic snaking bifurcation diagram. Phys. Rev. E 78, 036214.
Bortolozzo, U., Ramazza, P. L., Boccaletti, S., 2005. Dissipative solitons driving and bound state control via parameter gradients. Chaos 15, 013501.
Bortolozzo, U., Residori, S., 2006. Storage of localized structure matrices in nematic liquid crystals. Phys. Rev. Lett. 96, 037801.
Boyd, R. W., Gauthier, D., Gaeta, A. L., 2006. Applications of slow light in telecommunications. Opt. & Photon. News 17 (4), 18–23.
Brambilla, M., Lugiato, L. A., Stefani, M., 1996. Interaction and control of optical localized structures. Europhys. Lett. 34, 109–114.
Brambilla, M., Maggipinto, T., Patera, G., Columbo, L., 2004. Cavity light bullets: Three-dimensional loclaized structures in a nonlinear optical resonator. Phys. Rev. Lett. 93, 203901.
Bray, A., 1994. Theory of phase-ordering kinetics. Adv. Phys. 43, 357–459.
Burke, J., Knobloch, E., 2006. Localized states in the generalized Swift-Hohenberg equation. Phys. Rev. E 73, 056211.
Burke, J., Knobloch, E., 2007. Snakes and ladders: Localized states in the SwiftHohenberg equation. Phys. Lett. A 360, 681–688.
Camacho, R. M., Pack, M. V., Howell, J. C., 2006. Low-distortion slow light using two absorption resonances. Phys. Rev. A 73, 063812.
Champneys, A. R., 1998. Homoclinic orbits in reversible systems and their applications in mechanics, fluids and optics. Physica D 112, 158–186.
Chow, W. W., Koch, S. W., Sargent III, M., 1994. Semiconductor laser physics. Springer, New York.
Christodoulides, D., Joseph, R., 1988. Discrete self-focusing in nonlinear arrays of coupled waveguides. Opt. Lett. 13, 794–796.
Cleff, C., Gütlich, B., Denz, C., 2008. Gradient induced motion control of drifting solitary structures in a nonlinear optical single feedback experiment. Phys. Rev. Lett. 100, 233902.
Clerc, M. G., Falcon, C., 2005. Localized patterns and hole solutions in one-dimensional extended systems. Physica A 356, 48–53.
Columbo, L., Gil, L., Tredicce, J., 2008. Could cavity solitons exist in bidirectional ring lasers? Opt. Lett. 33, 995–997.
Coullet, P., 2002. Localized patterns and fronts in nonequilibrium systems. Int. J. Bif. Chaos 12 (11), 2445–2457.
Coullet, P., Elphick, C., Repaux, D., 1987. Nature of spatial chaos. Phys. Rev. Lett. 58, 431–434.
Coullet, P., Gil, L., Rocca, F., 1989. Optical vortices. Opt. Commun. 73, 403–408.
Coullet, P., Riera, C., Tresser, C., 2000. Stable static localized structures in one dimension. Phys. Rev. Lett. 84, 3069–3072.

Coullet, P., Riera, C., Tresser, C., 2004. A new approach to data storage using localized structures. Chaos 14, 193–198.

Cross, M. C., Hohenberg, P. C., 1993. Pattern formation outside of equilibrium. Rev. Mod. Phys. 65, 851–1112.

D'Alessandro, G., Firth, W. J., 1991. Spontaneous hexagon formation in a nonlinear optical medium with feedback mirror. Phys. Rev. Lett. 66, 2597–2600.

Dawes, A. M. C., Illing, L., Clark, S. M., Gauthier, D. J., 2005. All-optical switching in rubidium vapor. Science 308, 672–674.

Dawes, J. H. P., 2008. Localized Pattern Formation with a Large-Scale Mode: Slanted Snaking. SIAM J. Dyn. Sys 7, 186.

Drummond, P. D., Haelterman, M., Vilaseca, R., 2004. Editorial: Optical solitons. J. Opt. B: Quantum Semiclass. Opt. 6 (5), S159.

Editorial, 2007. Taking light slow. Nature Phot. 2, 447.

Egorov, O., Lederer, F., 2008. Midband solitons in an array of quadratically nonlinear cavities. Opt. Express 16, 6050.

Egorov, O., Lederer, F., Stagliunas, K., 2008. Subdiffractive discrete cavity solitons. Opt. Lett. 32, 2106–2108.

Egorov, O., Peschel, U., Lederer, F., 2005a. Discrete quadratic cavity solitons. Phys. Rev. E 71, 056612.

Egorov, O., Peschel, U., Lederer, F., 2005b. Mobility of discrete cavity solitons. Phys. Rev. E 72, 066603.

Eilbeck, J., Johansson, M., 2003. The discrete nonlinear Schrödinger equation – 20 years on. In: Vazquez, L. e. a. (Ed.), Proc. of the 3rd Conf. Localization & Energy Transfer in Nonlinear Systems (June 17-21 2002, San Lorenzo de El Escorial Madrid). World Scientific, New Jersey, pp. 44–68.

Eisenberg, H. S., Silberberg, Y., Morandotti, R., Boyd, A. R., Aitchison, J. S., 1998. Discrete spatial optical solitons in waveguide arrays. Phys. Rev. Lett. 81 (16), 3383–6.

Elsass, T., Barbay, S., Gauthron, K., Beaudoin, G., Sagnes, I., Kuszelewicz, R., Sep 29 - Oct 2, 2008 2008. Monolithic vertical cavity laser with a saturable absorber: towards an integrated cavity soliton laser.

Esteban-Martín, A., Martínez-Quesada, M., Taranenko, V. B., Roldán, E., de Valcárcel, G. J., 2006. Bistable phase locking of a nonlinear optical cavity via rocking: Transmuting vortices into phase patterns. Phys. Rev. Lett. 97, 093903.

Etrich, C., Michaelis, D., Lederer, F., 2002. Bifurcations, stability, and multistability of cavity solitons in parametric downconversion. J. Opt. Soc. Am. B 19, 792–801.

Etrich, C., Peschel, U., Lederer, F., 1997. Solitary waves in quadratically nonlinear resonators. Phys. Rev. Lett. 79, 2454–2457.

Fedorov, S. V., Khodova, G. V., Rosanov, N. N., 1991. Soliton-like field transverse structures in passive and active optical bistable systems. Proc. SPIE 1840, 208–215.

Fedorov, S. V., Vladimirov, A. G., Khodova, G. V., Rosanov, N. N., 2000.

Effect of frequency detunings and finite relaxation rates on laser localized structures. Phys. Rev. E 61, 5814–5824.
Firth, W. J., 1990. Spatial instabilities in a Kerr medium with single feedback mirror. J. Mod. Opt. 37, 151–153.
Firth, W. J., 2000. Processing information with arrays of spatial solitons. Proc. SPIE 4016, 388–394.
Firth, W. J., 2001. Theory of cavity solitons. In: Boardman, A. D., Sukhorukov, A. P. (Eds.), Soliton-Driven Photonics. Kluwer Academic Publishers, London, pp. 459–485.
Firth, W. J., Ackemann, T., 2008. Unpublished.
Firth, W. J., Columbo, L., Maggipinto, T., 2007a. On homoclinic snaking in optical systems. Chaos 17, 037115.
Firth, W. J., Columbo, L., Scroggie, A. J., 2007b. Proposed resolution of theory-experiment discrepancy in homoclinic snaking. Phys. Rev. Lett. 99, 104503.
Firth, W. J., Harkness, G. K., 1998. Cavity solitons. Asian J. Phys. 7, 665–677.
Firth, W. J., Harkness, G. K., Lord, A., McSloy, J. M., Gomila, D., Colet, P., 2002. Dynamical properties of two-dimensional Kerr cavity solitons. J. Opt. Soc. Am. B 19 (4), 747–752.
Firth, W. J., Scroggie, A. J., 1994. Spontaneous pattern formation in an absorptive system. Europhys. Lett. 26, 521–526.
Firth, W. J., Scroggie, A. J., 1996. Optical bullet holes: robust controllable localized states of a nonlinear cavity. Phys. Rev. Lett. 76, 1623–1626.
Firth, W. J., Weiss, C. O., 2002. Cavity and feedback solitons. Opt. Photon. News 13 (2), 54–58.
Fischer, A. J., Chow, W. W., Choquette, K. D., Allerman, A. A., Geib, K. M., 2000a. Q-switched operation of a coupled-resonator vertical-cavity laser diode. Appl. Phys. Lett. 76, 1975–1977.
Fischer, A. P. A., Andersen, O. K., Yousefi, M., Stolte, S., Lenstra, D., 2000b. Experimental and theoretical study of filtered optical feedback in a semiconductor laser. IEEE J. Quantum Electron. 36 (3), 375–384.
Fischer, R., Träger, D., Neschev, D., Sukhorulov, A., Krolikowski, W., Denz, C., Kivshar, Y., 2006. Reduced-symmetry two-dimensional solitons in photonic lattices. Phys. Rev. Lett. 96, 023905.
Gallego, R., Miguel, M. S., Toral, R., 2000. Self-similar domain growth, localized structures, and labyrinthine patterns in vectorial Kerr resonators. Phys. Rev. E 61, 2241–4.
Gauthier, D. J., 2007. Solitons go slow. Nature Photonics, 92–93.
Geddes, J., Indik, R., Moloney, J., Firth, W. J., 1994. Hexagons and squares in a passive nonlinear optical system. Phys. Rev. A 50, 3471–3485.
Genevet, P., Barland, S., Giudici, M., Tredicce, J. R., 2008. Cavity soliton laser based on mutually coupled semiconductor microresonators. Phys. Rev. Lett. 101, 123905.
Gibbs, H. M., 1985. Optical Bistability: Controlling Light with Light. Academic Press, Orlando.

Giudici, M., Balle, S., Ackemann, T., Barland, S., Tredicce, J. R., 1999. Effects of optical feedback on vertical-cavity surface-emitting lasers: Experiment and model. J. Opt. Soc. Am. B 16, 2114–2123.

Gomila, D., Colet, P., Oppo, G.-L., San Miguel, M., 2001. Stable droplets and growth laws close to the modulational instability of a domain wall. Phys. Rev. Lett. 87, 194101.

Gomila, D., Colet, P., San Miguel, M., Scroggie, A., Oppo, G.-L., 2003. Stable droplets and dark-ring cavity solitons in nonlinear optical devices. IEEE J. Quantum Electron. 39, 238–244.

Gomila, D., Oppo, G.-L., 2005. Coupled-mode theory for photonic band-gap inhibition of spatial instabilities. Phys. Rev. E 72, 016614.

Gomila, D., Oppo, G.-L., 2007. Subcritical patterns and dissipative solitons due to intracavity photonic crystals. Phys. Rev. A 76, 043823.

Gomila, D., Scroggie, A. J., Firth, W. J., 2007. Bifurcation structure of dissipative solitons. Physica D 227, 70–77.

Gomila, D., Zambrini, R., Oppo, G.-L., 2004. Photonic band-gap inhibition of modulational instabilities. Phys. Rev. Lett. 92, 253904.

Große Westhoff, E., Kneisel, V., Logvin, Y. A., Ackemann, T., Lange, W., 2000. Pattern formation in the presence of an intrinsic polarization instability. J. Opt. B: Quantum Semiclass. Opt. 2, 386–392.

Grynberg, G., 1994. Drift instability and light-induced spin waves in an alkali vapor with a feedback mirror. Opt. Commun. 109, 483–486.

Gunton, J. D., Miguel, M. S., Sahni, P. S., 1983. The dynamics of first order phase transitions. In: Domb, C., Lebowitz, J. (Eds.), Phase transitions and critical phenomena. Academic Press, London, pp. 269–466.

Gütlich, B., Zimmermann, H., Cleff, C., Denz, C., 2007. Dynamic and static position control of optical feedback solitons. Chaos 17, 037113.

Gütlich, B., Zimmermann, H., Denz, C., Neubecker, R., Kreuzer, M., Tschudi, T., 2005. Forcing and control of localized states in optical single feedback systems. Appl. Phys. B 81, 927936.

Hachair, X., Barland, S., Furfaro, L., Giudici, M., Balle, S., Tredicce, J., Brambilla, M., Maggipinto, T., Perrini, I. M., Tissoni, G., Lugiato, L., 2004. Cavity solitons in broad-area vertical-cavity surface-emitting lasers below threshold. Phys. Rev. A 69, 043817.

Hachair, X., Furfaro, L., Javaloyes, J., Giudici, M., Balle, S., Tredicce, J., Tissoni, G., Lugiato, L., Maggipinto, T., Brambilla, M., 2005. Cavity-solitons switching in semiconductor microcavities. Phys. Rev. A 72, 013815–1–4.

Hachair, X., Pedaci, F., Caboche, E., Barland, S., Giudici, M., Tredicce, J. R., Prati, F., Tissoni, G., Kheradmand, R., Lugiato, L. A., Protsenko, I., Brambilla, M., 2006. Cavity solitons in a driven VCSEL above threshold. IEEE J. Sel. Top. Quantum Electron. 12, 339–351.

Hachair, X., Tissoni, G., Thienpnt, H., Panajotov, K., 2009. Linearly polarized bistable localized structure in medium-size vertical-cavity surface-emitting lasers. Phys. Rev. A 79, 011801(R).

Haelterman, M., Vitrant, G., 1992. Drift instability and spatiotemporal dissi-

pative structures in a nonlinear Fabry- Perot resonator under oblique incidence. J. Opt. Soc. Am. B 9, 1563–1570.

Harkness, G. K., Firth, W. J., Oppo, G.-L., McSloy, J. M., 2002. Computationally determined existence and stability of transverse structures: I. periodic optical patterns. Phys. Rev. E 66, 046605.

Henry, C. H., 1982. Theory of the linewidth of semiconductor lasers. IEEE J. Quantum Electron. 18, 259–264.

Hoyuelos, M., Colet, P., Miguel, M. S., Walgraef, D., 1998. Polarization patterns in Kerr media. Phys. Rev. E 58, 2992–3007.

IST-STREP 004868, 2005-2008. Fundamentals, Functionalities and Applications of Cavity Solitons (FunFACS). www.funfacs.org.

Jakobsen, P. K., Moloney, J. V., Newell, A. C., Indik, R., 1992. Space-time dynamics of wide-gain-section lasers. Phys. Rev. A 45, 8129–8137.

Jasim, K., Zhang, Q., Nurmikko, A. V., Ippen, E., Mooradian, A., Carey, G., Ha, W., 2004. Picosecond pulse generation from passively modelocked vertical cavity diode laser at up to 15 ghz pulse repetition rate. Electron. Lett. 40, 34–35.

Jiang, Z., McCall, M., 1992. A theoretical study of coupled laser systems. J. Mod. Opt. 39, 159–172.

K. S. Thornburg, J., Möller, M., Roy, R., Carr, T. W., Li, R.-D., Erneux, T., 1997. Chaos and coherence in coupled lasers. Phys. Rev. E 55, 3865–3869.

Kapral, R., Oppo, G.-L., 1986. Competition between stable states in spatially distributed systems. Physica D 23, 455–463.

Kawaguchi, H., 1994. Bistabilities and Nonlinearities in Laser Diodes. Artech House Publishers.

Kerner, B. S., Osipov, V. V., 1989. Autosolitons. Sov. Phys. Usp. 32, 101–138.

Khurgin, J. B., 2005. Adiabatically tunable optical delay lines and their performance limitations. Opt. Lett. 30, 2788–2791.

Kozyreff, G., Chapman, S. J., 2006. Asymptotics of large bound states of localized structures. Phys. Rev. Lett. 97, 044502.

Kreuzer, M., Gottschilk, H., Tschudi, T., Neubecker, R., 1991. Structure formation and self-organization phenomena in bistable optical elements. Mol. Cryst. Liquid Cryst. 207, 219–230.

Kuszelewicz, R., 1997. Unpublished.

Lang, R., Kobayashi, K., 1980. External optical feedback effects on semiconductor injection laser properties. IEEE J. Quantum Electron. 16, 347–355.

Le Berre, M., Leduc, D., Ressayre, E., Tallet, A., 1999. Striped and circular domain walls in the DOPO. J. Opt. B: Quantum Semiclass. Opt. 1, 153–160.

Le Berre, M. L., Ressayre, E., Tallet, A., 2000. Kinetics of domain walls in the degenerate optical parametric oscillator. J. Opt. B: Quantum Semiclass. Opt. 2, 347–352.

Lega, J., Moloney, J., Newell, A., 1994. Swift-Hohenberg equation for lasers. Phys. Rev. Lett. 73, 2978–2981.

Livi, R., Franzosi, R., Oppo, G.-L., 2006. Self-localization of Bose-Einstein condensates in optical lattices via boundary dissipation. Phys. Rev. Lett.

97, 060401.
Lloyd, D. J. B., Sandstede, B., Avitabile, D., Champneys, A. R., 2008. Localised patterns in the 2D Swift-Hohenberg equation. SIAM J. Dyn. Sys. 7, 1049.
Loiko, N. A., Babushkin, I. V., 2001. Competition of orthogonally polarized transverse Fourier modes in a VCSEL. J. Opt. B: Quantum Semiclass. Opt. 3, S234–S243.
Longhi, S., 1997. Localized structures in optical parametric oscillation. Physica Scripta 56, 611–618.
Lugiato, L. A., 1984. Theory of optical bistability. Progress in Optics XXI, 70–216.
Lugiato, L. A., 2003. Introduction to the feature section on cavity solitons: An overview. IEEE J. Quantum Electron. 39 (2), 193–196.
Lugiato, L. A., Brambilla, M., Gatti, A., 1999. Optical pattern formation. Adv. Atom. Mol. Opt. Phys. 40, 229–306.
Lugiato, L. A., Kaige, W., Abraham, N. B., 1994. Pattern formation and instabilities in resonators with nonlinear dispersive media. Phys. Rev. A 49, 2049–2064.
Lugiato, L. A., Lefever, R., 1987. Spatial dissipative structures in passive optical systems. Phys. Rev. Lett. 58, 2209–2211.
Lugiato, L. A., Oldano, C., 1988. Stationary spatial patterns in passive optical systems: Two-level atoms. Phys. Rev. A 37, 3896–3908.
Lugiato, L. A., Prati, F., Tissoni, G., Brambilla, M., Barland, S., Giudici, M., Tredicce, J. R., 2008. Cavity solitons in semiconductor devices. In: Akhmediev, N., Ankiewicz, A. (Eds.), Dissipative Solitons: From Optics to Biology and Medicine. Lect. Notes Phys. Springer, p. 978.
Maggipinto, T., Brambilla, M., Firth, W. J., 2003. Characterization of stationary patterns and their link with cavity solitons in semiconductor microresonators. IEEE J. Quantum Electron. 39, 206–215.
Maggipinto, T., Brambilla, M., Harkness, G. K., Firth, W. J., 2000. Cavity solitons in semiconductor microresonators: Existence, stability, and dynamical properties. Phys. Rev. E 62 (6), 8726–8739.
Mahmoud Aghdami, K., Prati, F., Caccia, P., Tissoni, G., Lugiato, L. A., Kheradmand, R., Tajalli, H., 2008. Comparison of different switching techniques in a cavity soliton laser. Eur. Phys. J. D 47, 447455.
Mandel, P., Tlidi, M., 2004. Transverse dynamics in cavity nonlinear optics (20002003). J. Opt. B: Quantum Semiclass. Opt. 6, R60R75.
Manneville, P., 1990. Dissipative structures and weak turbulence. Academic Press, Boston.
Martin, R., Scroggie, A. J., Oppo, G.-L., Firth, W. J., 1996. Stabilization, selection and tracking of unstable patterns by Fourier space techniques. Phys. Rev. Lett. 77, 4007–4010.
Maywar, D. N., Agrawal, G. P., Nakano, Y., 2000. Robust optical control of an optical-amplifier-based flip-flop. Opt. Express 6, 75–80.
McDonald, G. S., Firth, W. J., 1990. Spatial solitary-wave optical memory. J.

Opt. Soc. Am. B 7, 1328–1335.
McLaughlin, D. W., Moloney, J. V., Newell, A. C., 1983. Solitary waves as fixed points of infinite-dimensional maps in an optical bistable ring cavity. Phys. Rev. Lett. 51, 75–78.
McSloy, J. M., Firth, W. J., Oppo, G.-L., Harkness, G. K., 2002. Computationally determined existence and stability of transverse structures: II. multi-peaked cavity solitons. Phys. Rev. E 66, 046606.
Menesguen, Y., Barbay, S., Hachair, X., Leroy, L., Sagnes, I., Kuszelewicz, R., 2006. Optical self-organization and cavity solitons in optically pumped semiconductor microresonators. Phys. Rev. A 74, 023818.
Michaelis, D., Peschel, U., Etrich, C., Lederer, F., 2003. Quadratic cavity solitons – the up-conversion case. IEEE J. Quantum Electron. 39, 255–268.
Michaelis, D., Peschel, U., Lederer, F., 1997. Multistable localized structures and superlattices in semiconductor optical resonators. Phys. Rev. A 56, R3366–R3369.
Miguel, M. S., Feng, Q., Moloney, J. V., 1995. Light polarization dynamics in surface-emitting semiconductor lasers. Phys. Rev. A 52, 1728–1739.
Mok, J. T., Martjin de Sterke, C., Littler, I. C. M., Eggleton, B. J., 2006. Dispersionless slow light using gap solitons. Nature Phys. 2, 775–780.
Mori, T., Yamayoshi, Y., Kawaguchi, H., 2006. Low-switching-energy and high-repetition-frequency all-optical flip-flop operations of a polarization bistable vertical-cavity surface-emitting laser. Appl. Phys. Lett. 88, 101102.
Müller, I., Ammelt, E., Purwins, H.-G., 1999. Self-organized quasiparticles: Breathing filaments in a gas discharge system. Phys. Rev. Lett. 82, 3428–3431.
Murray, J. D., 2003. Mathematical Biology: Spatial Models and Biomedical Applications, 3rd Edition. Springer, Berlin, Heidelberg, New York.
Naumenko, A., Loiko, N. A., Sondermann, M., Jentsch, K. F., Ackemann, T., 2006. Abrupt turn-on and hysteresis in a VCSEL with frequency-selective optical feedback. Opt. Commun. 259, 823–833.
Naumenko, A. V., Loiko, N. A., Ackemann, T., 2007. Analysis of bistability conditions between lasing and nonlasing states for a vertical-cavity surface-emitting laser with frequency-selective optical feedback using an envelope approximation. Phys. Rev. A 76, 023802.
Neubecker, R., 1996. Characterization of symmetry properties of patterns by generalized autocorrelation functions. Opt. Commun. 132, 593–605.
Neubecker, R., Oppo, G.-L., Thuering, B., Tschudi, T., 1995. Pattern formation in a liquid crystal light valve with feedback, including polarization, saturation, and internal threshold effects. Phys. Rev. A 52, 791–808.
Neubecker, R., Thüring, B., Kreuzer, M., Tschudi, T., 1999. Transition from spatio-temporal order to disorder in a single-feedback experiment. Chaos, Solitons & Fractals 10, 681–692.
Neubecker, R., Tschudi, T., 1994. Self-induced mode as a building element of transversal pattern formation. J. Mod. Opt. 41, 885–906.
Neubecker, R., Zimmermann, A., 2002. Spatial forcing of spontaneous optical

patterns. Phys. Rev. E 65, 035205(R).
Nishiura, Y., Ueyama, D., 1999. A skeleton structure of self-replicating dynamics. Physica D 130, 73–104.
Notomi, M., Kuramochi, E., Tanabe, T., 2008. Large-scale arrays of ultrahigh-Q coupled nanocavities. Nature Phot. 2, 741–747.
Okawachi, Y., Sharping, J. E., Xu, C., Gaeta, A. L., 2006. Large tunable optical delays via self-phase modulation and dispersion. Opt. Exp. 14, 12022–12027.
Oppo, G.-L., 2009. Formation and control of Turing patterns and phase fronts in photonics and chemistry. J. Math. Chem. 45, 95–112.
Oppo, G.-L., Brambilla, M., Lugiato, L. A., 1994. Formation and evolution of roll patterns in optical parametric oscillators. Phys. Rev. A 49, 2028–2032.
Oppo, G.-L., D'Alessandro, G., Firth, W. J., 1991. Spatiotemporal instabilities of lasers in models reduced via center manifold techniques. Phys. Rev. A 44, 4712–4719.
Oppo, G.-L., Kapral, R., 1987. Domain growth and nucleation in a discrete bistable system. Phys. Rev. A 36, 5820–5831.
Oppo, G.-L., Scroggie, A. J., Firth, W. J., 1999. From domain walls to localized structures in degenerate optical parametric oscillators. J. Opt. B: Quantum Semiclass. Opt. 1, 133–138.
Oppo, G.-L., Scroggie, A. J., Firth, W. J., 2001. Characterization, dynamics and stabilization of diffractive domain walls and dark ring cavity solitons in parametric oscillators. Phys. Rev. E 63, 066209.
Oppo, G.-L., Yao, A., Prati, F., Valcrcel, G. J. d., 2009. Long-term spatiotemporal dynamics of solid-state lasers and VCSELs. Phys. Rev. A, accepted for publication.
Ouchi, K., Fujisaka, H., 1996. Phase ordering kinetics in the Swift-Hohenberg equation. Phys. Rev. E 54, 3895–3898.
Paré, C., Gagnon, L., Bélanger, P.-A., 1989. Spatial solitary wave in a weakly-saturated amplifying/absorbing medium. Opt. Commun. 74, 228–232.
Paulau, P. V., Gomila, D., Ackemann, T., Loiko, N. A., Firth, W. J., 2008. Self-localized structures in vertical-cavity surface-emitting lasers with external feedback. Phys. Rev. E 78, 016212.
Paulau, P. V., Scroggie, A. J., Naumenko, A., Ackemann, T., Loiko, N. A., Firth, W. J., 2007. Localized traveling waves in vertical-cavity surface-emitting lasers with frequency-selective optical feedback. Phys. Rev. E 75, 056208.
Pedaci, F., Barland, S., Caboche, E., Genevet, P., Giudici, M., Tredicce, J. R., Ackemann, T., Scroggie, A. J., Firth, W. J., Oppo, G.-L., Tissoni, G., 2008a. All-optical delay line using semiconductor cavity solitons. Appl. Phys. Lett. 92, 011101.
Pedaci, F., Genevet, P., Barland, S., Giudici, M., Tredicce, J. R., 2006. Positioning cavity solitons with a phase mask. Appl. Phys. Lett. 89, 221111.
Pedaci, F., Tissoni, G., Barland, S., Giudici, M., Tredicce, J. R., 2008b. Mapping local defects of extended media using localized structures. Appl. Phys.

Lett. 93, 111104.
Pérez-Arjona, I., Sánchez-Morcillo, V. J., Roldán, E., 2007. Cavity solitons in bidirectional lasers. Opt. Lett. 32, 3221–3223.
Pesch, M., Große Westhoff, E., Ackemann, T., Lange, W., 2005. Observation of a discrete family of dissipative solitons in a nonlinear optical system. Phys. Rev. Lett. 95, 143906.
Pesch, M., Lange, W., Gomila, D., Ackemann, T., Firth, W. J., Oppo, G.-L., 2007. Two-dimensional front dynamics and spatial solitons in a nonlinear optical system. Phys. Rev. Lett. 99, 153902.
Peschel, U., Egorov, O., Lederer, F., 2004. Discrete cavity solitons. Opt. Lett. 29, 1909–1911.
Pikovsky, A., Rosenblum, M., Kurths, J., 2001. Synchronization - A universal concept in nonlinear sciences. Vol. 12 of Cambridge Nonlinear Science Series. Cambrifge University Press, Cambridge.
Pomeau, Y., 1986. Front motion, metastability and subcritical bifurcations in hydrodynamics. Physica D 23, 3–11.
Prati, F., Caccia, P., Tissoni, G., Lugiato, L. A., Mahmoud Aghdami, K., Tajalli, H., 2007. Effects of carrier radiative recombination on a VCSEL-based cavity soliton laser. Appl. Phys. B 88, 405–410.
Prati, F., Tissoni, G., Lugiato, L. A., Aghdami, K. M., Brambilla, M., 2009. Moving solitons in a cavity soliton laser.Unpublished.
Rabbiosi, I., Scroggie, A. J., Oppo, G.-L., 2002. Suppression of spatial chaos via noise-induced growth of arrays of spatial solitons. Phys. Rev. Lett. 89, 254102.
Rabbiosi, I., Scroggie, A. J., Oppo, G.-L., 2003. Stochastic resonance in the presence of spatially localized structures. Phys. Rev. E 68, 036602.
Radwell, N., Ackemann, T., Jäger, R., 2008. EOS Annual Meeting TOM 6, Paris, France, Sep 29 - Oct 2, 2008. Cavity solitons in vertical-cavity surface-emitting lasers with feedback from a volume Bragg grating.
Radwell, N., Ackemann, T., Rose, P., Cleff, C., Denz, C., 2009. Unpublished.
Radwell, N., Tanguy, Y., Ackemann, T., 2007. Unpublished.
Remoissenet, M., 1994. Waves called solitons: Concepts, Experiments. Springer, Berlin, Heidelberg, New York.
Residori, S., 2005. Patterns, fronts and structures in a liquid-crystal-light-valve with optical feedback. Phys. Rep. 416, 201272.
Richter, R., Barashenkov, I. V., 2005. Two-dimensional solitons on the surface of magnetic fluids. Phys. Rev. Lett. 94, 184503.
Riecke, H., 1999. Localized structures in pattern-forming systems. In: Pattern Formation in Continuous and Coupled Systems. Vol. 115 of IMA. Springer, New York, pp. 215–228.
Rosanov, N. N., 1991. Switching waves, autosolitons, and parallel digital-analogous optical computing. Proc. SPIE 1840, 130–143.
Rosanov, N. N., 1996. Transverse patterns in wide-aperture nonlinear optical systems. Progress in Optics XXXV, 1–60.
Rosanov, N. N., 2002. Spatial hysteresis and optical patterns. Springer Series

in Synergetics. Springer, Berlin.
Rosanov, N. N., 2005. Solitons in laser systems with saturable absorption. In: Akhmediev, N., Ankiewicz, A. (Eds.), Dissipative Solitons. Lecture Notes in Physics. Springer, New York, pp. 101–130.
Rosanov, N. N., Fedorov, S. V., 1992. Diffractive switching waves and autosolitons in a laser with saturable absorption. Opt. Spectr. 72, 782–787.
Rosanov, N. N., Fedorov, S. V., Shatsev, A. N., 2005. Curvilinear motion of multivortex laser-soliton complexes with strong and weak coupling. Phys. Rev. Lett. 95, 053903.
Rosanov, N. N., Khodova, G. V., 1988. Autosolitons in nonlinear interferometers. Opt. Spectrosc. 65, 449–450.
Rosanov, N. N., Khodova, G. V., 1990. Diffractive autosolitons in nonlinear interferometers. J. Opt. Soc. Am. B 7, 1057–1065.
Rosanov, N. N., Semenov, V. E., 1980. Hysteresis variations of the beam profile in a nonlinear Fabry-Perot interferometer. Opt. Spectrosc. 48, 59–63.
Ross, J., Müller, S. C., Vidal, C., 1988. Chemical waves. Science 240, 460–465.
Rössler, T., Indik, R. A., Harkness, G. K., Moloney, J. V., 1998. Modeling the interplay of thermal effects and transverse mode behavior in native-oxide confined vertical-cavity surface-emitting lasers. Phys. Rev. A 58, 3279–3292.
Rozanov, N. N., Fedorov, S. V., Shatsev, A. N., 2004. Energy-flow patterns and bifurcations of two-dimensional cavity solitons. JETP 98, 427–437.
Saffman, M., Montgomery, D., Anderson, D. Z., 1994. Collapse of a transverse-mode continuum in a self-imaging photorefractively pumped ring resonator. Opt. Lett. 19, 518–520.
Sánchez-Morcillo, V. J., Staliunas, K., 1999. Stability of localized structures in the swift-hohenberg equation. Phys. Rev. E 60, 6153–6156.
Santagiustina, M., Hernandez-Garcia, E., San Miguel, M., Scroggie, A., Oppo, G. L., 2002. Polarization patterns and vectorial defects in type-ii optical parametric oscillators. Phys. Rev. E 65, 036610 1–14.
Schäpers, B., Ackemann, T., Lange, W., 2001. Characteristics and possible applications of localized structures in an optical pattern–forming system. Proc. SPIE 4271, 130–137.
Schäpers, B., Ackemann, T., Lange, W., 2002. Robust control of switching of localized structures and its dynamics in a single-mirror feedback scheme. J. Opt. Soc. Am. B 19 (4), 707–715.
Schäpers, B., Ackemann, T., Lange, W., 2003. Properties of feedback solitons in a single-mirror experiment. IEEE J. Quantum Electron. 39 (2), 227–237.
Schäpers, B., Feldmann, M., Ackemann, T., Lange, W., 2000. Interaction of localized structures in an optical pattern forming system. Phys. Rev. Lett. 85, 748–751.
Schreiber, A., Kreuzer, M., Thüring, B., Tschudi, T., 1997. Experimental investigation of solitary structures in a nonlinear optical feedback system. Opt. Commun. 136, 415–418.
Schulz-Ruhtenberg, M., Tanguy, Y., Huang, K. F., Jäger, R., Ackemann, T., 2009. Control of the spatial emission structure of broad-area vertical-cavity

surface emitting lasers by feedback. J. Phys. D: Appl Phys. 42, 055101.
Sciamanna, M., Erneux, T., Rogister, F., Deparis, O., Mégret, P., Blondel, M., 2002. Bifurcation bridges between external-cavity modes lead to polarization self-modulation in vertical-cavity surface-emitting lasers. Phys. Rev. A 65, 041801(R).
Scroggie, A. J., Firth, W. J., McDonald, G. S., Tlidi, M., Lefever, R., Lugiato, L. A., 1994. Pattern formation in a passive kerr cavity. Chaos, Solitons & Fractals 4, 1323–1354.
Scroggie, A. J., Firth, W. J., Oppo, G.-L., 2009. Cavity soliton laser with frequency selective feedback. Phys. Rev. A, submitted.
Scroggie, A. J., Jeffers, J., McCartney, G., Oppo, G.-L., 2005. Reversible soliton motion. Phys. Rev. E 71, 046602.
Scroggie, A. J., McSloy, J. M., Firth, W. J., 2002. Self-propelled cavity solitons in semiconductor microresonators. Phys. Rev. E 66, 036607.
Segev, M., 2002. Solitons: a universal phenomenon of self-trapped wave packets. Opt. & Photon. News 13 (2), 27, introduction to special issue on *Solitons*.
Seipenbusch, J. P., Ackemann, T., Schäpers, B., Berge, B., Lange, W., 1997. Drift instability and locking behavior of optical patterns. Phys. Rev. A 56, R4401–R4404.
Skryabin, D. V., Champneys, A. R., Firth, W. J., 2000. Frequency selection by soliton excitation in nondegenerate intracavity down-conversion. Phys. Rev. Lett. 84, 463–466.
Sondermann, M., Weinkath, M., Ackemann, T., Mulet, J., Balle, S., 2003. Two-frequency emission and polarization dynamics at lasing threshold in vertical-cavity surface-emitting lasers. Phys. Rev. A 68, 033822.
Spinelli, L., Tissoni, G., Brambilla, M., Prati, F., Lugiato, L. A., 1998. Spatial solitons in semiconductor microcavities. Phys. Rev. A 58, 2542–2559.
Staliunas, K., 2003. Midband dissipative spatial solitons. Phys. Rev. Lett. 91, 053901.
Staliunas, K., Egorov, O., Kivshar, Y. S., F., L., 2008. Bloch cavity solitons in nonlinear resonators with intracavity photonic crystals. Phys. Rev. Lett. 101, 153903.
Staliunas, K., Sánchez-Morcillo, V., 2003. Transverse Patterns. Vol. 183 of Springer Tracts in Modern Physics. Springer.
Staliunas, K., Sánchez-Morcillo, V. J., 1997. Localized structures in degenerate optical parametric oscillators. Opt. Commun. 139, 306–312.
Staliunas, K., Slekys, G., Weiss, C. O., 1997. Nonlinear pattern formation in active optical systems: shocks, domains of tilted waves, and cross-roll patterns. Phys. Rev. Lett. 79, 2658–2661.
Stegeman, G. I., Segev, M., 1999. Optical spatial solitons and their interactions: universality and diversity. Science 286, 1518–1523.
Tanguy, Y., Ackemann, T., Firth, W. J., Jäger, R., 2008a. Realization of a semiconductor-based cavity soliton laser. Phys. Rev. Lett. 100, 013907.
Tanguy, Y., Ackemann, T., Jäger, R., 2006. Characteristics of bistable lo-

calized emission states in broad-area vertical-cavity surface-emitting lasers with frequency-selective feedback. Phys. Rev. A 74, 053824.

Tanguy, Y., Ackemann, T., Jäger, R., 2007. Characteristics of switching in a semiconductor based cavity-soliton laser. Opt. Exp. 15, 16773–16780.

Tanguy, Y., Radwell, N., Ackemann, T., Jäger, R., 2008b. Characteristics of cavity solitons and drifting excitations in broad-area vertical-cavity surface-emitting lasers with frequency-selective feedback. Phys. Rev. A 78, 023810.

Taranenko, V. B., Staliunas, K., Weiss, C. O., 1997. Spatial soliton laser: localized structures in a laser with a saturable absorber in a self-imaging resonator. Phys. Rev. A 56, 1582–1591.

Taranenko, V. B., Weiss, C. O., 2001. Incoherent optical switching of semiconductor resonator solitons. Appl. Phys. B 72 (7), 893–895.

Taranenko, V. B., Weiss, C. O., Schäpers, B., 2001. From coherent to incoherent hexagonal patterns in semiconductor resonators. Phys. Rev. A 65, 013812.

Terhalle, B., Radwell, N., Rose, P., Denz, C., Ackemann, T., 2008. Control of broad-area vertical-cavity surface emitting laser emission by optically induced photonic crystals. Appl. Phys. Lett. 93, 151114.

Tissoni, G., Spinelli, L., Brambilla, M., Perrini, I., Maggipinto, T., Lugiato, L. A., 1999. Cavity solitons in bulk semiconductor microcavities: microscopic model and modulational instabilities. J. Opt. Soc. Am. B 16, 2083-2094.

Tissoni, G., Spinelli, L., Brambilla, M., Perrini, I., Maggipinto, T., Lugiato, L. A., 1999. Cavity solitons in bulk semiconductor microcavities: dynamical properties and control. J. Opt. Soc. Am. B 16, 2095–2105.

Tlidi, M., Le Berre, M., Ressayre, E., Tallet, A., Di Menza, L., 2000. High-intensity localized structures in the degenerate optical parametric oscillator: Comparisom between the propagation and the mean-field model. Phys. Rev. A 61, 043806.

Tlidi, M., Mandel, P., Lefever, R., 1994. Localized structures and localized patterns in optical bistability. Phys. Rev. Lett. 73, 640–643.

Tredicce, J. R., 2004. Personal Communication.

Trillo, S., Haelterman, M., Sheppard, A., 1997. Stable topological spatial solitons in optical parametric oscillators. Opt. Lett. 22, 970–2.

Trillo, S., Torruellas, W. E. (Eds.), 2001. Spatial Solitons. Vol. 82 of Springer Series in Optical Sciences. Springer, Berlin.

Tucker, R., Ku, P., Chang-Hasnain, C., 2005. Delaybandwidth product and storage density in slow-light optical buffers. Electron. Lett. 41, 208–209.

Ultanir, E. A., Stegeman, G. I., Lange, C. H., 2006. Stability properties of multiwavelength, incoherent, dissipative spatial solitons. Opt. Lett. 30, 531–533.

Ultanir, E. A., Stegeman, G. I., Lange, C. H., Lederer, F., 2004. Coherent interactions of dissipative spatial solitons. Opt. Lett. 29, 283–285.

Ultanir, E. A., Stegeman, G. I., Michaelis, D., Lange, C. H., Lederer, F., 2003. Stable dissipative solitons in semiconductor optical amplifiers. Phys. Rev.

Lett., 253903.
Ultanir, E. A., Stegeman, G. I., Michaelis, D., Lange, C. H., Lederer, F., 2005. Dissipative solitons in semiconductor optical amplifiers. In: Akhmediev, N., Ankiewicz, A. (Eds.), Dissipative Solitons. Springer, Berlin, pp. 37–54.
Umbanhowar, P. B., Melo, F., Swinney, H. L., 1996. Localized excitations in a vertically vibrated granular layer. Nature 382, 793–796.
Vaschenko, G., Giudici, M., Rocca, J. J., Menoni, C. S., Tredicce, J. R., Balle, S., 1998. Temporal dynamics of semiconductor lasers with optical feedback. Phys. Rev. Lett. 81, 5536–5539.
Viktorov, E. A., Mandel, P., 2000. Low frequency fluctuations in a multimode semiconductor laser with optical feedback. Phys. Rev. Lett. 85 (15), 3157–3160.
Vilaseca, R., Torrent, M. C., García-Ojalvo, J., Brambilla, E., San Miguel, M., 2001. Two-photon cavity solitons in active optical media. Phys. Rev. Lett. 87, 083902.
Vladimirov, A. G., Fedorov, S. V., Khodova, G. V., Kaliteevskii, N. A., Rozanov, N. N., 1999. Numerical investigation of laser localized structures. J. Opt. B: Quantum Semiclass. Opt. 1, 101–105.
Vladimirov, A. G., McSloy, J. M., Skryabin, D. V., Firth, W. J., 2002. Two-dimensional clusters of solitary structures in driven optical cavities. Phys. Rev. E 65, 046606.
Weiss, C., Larionova, Y., 2005. Pattern formation in optical resonators. Rep. Prog. Phys. 70, 255335.
Weiss, C. O., Vaupel, M., Staliunas, K., Slekys, G., Taranenko, V. B., 1999. Solitons and vortices in lasers. Appl. Phys. B 68, 151–168.
Wilmsen, C., Temkin, H., Coldren, L. A., 1999. Vertical-cavity surface-emitting lasers. Cambridge University Press, Cambridge.
Wise, F. W., Di Trapani, P., 2002. The hunt for light bullets – spatiotemporal solitons. Opt. Photon. News 13 (2), 28–32.
Woods, P., Champneys, A., 1999. Heteroclinic tangles and homoclinic snaking in the unfolding of a degenerate reversible Hamiltonian Hopf bifurcation. Physica D 129, 147–170.
Wright, E. M., Firth, W. J., Galbraith, I., 1985. Diffusion and diffraction in dispersive optical bistability. J. Opt. Soc. Am. B 2, 1005–1009.
Xia, F., Sekaric, L., Vlasov, Y., 2007. Ultracompact optical buffers on a silicon chip. Nature Photonics 1, 65–71.
Yabuzaki, T., Okamoto, T., Kitano, M., Ogawa, T., 1984. Optical bistability with symmetry breaking. Phys. Rev. A 29, 1964–1972.